Study of Interactions between Surfactant, Polymer and Dye in Solution and at Interfaces

Inaugural-Dissertation

zur Erlangung des Doktorgrades
der Mathematisch-Naturwissenschaftlichen Fakultät
der Heinrich-Heine-Universität Düsseldorf

vorgelegt von

Yifei Zhan
aus Fujian, China

Düsseldorf, July 2020

aus dem Institut für Physikalische Chemie
der Heinrich-Heine-Universität Düsseldorf

Gedruckt mit der Genehmigung der
Mathematisch-Naturwissenschaftlichen Fakultät der
Heinrich-Heine-Universität Düsseldorf

Berichterstatter:

1. Prof. Dr. Wolfgang von Rybinski
2. Prof. Dr. Claus A. M. Seidel

Co-Betreuung:

Prof. Dr. Birgit Glüsen (Technische Hochschule Köln)

Tag der mündlichen Prüfung: 11.09.2020

Acknowledgements

I would like to show my deep appreciation to the people who gave me generous support and assistance for the completion of my doctoral thesis.

I would first like to thank my supervisor Prof. Dr. Wolfgang von Rybinski for his guidance, constructive comments and timely feedback whenever I had questions and problems. His expertise in the field of colloid and surface science was invaluable for the academic discussion during my PhD study and helped me proceed with my research work.

My special thanks go to Prof. Dr. Claus A. M. Seidel for providing the chance of cooperation with his group molecular physical chemistry and his very helpful advices and discussion in the group seminars and for my thesis.

I am particularly grateful to Prof. Dr. Birgit Glüsen, who gave me the opportunity to further pursue my research interest in this field and made it possible for me to present my results at various conferences. Her great support and encouragement during the time undertaking my work made a very important contribution to this doctoral thesis.

I would also like to thank the financial supporting from the Ministry of Culture and Science of the German State of North Rhine-Westphalia for the project of "FunktioPol–The Polymer Solution".

I am grateful to the colleagues in the office, who were always being supportive to my laboratory work and provided me assistance in numerous ways. Thanks especially to Lothar Müller for building the AFM acoustic enclosure, which reduced the disturbance from the surrounding vibration and light during imaging.

Thank you to Matthias Frangenberg for the UV-Vis spectroscopic study of three-component systems in solution and to Friedrich Grimm for the preparation of polyamide films for the AFM study. Special thanks to Julian van Megen for his help in the beginning phase of the AFM study, who shared his experimental experience and gave me valuable advices.

Finally, I want to thank my parents, my sister and my brother, who are always by my side, believing in me during every challenging period and encouraging me to follow my dreams.

Abstract

Dye transfer is an unwanted effect in laundering processes, which leads to the redeposition of released dyes from colored textiles onto other fabrics. The transfer of dye is influenced, among other parameters like washing time and temperature, by the components of detergent, especially by surfactants. Additionally, the dye transfer can be reduced by the so-called dye transfer inhibition (DTI) polymers. To elucidate the influence of surfactants and DTI polymers on dye transfer, it is necessary to understand the molecular interaction between surfactant, polymer and dye in solution and at interfaces.

Although the interaction of different types of dyes with surfactants in solution was studied[1–5] and the efficacy of DTI polymers in inhibiting dye adsorption on surfaces was shown for cotton dyes[6], a general understanding of the adsorption of dyes in the presence of surfactant and DTI polymer at solid-liquid interfaces is still scarce, partly because of the lack of suitable experimental methods. In recent years progress in studying aggregate structures of surfactants adsorbed at solid-liquid interfaces was made by atomic force microscopy (AFM).[7–10] In this work, the study of adsorption layers by AFM directly in aqueous mixtures was addressed to evaluate the molecular mechanism of surfactant and DTI polymer in dye transfer inhibition, especially for critical polyamide dyes.

The adsorption structures of single components and of binary mixtures of the dye Acid blue 113, the nonionic surfactant alkyl heptaglycolether ($C_{12\text{-}18}E_7$) as well as the anionic surfactant sodium dodecyl sulfate (SDS) and the DTI polymer poly(vinylpyrrolidone-vinylimidazole) (PVPVI) on the model surface graphite were identified by AFM in liquid for the first time. In addition, the adsorption of the dye and the dye in mixture with SDS at the carbon black-solution interface was analyzed in comparison with AFM studies. In order to present structural models for the systems investigated, the interaction of these components in solution was additionally studied by UV-Vis spectroscopy and dynamic light scattering (DLS) and the interaction at the air-solution interface was determined by surface tension measurements.

On graphite, Acid blue 113 adsorbs as single dye molecules and small dye aggregates with a lateral dimension in the range of 1−13 nm. The adsorbed amounts of the dye on graphite are increased at high dye solution concentrations. This observation on graphite by AFM agrees well with the results on carbon black powder, where the adsorbed amounts of the dye increase with increasing dye concentrations until to its solubility limit in water. Considering the molecular

area of the dye, the maximal adsorbed amount of dye corresponds to a coverage of about 40% for the total carbon black surface.

Surfactants have high adsorption preference for hydrophobic surfaces like graphite and carbon black.[7,8,11,12] The nonionic surfactant $C_{12\text{-}18}E_7$ adsorbs onto the surfaces much more strongly and at lower surfactant concentrations than the anionic surfactant SDS.[13(p. 102)] Hence, these surfactants can compete with the dye during adsorption. As shown in AFM studies, in the mixture of the dye with $C_{12\text{-}18}E_7$ of even a very low concentration (0.003 mM) below the critical micelle concentration (CMC), the typical dye structure on graphite was not seen. At surfactant concentrations above the CMC only the hemicylindrical structure[8] of surfactants was observed on the surface, where the adsorption of the dye on the surface is obviously inhibited due to the adsorption of surfactants. In addition, the size of the hemicylindrical structure is increased in the presence of the dye from about 5.9 nm to 7.2 nm with respect to the periodicity of the structure. This indicates the incorporation of small amounts of the dye into the surfactant aggregates adsorbed on graphite. According to the UV-Vis spectroscopic study in solution, at saturation one $C_{12\text{-}18}E_7$ micelle can bind 2−3 dye molecules. Therefore, for the first time two different mechanisms for the dye adsorption on graphite were identified: on the one hand the adsorption of the dye is inhibited due to the strong adsorption of the surfactant $C_{12\text{-}18}E_7$. On the other hand, the dye may be incorporated into surfactant aggregates adsorbed in small amounts at surfactant concentrations above the CMC.

A similar effect in the AFM studies on graphite was also found for the mixture of the dye with the anionic surfactant SDS only at high surfactant concentrations. At high SDS concentrations (> CMC), only the hemicylindrical structure[7] of surfactants was observed. In addition, the adsorbed amounts of the dye in mixture with SDS on carbon black were determined to further interpret the adsorption of the dye. It was found that at low dye concentrations the adsorption of the dye is obviously not changed due to different surfactant concentrations, showing comparable Langmuir constants of 522−535 m^3/mol. At high dye concentrations the adsorbed amounts of dye decrease in the presence of high surfactant concentration, resulting in a plateau of lower level in the adsorption isotherm. This indicates that the adsorption of the dye on the solid surface can be inhibited by the anionic surfactant SDS of high concentrations (> CMC) to some extent. In addition, according to the spectroscopic study Acid blue 113 shows a weak interaction with SDS in solution and on average 7−8 SDS micelles can bind only one dye molecule, which is lower than that for the nonionic surfactant $C_{12\text{-}18}E_7$.

The DTI polymer PVPVI forms single globular structures on graphite at high concentrations ($\geq$ 0.1 mM). The size (diameter) of the globules is mostly in the range of 15−17 nm, which corresponds to the size of one polymer molecule in water determined by DLS. In mixture of the dye with the polymer, above the critical aggregation concentration (CAC) of the polymer ($\sim 1 \cdot 10^{-4}$ mM), an adsorption of the dye-polymer complex was found on the surface. This interaction between Acid blue 113 and PVPVI was also observed in solution above the CAC forming a dye-polymer (1:1) complex. In the presence of the dye the polymer globules could not be observed even at high polymer concentrations.

In the presence of $C_{12\text{-}18}E_7$ at even a very low concentration (0.003 mM) below the CMC, the globular structure of the DTI polymer was hardly observed on graphite, whereas the globular polymers could still be seen at the SDS concentration of 0.1 mM. For both surfactants at concentrations above the CMC, the adsorption of the polymer is markedly inhibited on the surface, where almost only the hemicylindrical structure of surfactants was observed, which is not changed in the presence of polymer. Hence, the study at solid-liquid interfaces confirms that the adsorption of individual components onto surfaces in the binary system is competitive, which has a very important influence on the adsorption of dye on surfaces.

In summary, AFM proves to be a very powerful tool to characterize the adsorbed layers from binary aqueous mixtures of dye, surfactant and DTI polymer at solid-liquid interfaces. It enables the identification of adsorption structures on the nanometer scale and allows the allocation of individual components. The studies on nonpolar model surfaces reveal that two different mechanisms play a decisive role in the adsorption of dye on surfaces in the presence of surfactants: the competitive adsorption of individual components and the incorporation of dyes into micellar surfactant aggregates on model surfaces. $C_{12\text{-}18}E_7$ has a higher adsorption preference than the dye to model surfaces, and on the other hand, the dye can be incorporated into surfactant micelles in solution as well as into surfactant aggregates adsorbed on surface, which can result in additive or adverse effects of the two mechanisms on dye transfer inhibition. In comparison with the anionic surfactant SDS, the nonionic surfactant $C_{12\text{-}18}E_7$ shows a greater effect due to its higher affinity for model surfaces and stronger incorporation of the dye into surfactant micelles in solution. The DTI polymer PVPVI forms a dye-polymer complex with the dye on model surfaces above the CAC of the polymer, as also shown in solution. In the presence of surfactants ($>$ CMC), the adsorption of the polymer onto surfaces is inhibited due to the dominant adsorption of surfactants.

In this work, adsorption mechanisms were identified to get an in-depth understanding of the influence of surfactant and DTI polymer on dye transfer at a molecular level for a hydrophobic model surface. Based on these fundamental results, further studies on textile or textile-like surfaces would give additional insights in the mode of action of DTI in real washing processes.

Zusammenfassung

Die Farbübertragung ist ein unerwünschter Effekt bei Waschprozessen, der dazu führt, dass abgelöste Farbstoffe aus farbigen Textilien auf andere Textilien übertragt werden. Die Übertragung des Farbstoffs wird unter anderem wie Waschzeit und Waschtemperatur durch die Komponenten des Waschmittels, insbesondere durch Tenside, beeinflusst. Zusätzlich kann die Farbübertragung durch die sogenannten Farbübertragungsinhibitoren (DTI-Polymere) verringert werden. Um den Einfluss von Tensiden und DTI-Polymeren auf die Farbübertragung aufzuklären, ist es notwendig, die molekulare Wechselwirkung zwischen Tensid, Polymer und Farbstoff in Lösung und an Grenzflächen zu verstehen.

Obwohl die Wechselwirkung von verschiedenen Farbstoffen und Tensiden in Lösung untersucht[1–5] und die Wirksamkeit von DTI-Polymeren bei der Farbübertragungsinhibition (*dye transfer inhibition*, DTI) für Baumwollfarbstoffe gezeigt[6] wurde, ist wegen des Fehlens geeigneter experimenteller Methoden ein allgemeines Verständnis der Adsorption von Farbstoffen an fest-flüssigen Grenzflächen in Gegenwart von Tensid und DTI-Polymer immer noch sehr gering. Fortschritte bei der Untersuchung der an fest-flüssigen Grenzflächen adsorbierten Aggregatstrukturen von Tensiden wurden durch Rasterkraftmikroskopie (AFM) erzielt.[7–10] Im Rahmen dieser Arbeit wurden die Untersuchungen von Adsorptionsschichten durch AFM direkt in wässrigen Mischungen durchgeführt um den molekularen Mechanismus von Tensid und DTI-Polymer bei der Farbübertragungsinhibition zu verstehen, besonders für kritische Polyamidfarbstoffe.

In der vorliegenden Arbeit wurden daher die Adsorptionsstrukturen der Einzelkomponenten und binärer Mischungen von dem Farbstoff Acid blue 113, dem nichtionischen Tensid Alkylheptaglycolether ($C_{12\text{-}18}E_7$) sowie anionischen Tensid Natriumdodecylsulfat (SDS) und dem DTI-Polymer Poly(Vinylpyrrolidon-Vinylimidazol) (PVPVI) auf der Modelloberfläche Graphit erstmals durch AFM in Flüssigkeit identifiziert. Zusätzlich wurde die Adsorption des Farbstoffs und dessen Mischung mit SDS an der Ruß-Lösung Grenzfläche im Vergleich zu den AFM-Studien analysiert. Um Strukturmodelle für die untersuchten Systeme aufstellen zu können, wurde auch die Wechselwirkung dieser Komponenten in Lösung durch UV-Vis-Spektroskopie und dynamische Lichtstreuung (DLS) untersucht und die Wechselwirkung an der Luft-Lösung Grenzfläche durch Oberflächenspannungsmessungen bestimmt.

Acid blue 113 adsorbiert auf Graphit als einzelne Farbstoffmoleküle und kleine Farbstoffaggregate mit einer lateralen Dimension von 1−13 nm. Die adsorbierten Mengen des Farbstoffs auf Graphit nehmen bei hohen Farbstoffkonzentrationen zu. Diese Beobachtung an Graphit durch AFM stimmt gut mit den Ergebnissen an Rußpulver überein, wo die adsorbierten Mengen des Farbstoffs mit zunehmenden Farbstoffkonzentrationen bis zu seiner Löslichkeitsgrenze in Wasser zunehmen. Gemäß der molekularen Fläche des Farbstoffs entspricht die maximal adsorbierte Farbstoffmenge einer Bedeckung von etwa 40% für die gesamte Rußoberfläche.

Tenside haben eine hohe Adsorptionsaffinität zu hydrophoben Oberflächen wie Graphit und Ruß.[7,8,11,12] Das nichtionische Tensid $C_{12\text{-}18}E_7$ adsorbiert viel stärker und bei niedrigerer Tensidkonzentration an den Oberflächen als das anionische Tensid SDS.[13(p. 102)] Daher können diese Tenside während der Adsorption mit dem Farbstoff konkurrieren. Die AFM-Studie zeigte, dass in der Mischung des Farbstoffs mit $C_{12\text{-}18}E_7$ sogar bei einer sehr niedrigen Konzentration (0,003 mM) unterhalb der kritischen Mizellbildungskonzentration (CMC) die typische Farbstoffstruktur auf Graphit nicht gesehen wurde. Bei den Tensidkonzentrationen oberhalb der CMC wurde nur die Hemizylinderstruktur[8] von Tensiden auf der Oberfläche beobachtet. Die direkte Adsorption des Farbstoffs auf der Oberfläche wurde aufgrund der Adsorption von Tensiden gehemmt. Zusätzlich vergrößerte sich die Periodizität der Hemizylinderstruktur in Gegenwart des Farbstoffs von etwa 5,9 nm auf 7,2 nm. Dies kann auf die Einlagerung des Farbstoffs von kleinen Mengen in die adsorbierten Tensidaggregate hindeuten. Gemäß der UV-Vis-spektroskopischen Untersuchung in Lösung kann eine $C_{12\text{-}18}E_7$-Mizelle bei Sättigung 2−3 Farbstoffmoleküle binden. Es wurden daher erstmals zwei verschiedene Mechanismen für die Adsorption des Farbstoffs auf Graphit identifiziert: Die Hemmung der direkten Adsorption des Farbstoffs aufgrund der starken Adsorption des Tensids $C_{12\text{-}18}E_7$ und die geringe Einlagerung des Farbstoffs in hemizylindrische Tensidaggregate bei Tensidkonzentrationen oberhalb der CMC.

Ein ähnlicher Effekt in AFM-Studien auf Graphit wurde auch in der Mischung des Farbstoffs mit dem anionischen Tensid SDS allerdings nur bei hohen Tensidkonzentrationen gefunden. Bei hohen SDS-Konzentrationen (> CMC) wurde nur die hemizylindrische Tensidstruktur[7] beobachtet. Außerdem wurden die adsorbierten Mengen des Farbstoffs in Mischung mit SDS auf Ruß bestimmt, um die Adsorption des Farbstoffs weiter zu interpretieren. Es wurde gefunden, dass bei niedrigen Farbstoffkonzentrationen die Adsorption des Farbstoffs offensichtlich nicht von unterschiedlichen Tensidkonzentrationen beeinflusst wird, wie die

vergleichbaren Langmuir-Konstanten von 522 – 535 m^3/mol zeigen. Bei hohen Farbstoffkonzentrationen nimmt die adsorbierte Farbstoffmenge in Gegenwart einer hohen Tensidkonzentration ab, was zu einem niedrigeren Plateau in der Adsorptionsisotherme führt. Dies weist darauf hin, dass die Adsorption des Farbstoffs an der Oberfläche auch durch das anionische Tensid SDS mit hohen Konzentrationen (> CMC) gehemmt werden kann. Laut spektroskopischer Untersuchung zeigt Acid blue 113 eine schwache Wechselwirkung mit SDS in Lösung und im Durchschnitt können 7−8 SDS-Mizellen nur ein Farbstoffmolekül binden, was niedriger ist als für das nichtionische Tensid $C_{12\text{-}18}E_7$.

Das DTI-Polymer PVPVI bildet einzelne kugelförmige Strukturen auf Graphit bei hohen Konzentrationen (≥ 0,1 mM). Die Größe (der Durchmesser) der Kugeln liegt meistens im Bereich von 15−17 nm, was der Größe eines Polymermoleküls in Wasser entspricht, die mittels DLS bestimmt wurde. In Mischung des Farbstoffs mit dem Polymer wurde oberhalb der kritischen Aggregationskonzentration (CAC) des Polymers (~$1 \cdot 10^{-4}$ mM) eine Adsorption des Farbstoff-Polymer-Komplexes auf der Oberfläche gefunden. Diese Wechselwirkung zwischen Acid blue 113 und PVPVI wurde auch in Lösung oberhalb der CAC beobachtet, wobei ein (1:1) Farbstoff-Polymer-Komplex gebildet wird. In Gegenwart des Farbstoffs konnten die Polymerkugeln auch bei hohen Polymerkonzentrationen nicht beobachtet werden.

In Gegenwart von $C_{12\text{-}18}E_7$ mit einer sehr geringen Konzentration (0,003 mM) unterhalb der CMC wurde die Kugelstruktur des Polymers auf Graphit kaum beobachtet, während die Polymerkugeln bei einer SDS-Konzentration von 0,1 mM noch zu sehen waren. Für beide Tenside bei Konzentrationen oberhalb der CMC wurde die Adsorption des Polymers auf der Oberfläche deutlich gehindert, wo fast nur die Hemizylinderstrukturen der Tenside beobachtet wurden, die in Gegenwart des Polymers nicht verändert sind. Somit bestätigt die Studie an fest-flüssigen Grenzflächen, dass die Adsorption einzelner Komponenten auf Oberflächen im binären System konkurrierend ist, was einen sehr wichtigen Einfluss auf die Adsorption von Farbstoff auf Oberflächen hat.

Zusammenfassend erweist sich AFM als eine sehr gute Methode zur Charakterisierung der adsorbierten Schichten von binären wässrigen Mischungen aus Farbstoff, Tensid und DTI-Polymer an fest-flüssigen Grenzflächen. Damit können Adsorptionsstrukturen im Nanometerbereich identifiziert und einzelnen Komponenten zugeordnet werden. Die Untersuchungen an unpolaren Modelloberflächen zeigten, dass zwei verschiedene Mechanismen bei der Adsorption von Farbstoff auf Oberflächen in Gegenwart von Tensiden

eine entscheidende Rolle spielen: die Konkurrenzadsorption der einzelnen Komponente und die Einlagerung der Farbstoffe in mizellaren Tensidaggregaten auf Modelloberflächen. $C_{12\text{-}18}E_7$ hat eine höhere Adsorptionsaffinität zu Modelloberflächen als der Farbstoff und verdrängt diesen von der Oberfläche. Andererseits kann der Farbstoff sowohl in Tensidmizellen in Lösung als auch in adsorbierten Tensidaggregaten auf Oberflächen eingelagert werden, was zu additiven oder gegenläufigen Auswirkungen auf die Farbübertragungsinhibition führen kann. Im Vergleich zum anionischen Tensid SDS zeigt das nichtionische Tensid $C_{12\text{-}18}E_7$ aufgrund seiner höheren Affinität zu Modelloberflächen und stärkeren Einlagerung des Farbstoffs in Tensidmizellen in Lösung eine größere Wirkung. Das DTI-Polymer PVPVI bildet mit dem Farbstoff einen Farbstoff-Polymer-Komplex auf Modelloberflächen oberhalb der CAC des Polymers, wie es auch in Lösung gezeigt wird. In Gegenwart von Tensiden ($>$ CMC) wird die Adsorption des Polymers auf Oberflächen aufgrund der dominanten Adsorption von Tensiden gehemmt.

In dieser Arbeit wurden Adsorptionsmechanismen identifiziert, um den Einfluss von Tensid und DTI-Polymer auf die Farbübertragung für eine hydrophobe Modelloberfläche auf molekularer Ebene zu verstehen. Basierend auf diesen grundlegenden Ergebnissen werden weitere Untersuchungen auf textilen bzw. textilähnlichen Oberflächen zusätzliche Erkenntnisse über die Wirkungsweise von DTI in realen Waschprozessen liefern.

Contents

1 Introduction

With the vast application of coloration in textile materials, dye transfer has become an important issue in laundering processes. During washing, the dye can be released from colored textiles and dissolved in washing liquid, a part of which can redeposit onto other fabrics. It is possible to reduce dye transfer by the development of better dyes and the reduction of washing time and temperature.[14] Additionally, dye transfer can also be impacted by the components of detergents, therefore, the optimization of detergents is a very important factor to decrease the unwanted effect.

Surfactants are the most important components in detergents. In a washing procedure, surfactants are able to remove dyes from textiles[15,16] and solubilize dyes[17–20]. The removal of dyes from textile surfaces is related to the interaction of surfactants with the surfaces and with dyes at solid-liquid interfaces.[15] The solubilization of dyes can result in the stabilization of dyes in surfactant solution preventing the redeposition of dyes.[6] Surfactants consist of both hydrophilic and hydrophobic parts. The interaction between surfactants and dyes is mainly caused by the electrostatic[1,3] and hydrophobic forces[16,21], which is greatly dependent on the structure and property of surfactants and dyes. Hence, the choice of surfactants is decisive for the effect on dye transfer inhibition (DTI).

In addition, some water-soluble polymers such as polyvinylpyrrolidone (PVP), polyvinylpyridine N-oxide (PVP-NO) and the copolymer of vinylpyrrolidone and vinylimidazole (PVPVI) are found to be effective as dye transfer inhibitors for cottons,[14,22] some of which show also selectivity for dyes. These DTI polymers can bind dyes by the electrostatic attraction between the polar groups of dyes and the polyelectrolytes in addition to the hydrophobic interaction.[23]

Therefore, the complete picture of a complex washing process involves the interaction in solution and at solid-liquid interfaces. Actually, in a real washing process these interactions take place simultaneously. The key factor of DTI efficacy is the interaction between dyes and additives both in solution and at interfaces, which is essential to understand the influence of detergent components on dye transfer as well as dye transfer inhibition and to further improve the formulation of detergents.

The interaction of different types of dyes with surfactants in solution has been intensively studied in the past.[1–5] Oakes et al. demonstrated the interaction between dyes and DTI polymers

in solution[24] and indicated the DTI effect of these polymers by measuring the loss of adsorbed dyes on cotton after washing dyed fabrics with DTI polymer solutions[25,26]. Although the efficacy of DTI polymers in inhibiting dye adsorption on surfaces was shown for cotton dyes[6], the mechanism of the influence of DTI polymers on dye adsorption was not pointed out. In addition, synthetic fibers such as polyamide fibers gain more and more importance in textiles[27] and the classical DTI polymers are usually not effective for polyamide dyes.[23] Because of the lack of suitable experimental methods, a general understanding of the adsorption of dyes in the presence of surfactant and DTI polymer at solid-liquid interfaces is still scarce. In recent years progress in studying aggregate structures of surfactants adsorbed at solid-liquid interfaces was made by atomic force microscopy (AFM).[7–10] In this work, the study of adsorption layers by AFM directly in aqueous mixtures is addressed to evaluate the molecular mechanism of surfactant and DTI polymer in influencing dye adsorption as well as in dye transfer inhibition, especially for critical polyamide dyes.

In the study, the anionic dye Acid blue 113 is chosen as the model dye. Acid blue 113 is a biazo dye, which is widely applied as coloring agent in textile dyeing for nylon, wool and silk fabrics[28]. A vinylpyrrolidone-vinylimidazole copolymer PVPVI is taken as the DTI polymer. As most detergents contain anionic and nonionic surfactants[29(p. 101-104)], the anionic surfactant sodium dodecyl sulfate (SDS) and the nonionic surfactant alkyl heptaglycolether ($C_{12\text{-}18}E_7$) are used as model surfactants. The study focuses on the molecular interaction between surfactants, the DTI polymer and the dye in solution and on nonpolar model surfaces in binary aqueous mixtures.

The adsorption structures of single components and of binary mixtures of surfactant, DTI polymer and dye on graphite are identified by AFM in solutions. In addition, the adsorbed amounts of the dye and the dye in mixture with SDS on carbon black powder are quantified in comparison with AFM studies. To develop structural models for the systems investigated, the interaction of these components in solution is studied by UV-Vis spectroscopy and particle size analysis using dynamic light scattering (DLS) and the interaction at the air-solution interface is determined by surface tension measurements with the Wilhelmy plate method. Based on the results obtained, structural models for the binary systems in solution and at solid-liquid interfaces are suggested and presented to give a comprehensive view of the influence of surfactant and DTI polymer on dye adsorption and dye transfer at a molecular level.

For the further study on textile or textile-like surfaces, different polyamide surfaces are characterized by AFM both in air and in water. The characterization of the polyamide surfaces provides basic information for future studies on textile surfaces in order to get a deeper insight into the mode of action of DTI in real washing processes.

2 Theories

2.1 Interaction of dyes with surfactants in solution

According to applications the dyes used to textile coloration can be classified mainly as acid, reactive, direct, disperse and basic dyes.[27] The dyes may be soluble or insoluble/poorly soluble in water. The water-insoluble dyes are mostly found to be solubilized in surfactant solutions.[17,18] For water-soluble dyes, despite surfactants are not decisive in their solubilization in water, the aggregation and adsorption of these dyes can still be influenced by surfactants[23,26]. Most dyes interact with surfactants above the critical micelle concentration (CMC), where dyes are incorporated in surfactant micelles.[30]

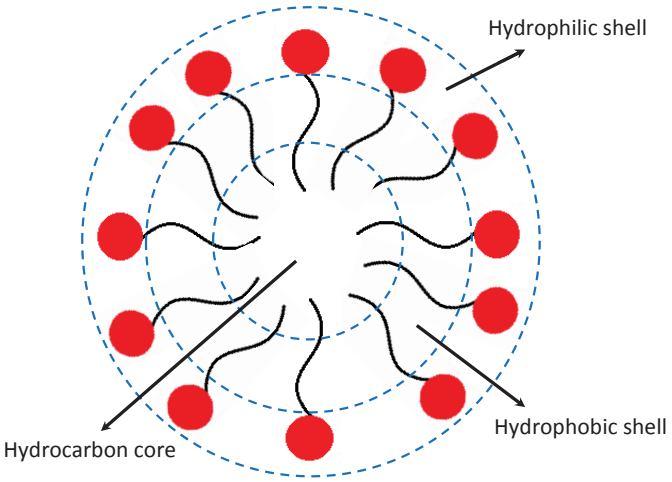

Figure 2-1 Illustration of a spherical surfactant micelle in solution (cross section) consisting of three regions:[16] the hydrophilic shell (outer region), the hydrophobic shell (palisade region) and the hydrocarbon core. The hydrophilic headgroup of surfactant is marked in red and the hydrophobic chain is indicated as the black line.

Surfactants can self-assemble or self-associate in aqueous solution to form micelles at a certain concentration, which is known as the critical micelle concentration (CMC).[31(p. 39-41)] Surfactant micelles have different structures, such as spherical, cylindrical (rod-like) or bilayer (lamellar) forms. Figure 2-1 shows an illustration of a spherical micelle (cross section). The micelle is composed of three regions: the hydrophilic shell (outer region), the hydrophobic shell (palisade region) and the hydrocarbon core.[16,32] The hydrophilic shell is referred to as the interfacial region between the micelle and the surrounding medium, where the hydrophilic headgroups of surfactant are present. The hydrophobic shell is related to the outer part of the hydrocarbon chain of surfactant, which is connected with the headgroup of surfactant. The hydrocarbon core is the extremely hydrophobic center of the micelle.

The location of dye molecules in a surfactant micelle is affected by the properties of dye and surfactant. A number of ionic dyes are found to interact with oppositely charged ionic surfactants even below the CMC, which may be driven by the electrostatic interaction between the ionic groups.[3] For the systems where no electrostatic interaction is present, like hydrophobic/nonionic dyes and ionic surfactants or ionic/nonionic dyes and nonionic surfactants, the hydrophobic interaction is essential for the association[23]. In most cases, the dye is accommodated in the hydrophilic and hydrophobic shell of surfactant micelle with a suitable orientation,[1,2,5,21] depending on the dye-surfactant interaction. A commonly used method to demonstrate the dye-surfactant interaction in solution is the UV-Vis spectroscopy. It is known that the incorporation of dyes in surfactant micelles can cause changes in the absorption spectrum of dye.[5,23,33] Moreover, the position of dyes in surfactant micelles can also be indirectly determined by UV-Vis spectroscopy.[21,34] In this method the change of the absorption spectrum of dye in various solvents with different polarity is recorded, which is compared with the spectrum of dye in surfactant solutions. The similarity between the spectrum of dye in surfactant solutions and that in solvents pinpoints the possible location of dye in surfactant micelles.[16] That is to say, if the absorption spectrum of the dye in surfactant solution is similar to that in a polar or more polar solvent, the dye is expected to be located in the hydrophilic shell of surfactant micelle.

2.2 Thermodynamics of adsorption at interfaces

The thermodynamics of adsorption on surface can be expressed by[35(p. 209)]

$$\Delta G = \Delta H - T\Delta S \tag{2-1}$$

ΔG is the change of Gibbs free energy, ΔH is the enthalpy change and ΔS the entropy change. The nature of any systems is to keep the lowest Gibbs free energy, which means that a spontaneous change is always related to a negative ΔG. After adsorption of substances in a system onto a surface, the entropy of the system usually decreases ($\Delta S < 0$). Therefore, ΔH must be negative (exothermic) for a spontaneous adsorption process. Depending on the magnitude of the enthalpy change ΔH, the adsorbate-substrate bonding can be due to physisorption or chemisorption. The bonding interaction in physisorption is weaker ($|\Delta H| <$ 35 kJ·mol^{-1}) than that in chemisorption ($|\Delta H| >$ 35 kJ·mol^{-1}).[36(p. 9-10)]

2.2.1 Adsorption at the gas-liquid interface

When two immiscible phases are in contact with each other, a boundary region forms between them, where the properties of both bulk phases change gradually at the dividing interface[37]. This interface is referred as the Gibbs dividing interface, which is considered as an infinitesimally thin two-dimensional layer with no volume.[38] The molecules presented in the interface cause excess interfacial quantities like moles of components, energy and entropy of the system. The formation of an interface is related to the surface free energy. The surface free energy is the work required to create a new surface/interface of one unit area (1 m^2), which is dimensionally equivalent to the surface tension γ.[38(p. 85)] The surface tension is usually also defined as the force per unit length acting normal to the interface formed.[38]

Because of the association of the surface free energy and the surface tension, the surface excess concentration of the component i Γ_i is given by the Gibbs adsorption law[39(p. 67)]

$$\Gamma_i = \frac{n_i}{A} \tag{2-2}$$

n_i is the surface excess amount of the component i at the interface and A is the interfacial area. At constant temperature the Gibbs equation gives a relationship of the surface tension γ and surface excess concentration[38(p. 99-100)]

$$d\gamma = -\sum_i \Gamma_i \, d\mu_i \tag{2-3}$$

$$\mu_i = X + RT \ln a_i \tag{2-4}$$

μ_i is the chemical potential of the component i and a_i the activity of the component i. R is the ideal gas constant (8.314 $J \cdot K^{-1} \cdot mol^{-1}$), X is a constant and T is the absolute temperature. For a two-component system (solvent Γ_1 and solute Γ_2), if the Gibbs interface plane is chosen in such a position that the surface excess concentration of solvent is zero ($\Gamma_1 = 0$), then the Gibbs equation is simplified as follows[37(p. 28-29)]

$$d\gamma = -\Gamma_2 RT d \ln a_2 \tag{2-5}$$

For a dilute solution, the surface excess concentration of solute adsorbed at the interface is calculated by the following equations

$$\Gamma_2 = -\frac{1}{RT}\left(\frac{d\gamma}{d\ln c_2}\right) \quad \text{(nonionic solute)} \tag{2-6}$$

$$\Gamma_2 = -\frac{1}{2RT}\left(\frac{d\gamma}{d\ln c_2}\right) \quad \text{(ionic solute of the form } A^+B^-\text{)} \tag{2-7}$$

c_2 is the molar concentration of the solute. For surface-active substances such as surfactants, the surface tension decreases with increasing surfactant concentrations in a certain concentration range. The surface tension at a gas-liquid or liquid-liquid interface can be measured directly. According to the equation 2-6 or 2-7, the surface excess concentration of solute can be calculated by plotting of the surface tension γ versus the logarithmic concentration. Furthermore, the molecular area of the solute at interfaces can also be determined by Equation 2-13 shown in Section 2.2.2.

2.2.2 Adsorption at the solid-liquid interface

As stated in Section 2.2.1, the Gibbs adsorption equation describes the amount of adsorbate at gas-liquid or liquid-liquid interfaces. For the adsorption of gas or liquid on solid surfaces, the surface excess concentration at equilibrium is related to the adsorptive gas pressure or the solution concentration. The dependence of the adsorbed amount on the gas pressure or solution concentration is called an adsorption isotherm.[36(p. 1)] It is experimentally determined by a plot of the adsorbed amounts as a function of the equilibrium pressure or concentration of the adsorptive substance. In practice, different models of adsorption isotherm are developed to analyze the experimental data. Here, three typical adsorption isotherm models will be given for describing the adsorption at solid-liquid interfaces.

Henry isotherm

For ideal gas and very dilute solutions, most adsorption isotherms obey the Henry's law[36(p. 1)],

$$\Gamma = k \cdot c \tag{2-8}$$

the adsorbed amount Γ is proportional to the equilibrium concentration c of the adsorptive substance.

Freundlich isotherm

For many systems studied, the adsorption isotherm is actually not linear as given by Equation 2-8. These systems can be generally described by the empirical Freundlich adsorption equation:[38(p. 302)]

$$\Gamma = k_{\mathrm{F}} \cdot c^{n} \tag{2-9}$$

c is the equilibrium concentration. k_{F} and n are two empirical constants, the relative adsorption capacity and the surface heterogeneity indicating the intensity of the adsorption. The smaller the n value is, the surface becomes more heterogeneous.[40] k_{F} and n can be determined according to the logarithmic form of Equation 2-9,

$$\log \Gamma = \log(k_{\mathrm{F}}) + n \cdot \log c \tag{2-10}$$

The plot of $\log \Gamma$ versus $\log c$ should give a straight line with the slope n and the intercept $\log(k_{\mathrm{F}})$. In the Freundlich adsorption isotherm, the adsorption sites have different adsorption energies, some of which may be more favorable, so the adsorption is not restricted to a completely saturated monolayer[40]. In addition, the heat of adsorption decreases with the increase of the fractional coverage.[38(p. 302-304)]

Langmuir isotherm

Langmuir adsorption isotherm is used to quantify the adsorption of one monolayer. It is assumed that the adsorptive molecules (adsorbates) and the surface are in dynamic equilibrium.[36(p. 2)] That means the rate of adsorption onto the substrate is equal to the rate of desorption from the substrate. Based on this assumption the Langmuir isotherm is expressed as[38(p. 298)]

$$\Gamma = \frac{\Gamma_{\mathrm{max}} \cdot k \cdot c}{1 + k \cdot c} \tag{2-11}$$

Γ_{max} is the adsorbed amount of a saturated monolayer, which is the moles of adsorbate per unit mass or area. k is the Langmuir constant and equals the ratio of the adsorption rate constant to the desorption rate constant[36(p. 2)], relating to the affinity of adsorbates to the substrate. c is the equilibrium concentration. Converting Equation 2-11 into a linear form as follows

$$\frac{1}{\Gamma} = \frac{1}{\Gamma_{\max} \cdot k \cdot c} + \frac{1}{\Gamma_{\max}} \tag{2-12}$$

the $\Gamma_{\max}$ and k can be determined by plotting of $1/\Gamma$ versus $1/c$. If $\Gamma_{\max}$ is related to the moles of adsorbed molecules per unit area, the molecular area can be calculated by

$$A_{ad} = \frac{1}{\Gamma_{\max} \cdot N_A} \tag{2-13}$$

A_{ad} is the molecular area (m^2) of the adsorbate and N_A is the Avogadro constant ($6.022 \cdot 10^{23}$ mol^{-1}).

The Langmuir isotherm model has some assumptions:[36,38,40]

- The adsorption energy of adsorption sites is equivalent and each specific site can be occupied only by one adsorbate.
- There is no interaction between adsorbates. All adsorption sites have equal affinity for adsorbates.
- Once the adsorbate is localized, no migration of the adsorbate exists on the surface.
- The enthalpy of adsorption is independent on the coverage of the surface.

Hence, the Langmuir isotherm model describes an ideal homogeneous adsorption regarding one monolayer.

2.3 Adsorption structures of surfactants at solid-liquid interfaces via AFM

Surfactant molecules often form micelles in solution above the CMC. Depending on the structure of surfactants and the properties of solvents, the aggregate structure of micelles can be spherical, cylindrical and lamellar. Unlike in the bulk phase, where the self-assembly of surfactants is mainly driven by the hydrophobic interaction between surfactants,[37(p. 376)] the aggregation at solid-liquid interfaces is also greatly influenced by the surfactant-substrate interaction[7,41,42]. At a solid-liquid interface, the surfactant aggregate structure may differ from that in the bulk phase. One of the most advanced approaches to investigate the aggregate structure of surfactants at solid-liquid interfaces is the atomic force microscopy (AFM), which can provide information of the morphology of aggregates adsorbed and evaluate the mechanical properties of adsorbates. In the last few years, a range of AFM studies of surfactant aggregates adsorbed at solid-liquid interfaces are reported.[7–10,41–44]

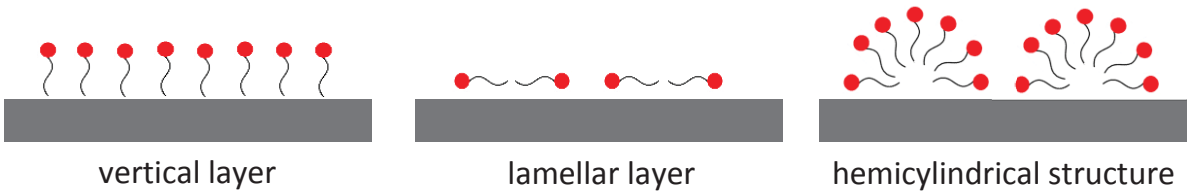

Figure 2-2 Schematic structures of possible surfactant aggregates at the solid-liquid interface.[41,43] The hydrophilic headgroup is marked in red and the hydrophobic tail is referred to as a black line. The substrate presented here is related to a hydrophobic surface.

Figure 2-2 shows three possible aggregate structures of adsorbed surfactants at solid-liquid interfaces, which can be demonstrated by AFM studies. In terms of a hydrophobic surface as shown here, all the aggregate structures benefit reduction of the water-solid interfacial free energy by minimization of the contact between water molecules and the hydrophobic surface[41]. It is found that the aggregate structure of ethylene oxide surfactants (C_iE_j) is affected by the alkyl-chain length, the polyoxyethylene number and the hydrophobicity of substrate.[45,42,41] Some of these nonionic surfactants form globular micelles on hydrophilic silica. On hydrophobic silica a range of C_iE_j surfactants present a continuous adsorption structure, where surfactant molecules may be out of the substrate plane (the left in Fig. 2-2) or parallel to it (the middle in Fig. 2-2). Surfactants with short hydrocarbon chains favor to form a vertical layer on hydrophobic surfaces; however, surfactants with long hydrocarbon chains may adsorb flat due to the strong hydrophobic interaction between the tail and the surface. In both cases, the aggregate structure shows a homogeneous adsorbed layer in AFM images.

Some surfactants adsorbed on graphite form the hemicylindrical structure (the right in Fig. 2-2), which was firstly suggested by Wanless et al.[7] for the structure of sodium dodecyl sulfate (SDS) adsorbed on graphite. This structure is considered to be induced by surfactant-substrate interaction and driven by the aggregate structure of surfactants in the bulk phase.[8,41] The hemicylindrical structure appears as long parallel periodic stripes in AFM images. The periodicities of the hemicylindrical structures of a wide variety of ionic and nonionic surfactants are determined by AFM. It is found that the periodicity of surfactant aggregates adsorbed is not very dependent on the headgroups rather than the hydrophobic chains.[8] This further confirms that the initial adsorption on graphite is due to the hydrophobic interaction between the hydrocarbon chain and graphite. The model for the adsorption of hydrocarbons on graphite was presented by A. J. Groszek[46], where the preferentially horizontal adsorption of long alkyl chains is attributed to the specific honeycomb lattice of graphite. The formation of

hemicylindrical structures for surfactants is therefore a very characteristic preference for the graphite surface.

2.4 Methods

2.4.1 Ultraviolet-visible (UV-Vis) spectroscopy

Absorption

Radiation in the ultraviolet (200−400 nm) and visible (400−800 nm) range of electromagnetic spectrum can cause electronic transitions.[47(p. 8)] The ultraviolet and visible light can be absorbed by molecules due to the interaction between the light and molecules, which results in electronic transitions of electrons of the molecule from lower (ground state) to higher (excited state) energy levels. The larger the energy gap is, the higher energy will be required for the electronic excitation.

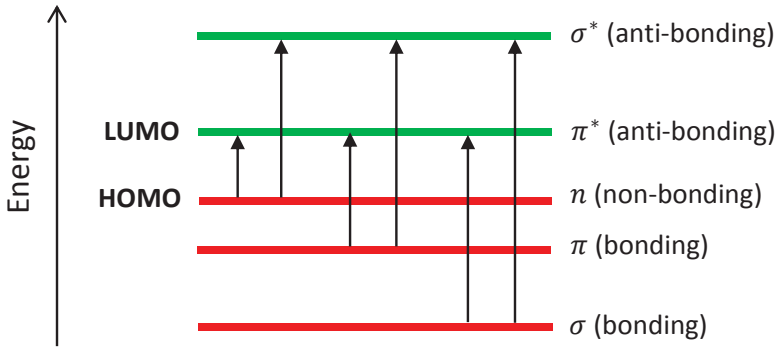

Figure 2-3 Simplified molecular orbitals (MOs) and possible electronic transitions by absorption of light. A molecular orbital consists of occupied (bonding and non-bonding) and unoccupied (anti-bonding) orbitals. After absorption of light, electrons can be excited from the lower to higher energy level. HOMO stands for the highest occupied molecular orbital and LUMO for the lowest unoccupied molecular orbital. The energy of light in the UV-Vis range (200−800 nm) can only cause an electronic excitation corresponding to low energy gaps, like the $n \rightarrow \pi^*$ or $\pi \rightarrow \pi^*$ transition.

Figure 2-3 shows the molecular orbitals (MOs) with possible electronic transitions. Molecular orbitals consist of occupied (bonding σ- and π-, non-bonding n-) and unoccupied (anti-bonding σ^*- and π^*-) orbitals. An electron can undergo a transition from the highest occupied molecular orbital (HOMO) to the lowest unoccupied molecular orbital (LUMO), when the energy of the absorbed wavelength equals the HOMO-LUMO energy gap. The energy of light in the UV-Vis range (200−800 nm) can only cause an electronic excitation corresponding to low energy gaps, such as the $n \rightarrow \pi^*$ or $\pi \rightarrow \pi^*$ transition.[48] Hence, molecules with conjugated π-systems, i.e. alternating single and double bonds, are of great interest for the studies by UV-Vis

spectroscopy. Parts of these molecules, which absorb light in the visible range, are also called chromophores, the HOMO-LUMO energy gap of which decreases with increasing double bonds.[48]

A spectrum band can be further explained by taking the vibrational states into account. During an electronic transition the molecule is able to move to a new vibrational level. Under the Franck-Condon principle, because the electronic excitation (ca. 10^{-15} s) is much quicker than the nuclear vibration (ca. 10^{-13} s), the motion of nuclei is neglected analogous to the Born-Oppenheimer approximation.[49,50] In Figure 2-4 the electronic vibrational states of the ground state (S_0) and of the first excited state (S_1) are shown. Due to the absorption of a photon, a molecule can be transferred from the lowest vibrational energy level of the ground state S_0 (ν=0) to different vibrational energy levels of the excited state S_1 (ν'=0, 1, 2, 3, ⋯).

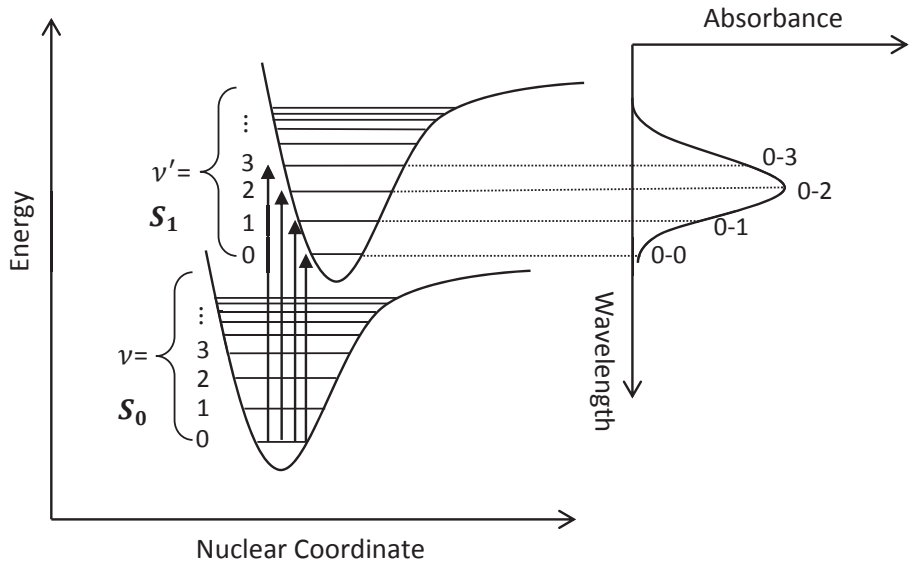

Figure 2-4 Explanation of spectral band according to the Franck-Condon principle, drawn based on the reference[28]. Taking the vibrational states into account, the molecule is able to move to a new vibrational level during an electron transition. Due to the absorption of a photon, a molecule can be transferred from the lowest vibrational energy level of the ground state S_0 (ν=0) to different vibrational energy levels of the excited state S_1 (ν'=0, 1, 2, 3, ⋯). The intensity (probability) of a vibronic transition is related to the absorbance in an absorption spectrum, corresponding to a certain wavelength (energy).

According to the Franck-Condon principle, the intensity (probability) of a vibronic transition is proportional to the square of the overlap integral between the vibrational wavefunctions of two involved states.[51] The intensity will be consequently represented as the absorbance in an absorption spectrum. For instance, as can be seen in Figure 2-4 the 0-2 vibrational transition is

the most favored transition corresponding to the maximal absorbance (the spectrum peak) and a certain wavelength (energy) in the spectrum.

A shift of the spectral band in the absorption spectrum to a larger wavelength (lower frequency/energy) is called bathochromic shift, and vice versa, a shift to a smaller wavelength (higher frequency/energy) is hypsochromic shift.[52] The spectral shift of dyes in solution can be caused by the change in chemical structure like tautomeric forms and/or solvatochromism.[23] The shift of solvatochromic compounds is affected by the polarity of solvent and solute as well as hydrogen bonding for complexation.[53,54] Thus, in a multicomponent system the spectral shift is considered complex, where the interaction between different solutes and the interaction between solute and solvent are characteristic for the system.

The Lambert-Beer law

If a monochromatic light passes through a light-absorbing substance, the light may be simultaneously transmitted, reflected, scattered and absorbed. As a result, the intensity of light will be decreased. According to the Lambert-Beer law[55(p. 3)], the attenuation of light is influenced by the substance and the pathlength of light. The intensity decreases exponentially through a sample:

$$I = I_0 \cdot e^{-\alpha x c} \tag{2-14}$$

where I_0 is the intensity of the incident light and I is the intensity of the transmitted light. c is the concentration of the sample in mol/L and x is the thickness of the sample (pathlength) in cm. α is a factor, which is dependent on the sample property and the wavelength of light. Equation 2-14 is usually expressed by a more common equation as follows:

$$A(\lambda) = \log\frac{I_0}{I} = \varepsilon(\lambda) \cdot x \cdot c \tag{2-15}$$

A is defined as the absorbance of the wavelength λ and ε is the molar decadic extinction coefficient ($\varepsilon = 0.43\alpha$ $M^{-1}\cdot cm^{-1}$). Because ε is a characteristic quantity of substance, it can be determined by the plot of the absorbance versus the concentration, i.e. the calibration graph, in turn, the concentration of sample can also be determined by the measured absorbance value.

The Lambert-Beer law can only be applied under certain conditions:[48]

- The incident light muss be monochromatic and parallel.

- The sample muss be homogeneous in the measured volume.
- The concentration of solution should be low in order to minimize the intermolecular interaction.
- The possible scattering and reflection of light are neglected.

2.4.2 Dynamic light scattering (DLS)

Dynamic light scattering (DLS), also known as quasi-elastic light scattering or photon correlation spectroscopy,[56] is a classical technique used to measure the size of particles in solution. When a light beam illuminates a suspension, which is composed of dispersed particles, the light will be scattered in all directions. The intensity of scattered light can be detected and measured to obtain the information of particles. Because of the Brownian motion[57(p. 17-18)] of particles in solution, which is the random movement of particles due to the collision of molecules with the surrounding molecules, the scattered intensity fluctuates over time. The interference of the scattered light will be either constructive or destructive. If the particles are small, which move faster, the intensity fluctuation is rapid and vice versa.[58(p. 21-29)] Therefore, the intensity fluctuation is related to the particle size.

In practice, the intensity autocorrelation function (second-order correlation function) $g_2(\tau)$ is analyzed, which is an integral over the product of intensities at the time t and the delayed time t+τ:[59,60(p. 135-136)]

$$g_2(\tau) = \frac{1}{\tau}\int_0^{\tau} I(t)I(t+\tau)dt \tag{2-16}$$

In a light scattering experiment, the second-order autocorrelation can be determined from the electric field correlation function (first-order correlation function) $g_1(\tau)$. The relationship between $g_1(\tau)$ and $g_2(\tau)$ can be expressed with the equation[61]

$$g_2(\tau) = 1 + \beta|g_1(\tau)|^2 \tag{2-17}$$

where β is the coherence factor, which depends on the uncorrelated scattering from the apparatus, solvent, contaminant and others.

For monodisperse particles, $g_1(\tau)$ is a single exponential decay with a certain decay constant, which is related to the translational diffusion coefficient. Hence, the $g_2(\tau)$ is simplified as follows:[61]

$$g_2(\tau) = 1 + \beta e^{-2D_t q^2 \tau} \tag{2-18}$$

q is the magnitude of scattering vector. D_t is the translational diffusion coefficient.

According to the Stokes-Einstein[60(p. 139)] equation, the hydrodynamic radius R_h can be calculated:

$$R_h = \frac{k_B T}{6\pi\eta D_t} \tag{2-19}$$

k_B is the Boltzmann constant ($1.38 \cdot 10^{-23}$ J·K^{-1}), T is the absolute temperature and η is the viscosity of the solution medium.

There are different methods[61] used in commercial equipments to analyze the autocorrelation function, for instance, the cumulant method, the exponential sampling method (Pike-Ostrowsky) and constrained regularization (CONTIN) by Provencher.

The cumulant method[62] is widely used to analyze a Gaussian-like distribution. In real measurements, the particles are not perfect uniform. The size of particles is usually in a size range regarding a size distribution. So for polydisperse particles $g_1(q,\tau)$ can be described as an intensity-weighted integral over a distribution of decay rate $G_i(\Gamma_i)$ corresponding to each of the species:[56]

$$g_1(q,\tau) = \sum_{i=1}^{n} G_i(\Gamma_i)\exp(-\Gamma_i \tau) = \int G(\Gamma)\exp(-\Gamma\tau)d\Gamma \tag{2-20}$$

Expanding this equation above, it can be rewritten as:[56,60]

$$g_1(q,\tau) = \exp\left\{-\bar{\Gamma}(\tau - \frac{k_2}{2!}\tau^2 + \frac{k_3}{3!}\tau^3 - \frac{k_4}{4!}\tau^4 \cdots)\right\} \tag{2-21}$$

k_2, k_3 and k_4 are the variance, skewness and kurtosis of distribution respectively for a Gaussian distribution. $\bar{\Gamma}$ is the average decay rate constant, which refers to a z-averaged translational

diffusion coefficient D_z. The z-averaged hydrodynamic radius $R_{h,z}$ is therefore defined as follows:

$$R_{h,z} = \frac{k_B T}{6\pi\eta D_z} \tag{2-22}$$

The polydispersity index (PDI) can be derived from Equation 2-21:[62]

$$PDI = \frac{k_2}{\bar{\Gamma}^2} \tag{2-23}$$

A PDI value smaller than 0.05 indicates a highly monodisperse sample. The value greater than 0.7 implies a very broad size distribution. The PDI value in the range of 0.05−0.7 is considered to be suitable for the operation of distribution algorithms in DLS technique.[63]

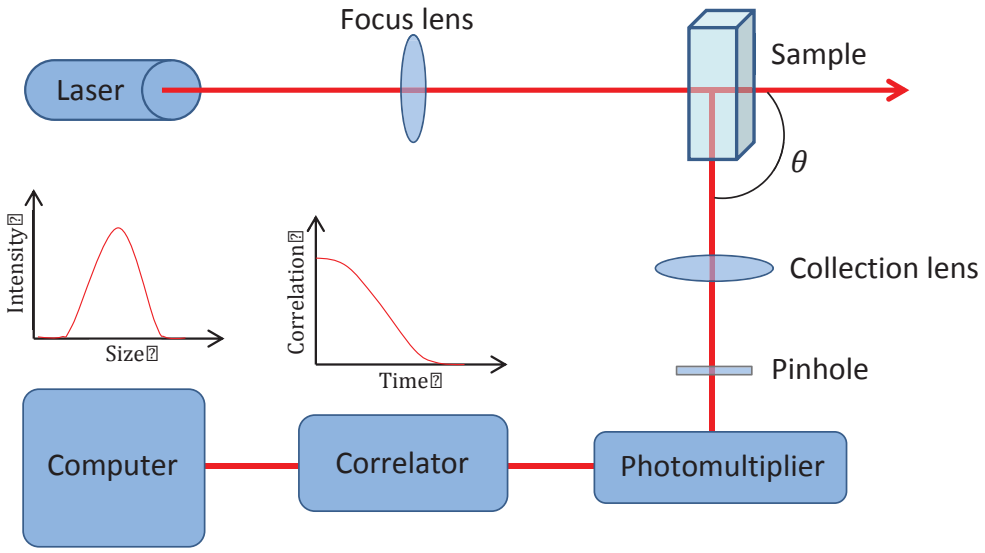

Figure 2-5 A typical DLS instrument, redrawn from the reference[60(p. 146)]. A light source generated from the laser is focused by a lens and illuminates the sample within a cell. The scattered light with a particular angle is selected by a pinhole and passes a photomultiplier to obtain a single electrical pulse for each photon detected. The change in the intensity of scattered light is recorded by a correlator deriving an autocorrelation function with respect to the time, which gives the information of particles, like a size distribution.

The main components of a typical DLS instrument are illustrated in Figure 2-5. A laser is used to generate light source. The light source is focused by a lens and illuminates the sample within a cell. The light is scattered theoretically in all directions. The scattered light can be collected by a lens, which is placed with a particular angle θ to the laser beam passing straight through the sample. The collected light is selected by a pinhole and passes a photomultiplier to obtain a

single electrical pulse for each photon detected. The intensity signal of scattered light is transmitted to a correlator. The correlator records the change in the intensity with respect to the time and derives an autocorrelation function. The autocorrelation function is analyzed by a computer, which gives the information of particles, like a size distribution.

2.4.3 Wilhelmy plate method

The Wilhelmy plate method is a widely used method to determine the surface or interfacial tension at an air-liquid or a liquid-liquid interface, which was firstly applied by Ludwig Wilhelmy[64]. In this method, a thin plate is suspended perpendicular to a liquid surface and coupled with a sensitive electrobalance (Fig. 2-6). The plate is vertically lowered and immersed into a liquid at a constant depth. In this way, a liquid lamella is formed around the perimeter of the plate. The forces causing imbalance are the weight of the plate, the tensile force and the buoyancy force generated by the liquid. The plates used in this method are usually made of platinum, platinum/iridium, glass, steel or plastic materials.[38] The weight of the plate is therefore known. Because the density of measured liquid is given, the buoyancy force can be calculated. In practice, the electrobalance is zeroed before measuring, so that the term concerning the weight of the plate and the buoyancy are eliminated by weighing systems.

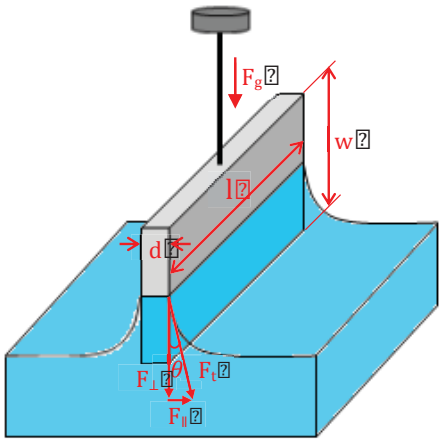

Figure 2-6 Surface tension determination by the Wilhelmy plate method, redrawn with reference to the analog[65]. A plate with the length l, width w and thickness d is immersed in a liquid. A liquid lamella with a contact angle θ is formed. The gravitational force F_g of the lamella can be converted to the surface tension of the interface.

As shown in Figure 2-6, the tensile force F_t can be divided into a force parallel ($F_\parallel$) and perpendicular ($F_\perp$) to the liquid surface, which are expressed by the following equations:

$$F_{\parallel} = F_t \cdot \sin\theta \tag{2-24}$$

$$F_{\perp} = F_t \cdot \cos\theta \tag{2-25}$$

θ is the contact angle formed by the meniscus, as indicated in Figure 2-6. Additionally, the perpendicular part of the tensile force ($F_{\perp}$) is equal to the gravitational force F_g measured by the weighing system,

$$F_g = F_{\perp} \tag{2-26}$$

According to the Wilhelmy equation[38(p. 239)], the surface tension γ is defined as the tensile force F_t per length of contact line (the perimeter of the plate contacting with the liquid):

$$\gamma = \frac{F_t}{2l + 2d} \tag{2-27}$$

l is the length of the plate and d the thickness of the plate. Consequently, Equation 2-27 can be rewritten as follows:

$$\gamma = \frac{F_g}{(2l + 2d) \cdot \cos\theta} \tag{2-28}$$

If the plate is completely wetted (θ = 0), the gravitational force F_g of the lamella is equal to the tensile force F_t. An alternative method[38(p. 240-241)] for completely wetting materials is to bring the plate into the liquid. The plate is then pulled back, detaching the liquid surface. The pull-off force is noted as the capillary force, which can be compared with the ring method.

The interfacial tension of two immiscible liquids can also be determined by the Wilhelmy plate method.[38(p. 241-242)] In this case, the gravitational force in Equation 2-28 refers to the measured force, when the plate is kept at the interface of the two different phases. The plate is submerged in the light phase and the balance is now tared. Afterwards the plate is submerged in the heavy phase, on top of which the light phase is filled carefully. The plate is placed back to the interfacial position. The interfacial tension can be calculated by the measured force corresponding to the gravitational force of the interfacial lamella (Equation 2-28).

2.4.4 Atomic force microscopy (AFM)

Atomic force microscopy (AFM) or scanning force microscopy (SFM) is a type of scanning probe microscopy (SPM) developed by Binnig et al.[35(p. 77)] in 1986. Similar to the scanning tunneling microscopy (STM), an AFM uses a force sensor to image the surface. Hence, AFM can be used to study conducting as well as non-conducting surfaces with demonstrated resolution on the order of fractions of nanometers.

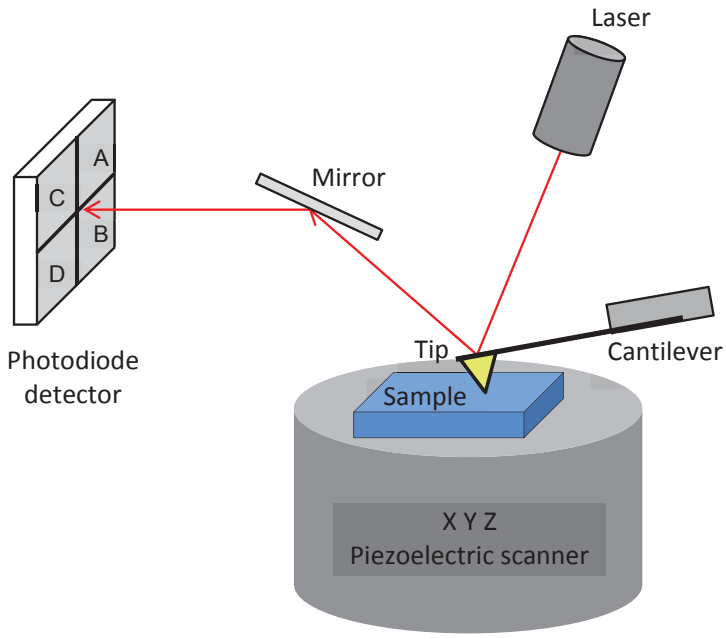

Figure 2-7 Setup of an AFM based on the beam deflection technique, redrawn from the reference[35(p. 79)]. When the tip is brought near a sample surface, forces between the tip and sample cause the cantilever to bend. The deflection of the cantilever can be detected by a position-sensitive detector and converted to electrical signals to form a topographic image.

Figure 2-7 shows a typical AFM apparatus, which is based on the beam deflection technique. A sharp tip is mounted at the end of a cantilever. When the tip is brought near a sample surface, forces between the tip and the sample cause the cantilever to bend. The deflection of the cantilever can be detected by reflection of a laser beam back off the cantilever.[35(p. 77)] A position-sensitive detector records the deflection of the cantilever and this motion will be converted to electrical signals to form a topographic image. The four-sectional photodetector allows measuring not only vertical but also lateral deflection of the cantilever.

AFM cantilevers are usually made of silicon or silicon nitride, which have two common shapes: rectangular and V-shaped. The back face of cantilever is usually coated with a metallic thin layer (often gold) in order to enhance the reflectivity. The most common methods used to

measure the cantilever deflection are the optical lever method[66] (see Fig. 2-7), the interferometric method and the electronic tunneling method. Most AFMs use a sample-moving or probe-moving scanner to control the position very accurately during imaging. The scanner is mostly made of piezoelectric materials. The piezoelectric drive moves the probe or sample in different dimensions, so that the tip can scan across a sample surface. An AFM image is a simulated image based on the height of each point of the surface. This topographic image reflects the geographical shape of the surface but not the exact real morphology of the surface.

Depending on the way of scanning and on the signals recorded, the imaging by AFM can be operated mainly in three modes[35(p. 79-80)]: noncontact, Tapping and contact mode.

- Noncontact mode. In noncontact mode, the piezoelectric drive makes the cantilever oscillate at a resonant or near-resonant frequency. The oscillation will be decreased due to the attractive interaction between the tip and the sample. The changes in frequency, amplitude and phase of the oscillation are measured to produce a topographical image of the surface. By noncontact mode the tip and sample suffer from less degradation or damage. However, the long-range interaction may lower the resolution. Because the tip may be either out of range of the van der Waals interaction or trapped in a thick adsorbed fluid layer.
- Tapping mode. In Tapping mode, the cantilever oscillates at a frequency near its resonance frequency. If the tip gets close to the sample, the tip touches the sample at the bottom of the cantilever oscillation. Because the tip "taps" the sample surface and less friction can be caused by the tip during imaging, Tapping mode is mostly used for soft materials or in liquid.
- Contact mode. In contact mode, the tip keeps a physical contact with the sample. During scanning the cantilever deflection is maintained constant. The value of deflection, i.e. the set point, is set through a feedback circuitry. In order to keep the deflection constant, the tip-sample distance must be adjusted during imaging. The change in piezo elongation is then converted to the topography of sample. Contact mode can provide high resolution, but the strong lateral forces (friction) may damage the sample or distort the sample feature.

Since AFM applies the force between the tip and sample, it is necessary to note the possible interactions between them. The interactions may arise from the electrostatic force, the van der Waals force, the chemical bonding and repulsive forces in short-ranges.[67] The interaction forces can be attractive or repulsive, depending on the tip-sample separation. In order to give a simplified expression of the complex interactions, the Lenard-Jones force law is used here[68(p. 30)]

$$F = 12\frac{C_1}{r^{13}} - 6\frac{C_2}{r^7} \tag{2-29}$$

C_1 and C_2 are constants depending on the tip and sample. r is the tip-sample distance.

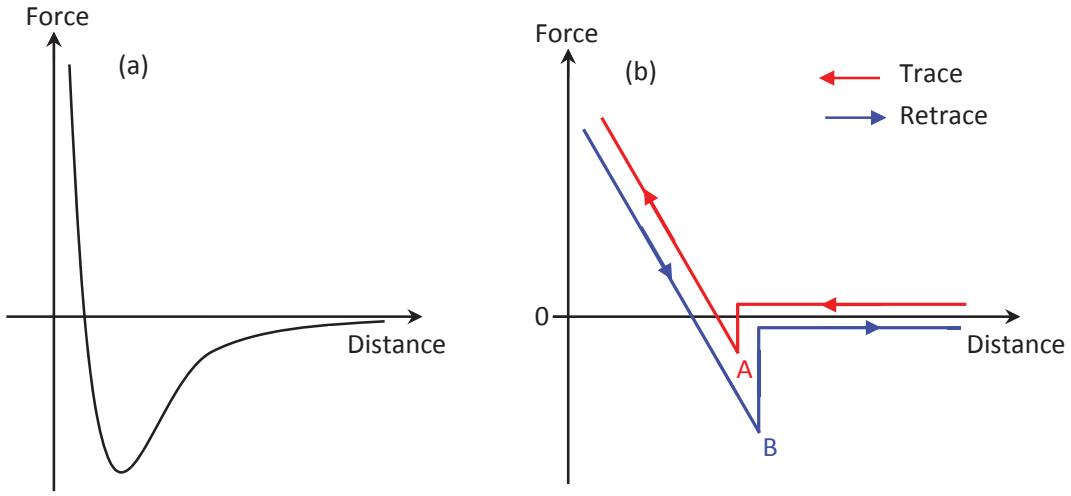

Figure 2-8 (a) Lenard-Jones force and (b) force-distance (F-D) curves in AFM. As the tip and the sample get gradually closer to each other, there is a weak attractive interaction between them. This electrostatic attraction (negative part) increases until the electrostatic repulsion occurs due to repelling of their electrons, which progressively complements the attractive force. With further decrease of their separation, the total force is dominated by the repulsive force corresponding to the positive part.

The graphical representation of Lenard-Jones law is shown in Figure 2-8 (a). As the tip and the sample get gradually closer to each other, there is a weak attractive interaction between them. This electrostatic attraction (negative part) increases with decreasing tip-sample distance until the electrostatic repulsion occurs due to repelling of their electrons, which progressively complements the attractive force. With further decrease of the distance, the total force is dominated by the repulsive force corresponding to the positive part presented in force-distance curves.

Figure 2-8 (b) shows typical force-distance (F-D) curves required by AFM. Force-distance curves are recorded by approaching the tip to the sample (red curve) and withdrawing it from the sample (blue curve). Therefore, an F-D measurement gives an approach and a retraction curve, which both can be composed of three regions: the zero line, the discontinuity and the contact region.[69(p. 5-9)] The zero line indicates that the tip is far from the sample, where no tip-sample interaction force is detected. The discontinuity region is characterized by the point jump-to contact (point A) in the approach curve and the point jump-off contact (point B) in the retraction curve. During approach if the attractive force between tip and sample exceeds the

elastic force of cantilever, the tip snaps onto the sample. Conversely, during withdrawal if the elastic force overcomes the adhesive force, the tip is detached from the contact region.

In the contact region, the tip is in physical contact with the sample. If the cantilever used is ideal elastic, the interaction force between the tip and sample is proportional to the deflection of the cantilever. The force F can be calculated by Hooke's law:[70]

$$F = -k_c \cdot \delta_c \tag{2-30}$$

k_c is the spring constant of cantilever and δ_c the cantilever deflection. Because the distance in a F-D curve is contributed by the deflection of the cantilever and the deformation of the sample,[70] the slope of the contact line is actually considered as a spring constant of the system investigated, thus, implying the stiffness of the sample.

As mentioned before, images obtained by AFM present the topography of the specimen surface. The structure in the topographic images can be very much affected by the geometry and characteristic of the used tip as well as the sample studied, resulting in reconstruction or distortion of the sample. Two major effects occurred in AFM images are the overestimation of lateral dimensions and the underestimation of vertical dimensions.[71] If the geometry of the tip and the sample is known, the dimension of the sample shown in AFM images can be corrected to derive the true structure of the sample. Figure 2-9 gives an example how the lateral dimension of a sample is broadened in the sample profile recorded by AFM.

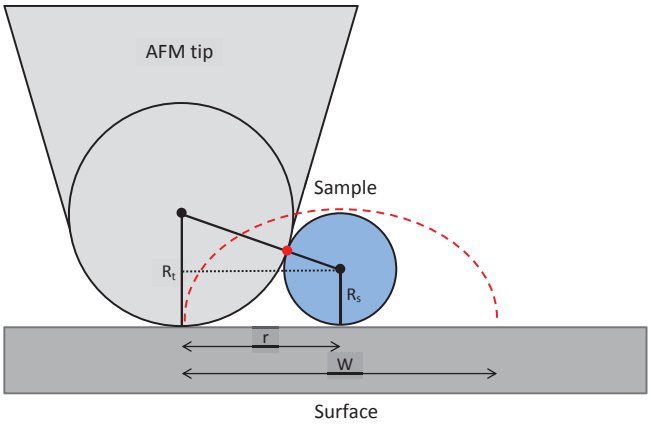

Figure 2-9 Schematic representation[72,73] of an AFM tip with a curvature radius of R_t and a spherical sample with a radius of R_s on surface, $R_t > R_s$. The red point refers to the first contact point between the tip and sample. The red dashed curve indicates the sample profile recorded in the AFM topographic image. The width of the sample profile W is the recorded lateral dimension of the sample in AFM images.

Here, the tip of AFM has a circle shape at the front with the curvature radius of R_t (tip radius) and the sample is simplified as a sphere with the radius of R_s. The first contact point between the tip and sample is marked in red, where two surfaces are tangent. During scanning, the tip moves across the sample reducing a sample profile with a broadened sample diameter in the AFM image, indicated as the red dashed curve. The width of the sample in image profile can be measured and the tip radius is known. Hence, the sample radius can be determined by the geometrical relation as follows:

$$r^2 + (R_t - R_s)^2 = (R_t + R_s)^2 \tag{2-31}$$

$$r = \frac{W}{2} \tag{2-32}$$

The radius of sample R_s can be calculated by the equation:

$$R_s = \frac{W^2}{16R_t} \tag{2-33}$$

W is the width (lateral dimension) of the sample in the AFM image profile and R_t the tip radius.

In the AFM studies presented, in cases where the adsorption structures are featureless or have no regular form, the roughness of surface is described by the area roughness parameter S_a and S_q given by the software XEI (Park Systems) of the used AFM, which are defined under the standard DIN EN ISO 25178-2[74] as follows:

$$S_a = \frac{1}{A}\iint_A |z(x,y)|dxdy \tag{2-34}$$

$$S_q = \sqrt{\frac{1}{A}\iint_A |z^2(x,y)|dxdy} \tag{2-35}$$

S_a: the arithmetic mean height of the surface.
S_q: the root mean square height of the surface.
z (x, y): the height of the surface along the z-axis relative to the fitting x-y plane.

3 Experimental

3.1 Substances

Substances used in this work are displayed in Table 3-1, where chemical structures and details of the used substances are shown.

Table 3-1 Substances used in this work.

Substance	Structure	Information
Acid blue 113	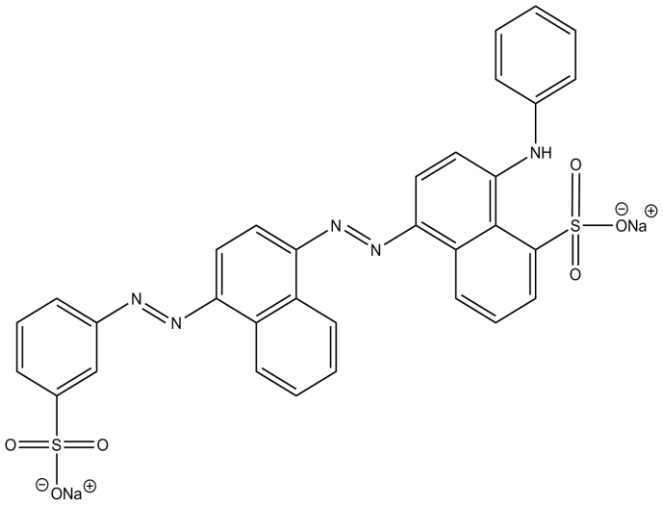	682 g/mol 50% Sigma-Aldrich
$C_{12\text{-}18}E_7$ (alkyl heptaglycolether)	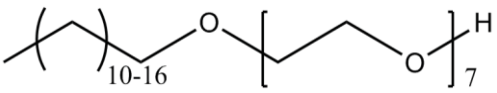	494 g/mol C_{12}: 48% C_{14}: 17% $\geq C_{16}$: 11% Dehydol LT 7 BASF
SDS (sodium dodecyl sulfate)	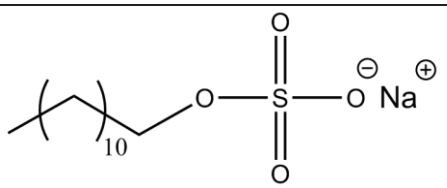	288 g/mol ≥99% Sigma-Aldrich
PVPVI (copolymer of vinylimidazole and vinylpyrrolidone)	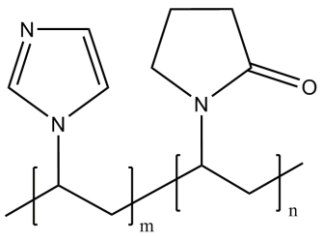	70000 g/mol 30% Sokalan HP 56K BASF

PA fiber (fabric)	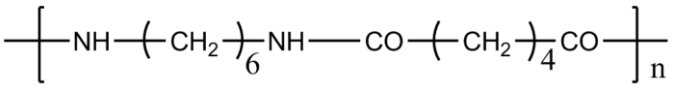	EMPA 406 Swissatest Testmaterialien
PA 66 granule	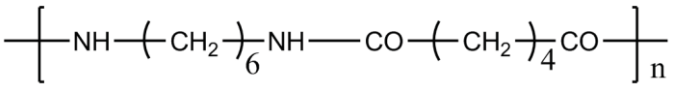	Sigma-Aldrich
Formic acid	CH_2O_2	98%−100% Merck
Acetic acid	CH_3COOH	25% and 100% Roth

In this work, the polyamide dye Acid blue 113, which is soluble in water, was applied. A water-soluble vinylpyrrolidone-vinylimidazole copolymer (PVPVI) was chosen as the DTI polymer. Two types of surfactants, the anionic surfactant sodium dodecyl sulfate (SDS) and the nonionic surfactant alkyl heptaglycolether ($C_{12\text{-}18}E_7$), were used. The used $C_{12\text{-}18}E_7$ is a technical polyoxyethylene-based surfactant containing different alkyl chains of C_{12} − C_{18} and polyoxyethylene chains of E_1−E_{20}.

Reagents as received were dissolved in deionized water without further purification. The used water has normally a specific conductivity not exceeding 0.065 μS/cm. The apparatus for water is named Astacus Bioscience from the firm MEMBRAPURE (Germany).

3.2 Methods

3.2.1 UV-Vis spectroscopy

UV-Vis spectroscopy was applied to quantify the interaction between dye, surfactant and polymer in solution. UV-Vis spectra were recorded using a spectrophotometer Evolution 220 supplied by Thermo Scientific. PMMA cells with a path length of 1 cm were used for detection of absorbance values. The solutions were measured at room temperature (23−25 °C) and the absorption spectra were recorded at the wavelength from 400 nm to 800 nm.

The purchased dye powder was dissolved in water under stirring for 16 − 17 h. For two-component systems, varied amounts of nonionic surfactant or polymer were added into the aqueous dye solution to obtain a stock solution. The stock solution was stirred overnight at

room temperature. The stock solution was then diluted with the prepared dye solution to get mixtures containing surfactant or polymer of various concentrations. For the mixture of the anionic surfactant and the dye, the anionic surfactant of different amounts was directly added into the aqueous dye solution to get the mixture with certain surfactant concentrations. For three-component systems, the dye-polymer solution was stirred for 24 h. Different amounts of the anionic surfactant were directly added into the dye-polymer solution. For nonionic surfactants a stock solution was prepared and diluted to obtain solutions with different surfactant concentrations. The two-component mixtures were equilibrated at room temperature for 5−7 h and the three-component mixtures for 24 h before UV-Vis measurements. The results of UV-Vis spectroscopic studies presented are an average of duplicates of two independent measurements.

3.2.2 Dynamic light scattering (DLS)

The DLS experiments were carried out using a Zetasizer nano-Zs (Malvern Instruments Ltd., UK). The incident beam is generated by a He-Ne laser with the wavelength of 633 nm. The scattering angle was 173°. The size range of particle size analyzer is 0.3 nm to 10 μm. The measurements were performed at room temperature and the data were analyzed with the Zetasizer software. The size (diameter) is calculated by the cumulant method.

One of the most important parameters from DLS analysis is the Z-average. Z-average is a calculated hydrodynamic diameter ($D_{h,z}$) by the method of cumulant, It is determined from the intensity-weighted size distribution. If there is only one peak in the distribution (monodisperse sample), Z-average provides a reliable size of particle. However, for polydisperse samples, whereas the distribution may show more than one peak, the peak size $D_{h,i}$ (i=1, 2, ...) will be preferred to describe the particle size. The peak size presented here is a statistical mean size from the mean intensity of single peak, which is considered as the respective component in solutions.

For one-component systems, the dye, surfactant or polymer was added into water to obtain the stock solution. For the mixture of surfactant and polymer, the stock solution was prepared by dissolving surfactants in the aqueous polymer solution of certain polymer concentration. For the mixture of the dye with surfactant or polymer, the stock solution was prepared by dissolving surfactant or polymer in the aqueous dye solution of certain dye concentration. All stock solutions were stirred overnight. The dilute solutions were equilibrated at room temperature for about 5 h before DLS measurements. The solutions were filtered by 0.45 μm PTFE filters and

filled into PMMA cuvettes for studies. The results of DLS studies presented are an average of duplicates of two independent measurements.

3.2.3 Wilhelmy plate method

Surface tension was measured with a DCAT 21 (Dataphysics) tensiometer using the Wilhelmy plate method. Measurements for single components were performed in triplicate independently at room temperature and the average value was taken. The critical micelle concentration (CMC) of surfactants was determined with the software DCATS 33 by plotting of the surface tension against the log concentration of surfactant. The minimum of surface tension was also evaluated according to the surface tension curve.

Single components were dissolved in water forming stock solutions for measurements. The concentration of stock solution for SDS, $C_{12\text{-}18}E_7$, PVPVI and Acid blue 113 was 100 mM, 1 mM, 1 mM and 0.05 g/L respectively. Surfactant stock solutions were stirred at room temperature for 3 h and the polymer or dye stock solution for 16 h. The stock solution for the surfactant-polymer system was prepared by directly dissolving surfactants in a very dilute polymer solution, which has stood for 7−8 h. The surfactant-polymer stock solution was stirred for 15−16 h. Before surface tension measurements, the one-component solution was stirred for 30 s at each concentration (data point) and equilibrated for 60 s. Nevertheless, the surfactant-polymer mixture was stirred for 10 s and left for 10 min before measurements.

3.2.4 Atomic force microscopy (AFM)

The used AFM was the mode XE7 from Park Systems (South Korea). Besides the passive vibration isolation supplied by the firm, a homemade acoustic enclosure was built up in order to further improve the resolution of the AFM. The acoustic enclosure is composed of a welded steel base frame (table) and an acoustic box fixed on the table. The acoustic box is made by thick (~50 mm) polyamide plates, which is entirely covered by Styrofoam. The home-built acoustic enclosure reduced the disturbance of environmental noise from mechanical vibration, acoustic vibration and ambient light.

A graphite plate and polyamide fiber or polyamide film served as model surfaces for AFM studies. Imaging at solid-liquid interfaces was performed by contact mode and imaging in air by noncontact or Tapping mode. The specifications of the cantilevers and substrates applied in AFM studies are given in Table 3-2. All images captured are deflection images (topography)

with the feedback gain (Z Gain) not more than 1 and the scan rate of 1−2 Hz. The presented images were not further treated other than flattened by the software XEI (Park Systems).

Table 3-2 Specifications of cantilevers and substrates used in AFM studies.

	Material	Producer	Information
Cantilever	Si_3N_4 (Au-Cr reflex coating)	Olympus	Spring constant: 0.02 & 0.08 N/m Tip radius: 15 nm Contact mode
	Si (Al reflex coating)	Olympus	Spring constant: 26 N/m Tip radius: 7 nm Tapping mode
	Si (Al reflex coating)	Nanosensors	Spring constant: 42 N/m Tip radius: 7 nm Noncontact mode
Substrate (model surface)	HOPG (highly oriented pyrolytic graphite)	Momentive Performance Materials	Grade: ZYH Size: 12 × 12 × 2 mm
	Polyamide fiber	EMPA 406 Swissatest Testmaterialien	Diameter: 12−15 μm
	Polyamide film	Reproduced	Thickness: 500 μm

The graphite plate fixed at the bottom of a petri dish (PS) was freshly cleaved by using adhesive tapes before each experiment. For the study of polyamide (PA) fiber, single fiber of the purchased PA fabrics (EMPA 406, Swissatest Testmaterialien) was fixed on the magnetic disk using double-sided tapes. The reproduced PA films were fixed on the magnetic disk using double-sided tapes for imaging in air. For imaging in liquid, the films were fixed at the bottom of a petri dish (PS) with a 2-part epoxy adhesive (UHU).

All solutions in AFM studies were prepared in water and left overnight at room temperature. Prior to measurements, the solution of ~3 mL was filled into the petri dish with certain model surface. The tip was then immersed in the studied solution for 1 h before imaging was

performed to minimize the thermal drift. All measurements were conducted at the water-surface or solution-surface interface in the temperature range of 22−26 ℃.

3.2.5 Adsorption experiments

The adsorbent carbon black powder used (Printex L, Evonik) is composed of particles with an average size of 23 nm. The surface area measured by the Brunauer–Emmett–Teller (BET) method[75] is 150 m^2/g given by the supplier.

The stock solutions of dye alone and of dye dissolved in a certain surfactant solution were stirred overnight at room temperature. An amount of carbon black powder was added into the Erlenmeyer flask containing 50 mL dye solution of certain concentrations. The suspension was mixed with a magnetic stirrer (IKA RT15) at 300 rpm for 2 h. The samples were centrifuged using MULTIFUGE 3 SR (Heraeus) at 16000 rpm for 20 min. In some experiments the dye solution was filtered by 0.45 μm PTFE filters after reaction with carbon black prior to centrifugation. The concentration of dye remained in solution was determined by UV-Vis spectrophotometer as mentioned in Section 3.2.1. The results of adsorption isotherms presented are an average of duplicates of two independent measurements.

4 Results and discussion

In this chapter, the results obtained from different methods are presented and analyzed. The UV-Vis spectroscopic study reveals the interaction of the dye with additives (surfactant and DTI polymer) in solution, which is also verified and evaluated by analysis of particle size using DLS. In order to clarify the interaction between surfactant and polymer, the interaction between them at the air-solution interface is interpreted by surface tension measurements. To understand the mechanism of the dye adsorption and the influence of surfactant and DTI polymer on dye adsorption at solid-liquid interfaces, the adsorption of the dye is investigated on the nonpolar model surfaces carbon black and graphite. The adsorption of the dye on carbon black is quantified by the analysis of adsorption isotherms. Adsorption structures of the dye and binary mixtures on graphite are identified by AFM, providing a further understanding of the influence of surfactant and DTI polymer on the adsorption of dye on surfaces at a molecular level. In addition, as preparation for further studies on textile or textile-like surfaces, polyamide surfaces are characterized by AFM to give basic information about textile-like surfaces.

4.1 Interaction in solution studied by UV-Vis spectroscopy

4.1.1 Dye + Nonionic surfactant

It is to note that the absorbance in all UV-Vis spectra shown is about zero at the maximal measured wavelength of 800 nm. The spectrum of the anionic dye Acid blue 113 in aqueous solution has a maximal absorbance at the wavelength of 566 ± 1 nm (Fig. 4-1).

In mixture of the dye with the nonionic surfactant $C_{12\text{-}18}E_7$, the spectrum of dye shifts to the larger wavelength (bathochromic shift) from a $C_{12\text{-}18}E_7$ concentration of about 0.02 mM. From this point, the maximal absorbance A_{max} and the corresponding wavelength λ_{max} increase with increasing surfactant concentrations. At about 0.4 mM of $C_{12\text{-}18}E_7$ the A_{max} and λ_{max} reaches a maximum respectively.

In order to characterize the dye-surfactant interaction, the maximal absorbance value A_{max} and the corresponding wavelength λ_{max} of mixtures are plotted against the concentration of $C_{12\text{-}18}E_7$ (Fig. 4-2). A bathochromic shift of the dye spectrum starts near to the critical micelle concentration (CMC) of $C_{12\text{-}18}E_7$ (0.02 mM) and ends at the concentration of 0.4 mM. The A_{max} value has an increase at 0.04 mM of $C_{12\text{-}18}E_7$ and reaches the maximum at 0.3 mM. In mixture with $C_{12\text{-}18}E_7$ Acid blue 113 has a shift from 566 ± 1 nm to 600 ± 1 nm. The spectra of mixtures remained almost unchanged after more than 20 h (see Appendix, Fig. 1).

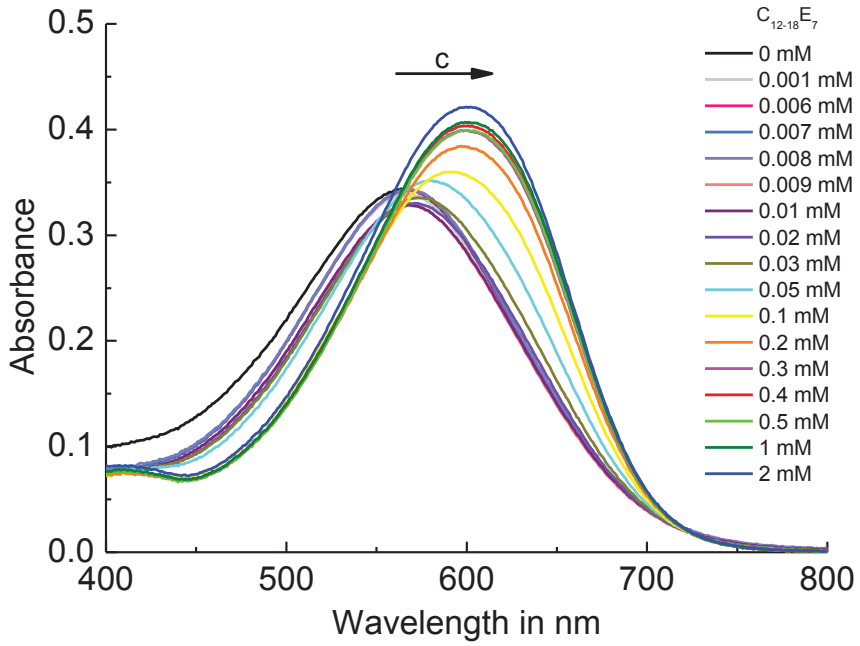

Figure 4-1 UV-Vis absorption spectra of mixtures of Acid blue 113 with $C_{12-18}E_7$ equilibrated for 5 h. The concentration of Acid blue 113 is 0.009 mM in all solutions and the concentration of $C_{12-18}E_7$ varies from 0 mM to 2 mM. From a $C_{12-18}E_7$ concentration of about 0.02 mM, the A_{max} and λ_{max} increase with increasing $C_{12-18}E_7$ concentrations and reach the maxima at about 0.4 mM of $C_{12-18}E_7$.

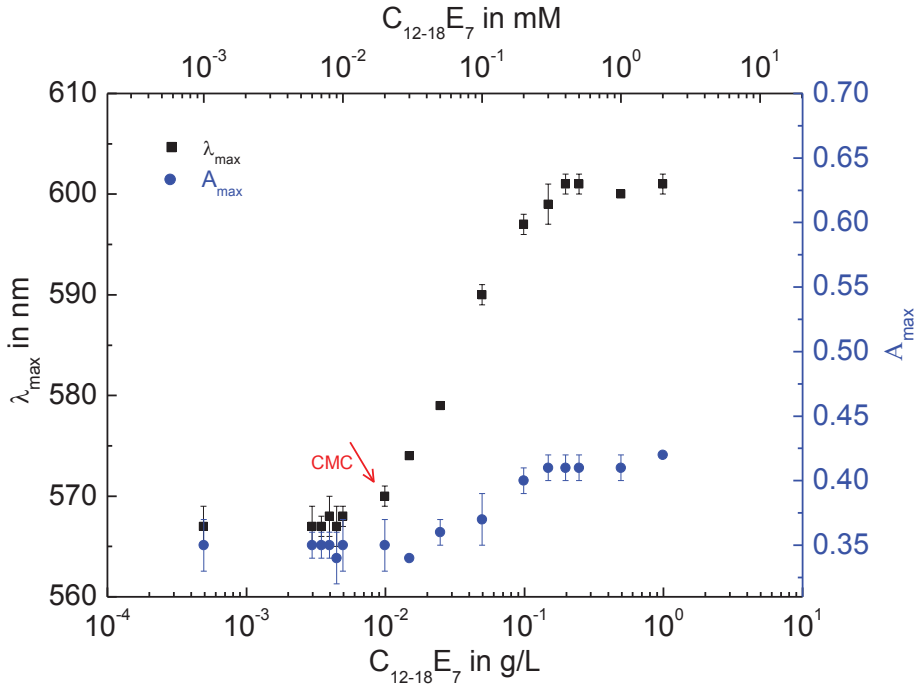

Figure 4-2 Plotting of the maximal absorbance values (A_{max}) and corresponding wavelengths (λ_{max}) of mixtures of Acid blue 113 with $C_{12-18}E_7$ depending on $C_{12-18}E_7$ concentrations. The equilibrium time was 5 h. The spectrum of Acid blue 113 begins to shift toward the larger wavelength at 0.02 mM of $C_{12-18}E_7$. The bathochromic shift reaches the maximum at 0.4 mM of $C_{12-18}E_7$. The spectrum peak (absorption maximum) shifts from 566 ± 1 nm to 600 ± 1 nm.

In UV-Vis spectroscopic studies, it was found that a range of anionic dyes interact with nonionic surfactants above the CMC.[4] The main driving force between them is interpreted as the hydrophobic and dispersion interaction.[76] The change in spectra can be explained by the effect of tautomerism and/or solvatochromism.[23] Some dyes with a naphtholic hydroxy group linked to the azo group exhibit commonly a hypsochromic shift due to a transition from hydrazone to tautomeric azo form in addition of nonionic surfactants.[4] The dyes, which are very sensitive to immediate environment, tend to undergo solvent shift and the direction of the shift is dependent on the polarity of the electronic state of the dye compared to that of solvent as well as the dye-solvent interaction.[23] That means if the excited state is more apolar than the ground state, a bathochromic shift is expected to happen in apolar or more apolar solvents. In other words, if an electronic excitation of molecules can benefit from the environment or from the interaction with surrounding solvents, the energy for the electronic transition can be lowered, corresponding to a spectral shift to a larger wavelength (lower frequency/energy) in the absorption spectrum, namely a bathochromic shift.

The interaction of the anionic dye Acid blue 113 with the nonionic surfactant $C_{12\text{-}18}E_7$ was observed above the CMC, which indicates the interaction of the dye with surfactant micelles by incorporation of dye into surfactant micelles. The bathochromic shift in the dye spectrum may originate from the stabilization of the dye in nonionic surfactant micelles mainly driven by the hydrophobic interaction between the dye and surfactant, since the tautomeric effect is not expected in the dye Acid blue 113 due to the chemical structure of the dye. Additionally, the bathochromic shift may be also attributed to the destruction of hydrogen bonding between azo groups of the dye in an aqueous media (water) in the presence of nonionic surfactants, resulting in more apolar environmental conditions that benefit the electronic excitation of the dye. It is assumed that Acid blue 113 may be accommodated in the hydrophilic region (polyoxyethylene shell) and partially penetrate into the hydrophobic region, which is suggested by Oakes et al.[4] for the system of similar azo dyes and the nonionic surfactant $C_{12}E_5$.

4.1.2 Dye + Anionic surfactant

Figure 4-3 shows the absorption spectra of Acid blue 113 in mixture with the anionic surfactant SDS of various concentrations. As can be seen, the spectrum of dye in the presence of SDS has only a small bathochromic shift in comparison with that of Acid blue 113 and $C_{12\text{-}18}E_7$. In presence of SDS up to 7 mM, the spectrum of dye shifts toward the larger wavelength. As the SDS concentration increases to 11 mM, there is no more shift observed with increasing

surfactant concentrations, where the maximal absorption lies at 584 ± 1 nm. The spectrum remains almost unchanged, as the SDS concentration is higher than 11 mM.

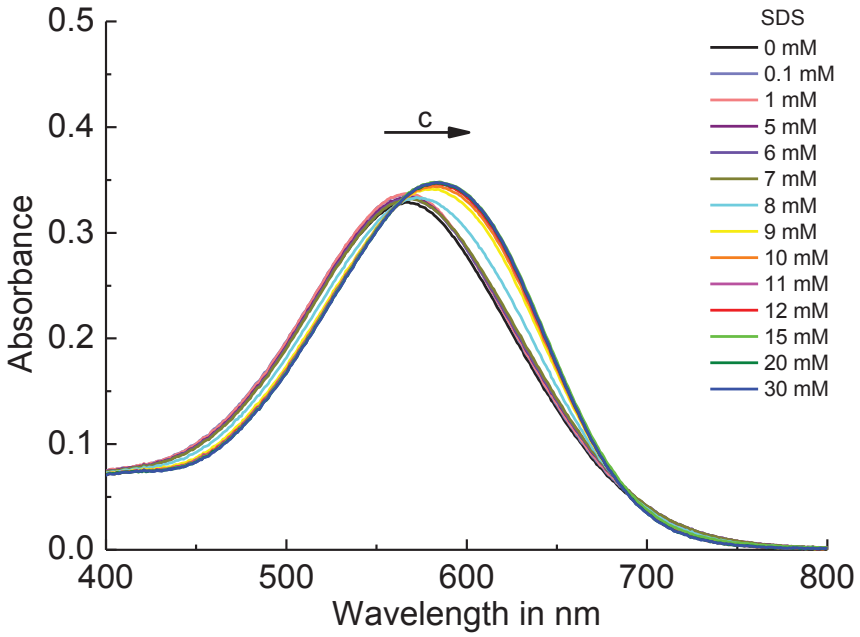

Figure 4-3 UV-Vis absorption spectra of mixtures of Acid blue 113 with SDS equilibrated for 5 h. The concentration of Acid blue 113 is 0.009 mM in all solutions and the concentration of SDS varies from 0 mM to 30 mM. From an SDS concentration of about 7 mM, the A_{max} and λ_{max} increase with increasing SDS concentrations and reach the maxima at about 11 mM.

Figure 4-4 shows the maximal absorbance value (A_{max}) and the corresponding wavelength (λ_{max}) of the mixtures in dependence of SDS concentrations. The A_{max} shifts to the larger value from 7 mM of SDS and the shift increases with increasing SDS concentrations until to 11 mM. The λ_{max} has an increase from the SDS concentration of 7 mM and reaches the maximum at SDS concentrations above 11 mM. The absorption maximum shifts from 567 nm to 584 ± 1 nm. It was found that the spectra of mixtures were not changed after more than 21 h (see Appendix, Fig. 2).

The anionic Acid blue 113 shows an interaction with SDS micelles, since the bathochromic shift of the dye spectrum occurs at the concentration above the CMC (7 mM). The interaction between Acid blue 113 and SDS is considered mainly as the hydrophobic interaction, resulting in stabilization of the dye by incorporation of the dye into surfactant micelles.

Comparing to the system of Acid blue 113-$C_{12\text{-}18}E_7$, the mixture of Acid blue 113 and SDS shows a relatively small spectral shift until to the maximal bathochromic shift. This may be

explained by a weak interaction between the dye and surfactant due to the repulsive interaction between anionic groups.

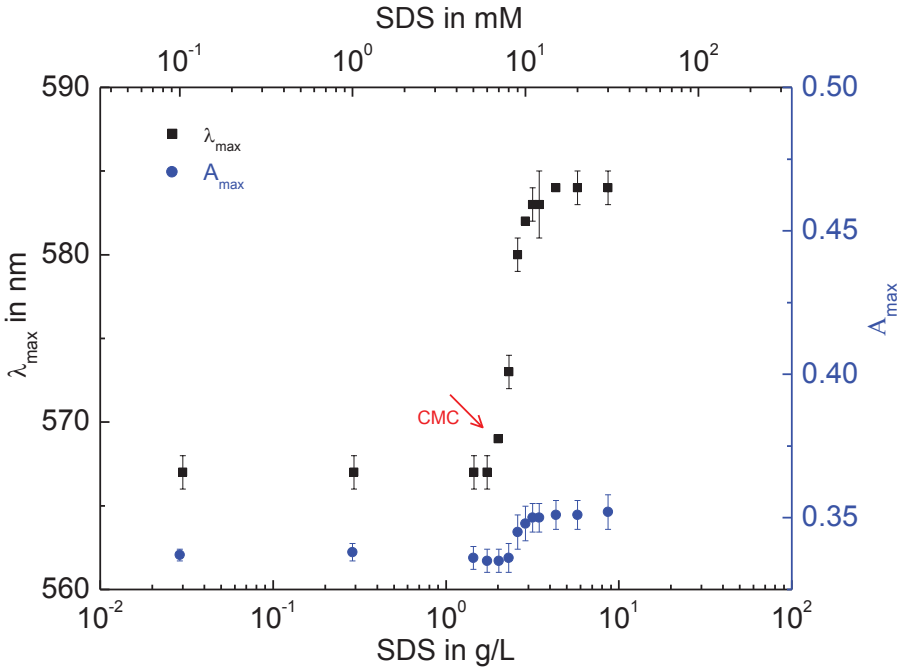

Figure 4-4 Plotting of the maximal absorbance values (A_{max}) and corresponding wavelengths (λ_{max}) of mixtures of Acid blue 113 with SDS depending on SDS concentrations. The equilibrium time was 5 h. The spectrum of Acid blue 113 begins to shift toward the larger wavelength at 7 mM of SDS. The bathochromic shift reaches the maximum at about 11 mM of SDS. The spectrum peak (absorption maximum) shifts from 567 ± 1 nm to 584 ± 1 nm.

In addition, the smaller bathochromic shift in the system of Acid blue 113-SDS compared to that of Acid blue 113-$C_{12\text{-}18}E_7$ may result from the weaker hydrophobic dye-surfactant interaction due to the smaller hydrophobic region (smaller size) of SDS micelle, which interacts with the dye, in comparison with that of $C_{12\text{-}18}E_7$ micelle.

4.1.3 Dye + Polymer

In comparison to the system of Acid blue 113-$C_{12\text{-}18}E_7$ and Acid blue 113-SDS, the mixtures of Acid blue 113 with the DTI polymer PVPVI present also bathochromic shifts, as shown in Figure 4-5.

By mixing with PVPVI of low concentrations, the maximal absorbance of Acid blue 113 decreases with increasing polymer concentrations to a minimum. At a PVPVI concentration of 0.006 g/L ($\sim 1 \cdot 10^{-4}$ mM), which is equal to the mass concentration of the dye, the spectrum begins to shift toward the larger wavelength as indicated by the arrow in Figure 4-5, where the maximal absorbance (A_{max}) and the corresponding wavelength (λ_{max}) increases with increasing

polymer concentrations respectively. A significant change in the dye spectrum was not observed until the PVPVI concentration is higher than about 0.6 g/L (~$1 \cdot 10^{-2}$ mM).

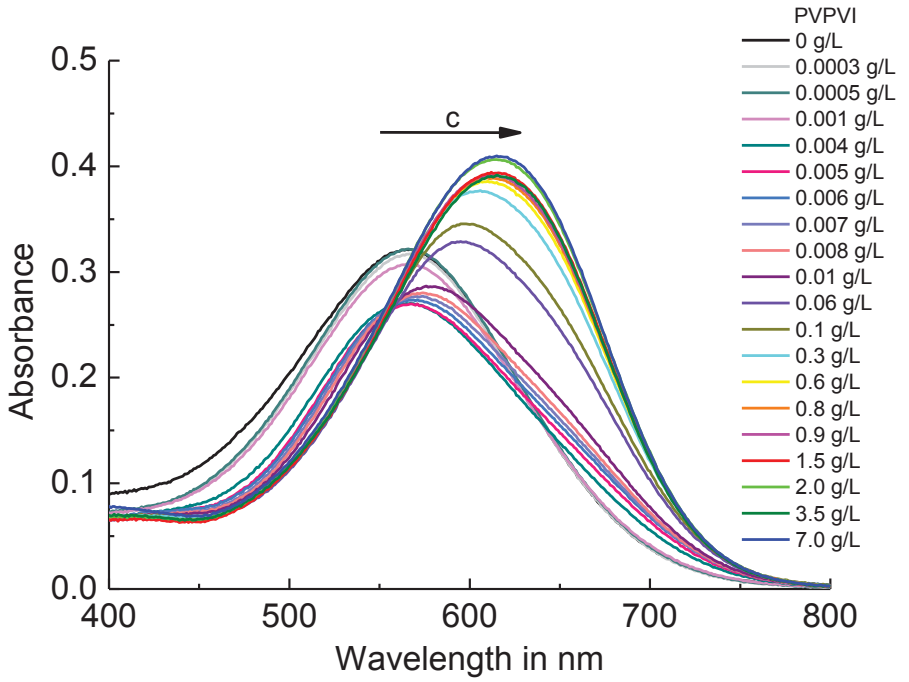

Figure 4-5 UV-Vis absorption spectra of mixtures of Acid blue 113 with PVPVI equilibrated for 7 h. The concentration of Acid blue 113 is 0.009 mM in all solutions and the concentration of PVPVI varies from 0 g/L to 7 g/L. From a PVPVI concentration of 0.006 g/L (~$1 \cdot 10^{-4}$ mM), the A_{max} and λ_{max} increase with increasing PVPVI concentrations and show no obvious increase at polymer concentrations above 0.6 g/L (~$1 \cdot 10^{-2}$ mM).

Based on the UV-Vis measurements, the maximal absorbance value A_{max} and the corresponding wavelength λ_{max} are plotted as a function of PVPVI concentrations (Fig. 4-6). The maximal absorbance of Acid blue 113 in mixture with PVPVI lowers to a minimum with increase of PVPVI to 0.005 g/L, where the form of spectrum is not changed (see Fig. 4-5). This effect may be caused by the change of polarity of the solution in the presence of the polymer electrolyte. As the PVPVI concentration is above 0.006 g/L, at which the spectrum begins to shift, A_{max} and λ_{max} increase with increasing PVPVI concentrations. The spectral maximum of the dye shifts from 566 ± 1 nm to 615 ± 1 nm. It was found that the spectra of mixtures were not distinctly changed until to 27 h (see Appendix, Fig. 3).

As seen in Figure 4-6, the polymer concentration at which the bathochromic shift begins is defined as the critical aggregation concentration (CAC), above which Acid blue 113 interacts with PVPVI.

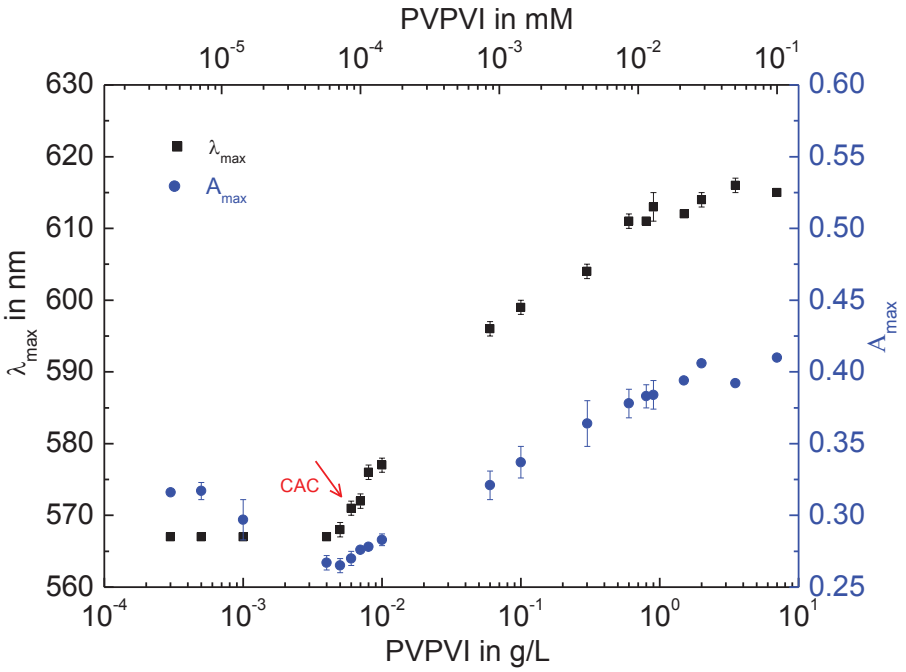

Figure 4-6 Plotting of the maximal absorbance values (A_{max}) and corresponding wavelengths (λ_{max}) of mixtures of Acid blue 113 with PVPVI depending on PVPVI concentrations. The equilibrium time was 7 h. The spectrum of Acid blue 113 begins to shift toward the larger wavelength at about 0.006 g/L ($\sim 1 \cdot 10^{-4}$ mM) of PVPVI. The bathochromic shift reaches the maximum at polymer concentrations above 0.6 g/L ($\sim 1 \cdot 10^{-2}$ mM). The spectrum peak (absorption maximum) shifts from 566 ± 1 nm to 615 ± 1 nm.

In the studies of binding properties of a comparable polymer poly(N-vinylpyrrolidone) (PVP) with different dyes, it is suggested that the driving force for binding of dyes to the polymer PVP is the dipolar, hydrogen binding, electrostatic and hydrophobic interaction[23,77–79]. According to the thermodynamic study by Takagishi et al.[78] the interaction between the anionic dye and PVP is contributed by the hydrophobic interaction, where the polymer backbone and the pyrrolidone ring may be binding sites for dyes. The thermodynamic study reported by Reeves et al.[79] indicates that the electrostatic interaction is predominant for the specific dye-polymer binding due to hydration of the polymer.

Similarly, PVPVI can also be considered as a polyelectrolyte. Therefore, the main interaction between Acid blue 113 and PVPVI may relate to the electrostatic attraction between the ionic parts of the dye and the polyelectrolyte as well as the hydrophobic interaction between the nonpolar parts of the dye and polymer. This may also explain the greater bathochromic shift of the system of Acid blue 113-PVPVI than that of Acid blue 113- $C_{12\text{-}18}E_7$ and Acid blue 113-SDS. In the systems of the dye with surfactants, only the hydrophobic interaction is considered to be responsible for the dye-surfactant interaction.

As the studies by UV-Vis spectroscopy present, the anionic dye interacts with the nonionic surfactant $C_{12\text{-}18}E_7$, anionic surfactant SDS and nonionic DTI polymer PVPVI respectively. The interaction occurs at certain concentration of additives and reaches the saturation to some point, where the binding of dye to additives is considered to be saturated. Under these conditions, the binding properties of Acid blue 113 with $C_{12\text{-}18}E_7$, SDS and PVPVI can be macroscopically determined with some certainty. In order to further understand the interaction between dye and surfactant as well as between dye and polymer, the binding properties of Acid blue 113 with additives are evaluated according to the plotting of wavelength shift at the maximal absorbance (λ_{max}). The binding property regarding the investigated system is quantified in terms of weight and mole ratio, as shown in Table 4-1. In the Table, the term C_{int} indicates the concentration of additive at which the λ_{max} begins to shift depending on the concentration of additives and C_{sat} refers to the concentration of additive at an initial saturation of the dye-additive interaction, where the binding of the dye with additives is considered saturated and no obvious spectral shift is observed.

Table 4-1 Binding properties of Acid blue 113 with additives determined from UV-Vis spectroscopic studies in terms of weight and mole ratio. The concentration of the dye is 0.009 mM in all systems.

System	C_{int} in mM	C_{sat} in mM	Weight ratio in g : g	Mole ratio in mol : mol
Acid blue 113 : $C_{12\text{-}18}E_7$	0.02	0.4	1: 31	1 : 42
Acid blue 113 : SDS	7	11	1 : 192	1 : 444
Acid blue 113 : PVPVI	$1{\cdot}10^{-4}$	$1{\cdot}10^{-2}$	1 : 116	1 : 1

C_{int}: the concentration of the additive, from which the λ_{max} begins to shift toward the larger wavelength (bathochromic shift).
C_{sat}: the concentration of the additive, at which no obvious spectral shift is observed indicating the saturation of interaction (initial saturation).
Weight ratio or mole ratio = C(dye) : ($C_{sat} - C_{int}$)

The weight ratios of $C_{12\text{-}18}E_7$ and SDS to the dye Acid blue 113 are about 31:1 and 192:1 respectively. The weight ratio for PVPVI interacting with the dye is about 116:1. The weight required for solubilizing per unit mass of the dye is therefore in this order: SDS > PVPVI > $C_{12\text{-}18}E_7$, which indicates correspondingly the affinity of additive for the dye with respect to mass, namely $C_{12\text{-}18}E_7$ > PVPVI > SDS.

In order to understand the binding properties from the viewpoint of molecular interactions between the dye and additives, the molar ratios in Table 4-1 are represented in Table 4-2.

Table 4-2 Binding properties of Acid blue 113 with additives determined from UV-Vis spectroscopic studies in terms of molecular interactions. The concentration of the dye is 0.009 mM in all systems.

System	C_{int} in mM	C_{sat} in mM	Molecule : Molecule	Molecule : Micelle
Acid blue 113 : $C_{12\text{-}18}E_7$	0.02	0.4	1 : 42	1: 0.38[a]
Acid blue 113 : SDS	7	11	1 : 444	1 : 7.4[b]
Acid blue 113 : PVPVI	$1 \cdot 10^{-4}$	$1 \cdot 10^{-2}$	1 : 1	-

a: with the aggregation number of surfactant micelle of 110.[80]
b: with the aggregation number of surfactant micelle of 60.[81]

The mole ratio of Acid blue 113 to PVPVI is determined to be ~1:1, which implies a 1:1 dye-polymer complex in solution. J. Oakes et al. found that acid dyes form 1:1 complex with cationic surfactant monomer (below the CMC), which implies a strong electrostatic interaction driving the binding.[76] Therefore, the polyelectrolyte PVPVI may bind with Acid blue 113 mainly driven by an attractive electrostatic interaction.

Because the dye interacts with both surfactants at concentrations above the CMC, it is more advisable to quantify the interaction between the dye and the surfactant micelle, i.e. the binding property of dye molecules with surfactant micelles. For the system of Acid blue 113-$C_{12\text{-}18}E_7$, a molecular ratio of ~42:1 is determined here for $C_{12\text{-}18}E_7$ to the dye. The aggregation number of $C_{12\text{-}18}E_7$ micelle was given in the range of 90−135,[80,82] therefore, it is suggested that one surfactant micelle binds 2−3 dye molecules if the aggregation number of $C_{12\text{-}18}E_7$ micelle is averaged to be 110. The molecular ratio of SDS to the dye is about 444:1. The aggregation number of spherical SDS micelles is about 60.[83–85] Hence, one dye molecule may be solubilized in 7−8 SDS micelles on average. The extremely high mole ratio of SDS to the dye can be attributed to the weak interaction between the dye and SDS. On the other hand, SDS has a much higher CMC than $C_{12\text{-}18}E_7$, which implies that above the CMC SDS requires a higher concentration of free surfactant monomers for equilibrium of the dye-surfactant interaction. Taking the aggregation number of both surfactants into account, the system of Acid blue 113-SDS still requires a higher concentration of micelles for equilibrium than that of Acid blue 113-$C_{12\text{-}18}E_7$. This can also result in a higher ratio of SDS monomers and consequently of SDS micelles to the dye by calculation.

Regarding the molecular ratio, the binding preference of additives for the dye decreases in the order: PVPVI > $C_{12\text{-}18}E_7$ > SDS. In solution, Acid blue 113 seems to have a much higher affinity for the polymer than for surfactants. It is assumed that the interaction of the dye with

surfactant micelles is driven by the hydrophobic interaction. Nevertheless, besides the hydrophobic interaction the electrostatic attraction also plays an important role in the dye-polymer interaction. The low affinity of the dye for SDS may be attributed to the weak interaction between the dye and the anionic surfactant due to the repulsion of the negatively charged groups. In addition, the lower affinity of the dye for SDS than that for $C_{12\text{-}18}E_7$ may be due to the smaller micelle size of SDS corresponding to a smaller hydrophobic part compared to that of $C_{12\text{-}18}E_7$, which is responsible for the hydrophobic interaction between the dye and surfactant.

4.1.4 Dye + Polymer + Nonionic surfactant

Figure 4-7 shows the maximal absorbance A_{max} and the corresponding wavelength λ_{max} for the three-component system of Acid blue 113 + PVPVI + $C_{12\text{-}18}E_7$ in dependence of $C_{12\text{-}18}E_7$ concentrations.

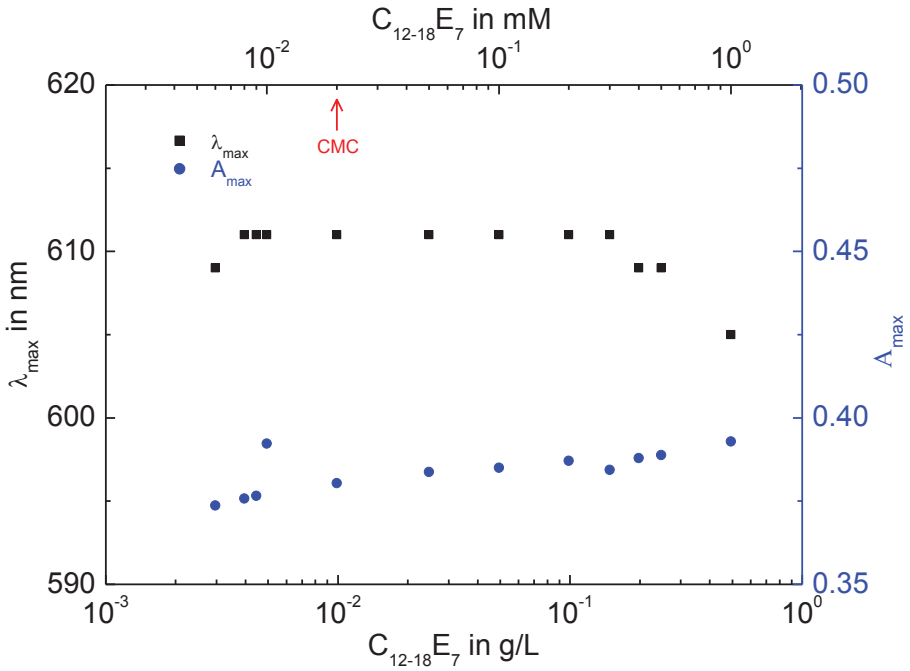

Figure 4-7 Plotting of the maximal absorbance values (A_{max}) and corresponding wavelengths (λ_{max}) for the ternary system Acid blue 113 + PVPVI + $C_{12\text{-}18}E_7$ in dependence of $C_{12\text{-}18}E_7$ concentrations. The concentration of Acid blue 113 is 0.009 mM and of PVPVI $1 \cdot 10^{-2}$ mM in all solutions. The concentration of $C_{12\text{-}18}E_7$ varies from 0 mM to 1 mM. The solutions of mixtures were equilibrated for 24 h before UV-Vis measurements. The λ_{max} for the three-component system is almost in the range of 609−611 nm and the A_{max} varies from 0.35 to 0.39, which are in good agreement with those of the two-component system of Acid blue 113 + PVPVI, indicating the dye-polymer complex. Additionally, in the three-component system no obvious influence of surfactant concentrations on the spectrum of dye was observed in a large range above the CMC.

In the presence of $1 \cdot 10^{-2}$ mM PVPVI, the λ_{max} for the ternary system is almost in the range of 609−611 nm and the A_{max} varies from 0.35 to 0.39. The values of λ_{max} and A_{max} are in good agreement with those of the two-component system of Acid blue 113 + PVPVI, where the averaged λ_{max} is 611 nm and A_{max} 0.38 (ref. Fig. 4-6). Therefore, the spectra of the three-component system indicate the dye-polymer binding. In addition, in the three-component system no obvious influence of surfactant concentrations on the spectrum of dye was observed in a large range above the CMC. At the $C_{12\text{-}18}E_7$ concentration of 1 mM, the value of λ_{max} for the ternary system decreases to 605 nm but the A_{max} is still comparable to that for the system of Acid blue 113 + PVPVI. Therefore, it is assumed that there may be some replacement of the polymer in dye-polymer complex by the nonionic surfactants at very high surfactant concentrations.

If the concentration of PVPVI is decreased to 10^{-3} mM, the λ_{max} for the three-component system is almost in the range of 594−596 nm and the A_{max} varies from 0.29 to 0.32, as shown in Figure 4-8.

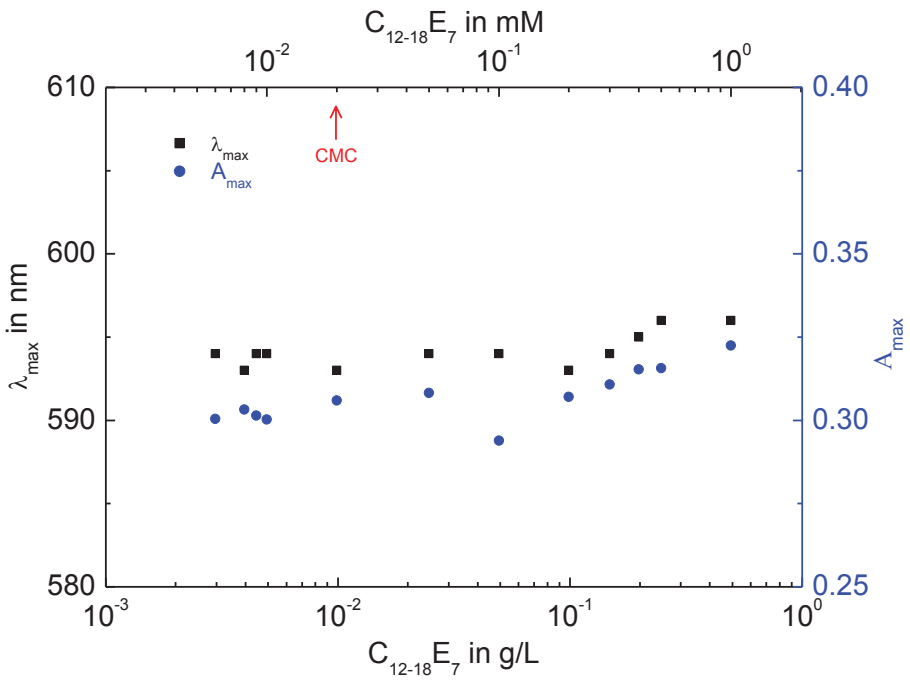

Figure 4-8 Plotting of the maximal absorbance values (A_{max}) and corresponding wavelengths (λ_{max}) for the ternary system Acid blue 113 + PVPVI + $C_{12\text{-}18}E_7$ in dependence of $C_{12\text{-}18}E_7$ concentrations. The concentration of Acid blue 113 is 0.009 mM and of PVPVI $1 \cdot 10^{-3}$ mM in all solutions. The concentration of $C_{12\text{-}18}E_7$ varies from 0 mM to 1 mM. The solutions of mixtures were equilibrated for 24 h before UV-Vis measurements. The λ_{max} for the three-component system is in the range of 594−596 nm and the A_{max} varies from 0.29 to 0.32, which are in good agreement with those of the two-component system of Acid blue 113 + PVPVI, indicating the dominant dye-polymer complex. Additionally, no obvious influence of the nonionic surfactant on the dye-polymer complex was observed even at concentrations above the CMC.

In the absence of $C_{12\text{-}18}E_7$ the λ_{max} for the binary system of dye-polymer is in the range of 598 ± 2 nm and the A_{max} 0.33 ± 0.01 (ref. Fig. 4-6). Moreover, as is shown in Figure 4-2, in the mixture of Acid blue 113 with $C_{12\text{-}18}E_7$ the absorption maximum (λ_{max}) shifts from 566 nm to 600 nm as the surfactant concentration increases from 0.02 mM to 0.4 mM. This further demonstrates that here the dye-polymer complex is not obviously influenced by the nonionic surfactant $C_{12\text{-}18}E_7$. This finding can be supported by the comparable study for the ternary system of Acid dye + PVP + Surfactant, where the nonionic surfactant $C_{12}E_8$ showed less influence on the dye-polymer binding[86].

4.1.5 Dye + Polymer + Anionic surfactant

In the three-component system of Acid blue 113 + PVPVI + SDS (Fig. 4-9), in the presence of $1{\cdot}10^{-2}$ mM PVIVI the λ_{max} is in the range of 610−615 nm and the A_{max} varies from 0.40 to 0.41, which are comparable with the value of λ_{max} (611 nm) and A_{max} (0.38) of the two-component system of Acid blue 113 + PVPVI (ref. Fig. 4-6). This indicates the dominant dye-polymer complex in the ternary system.

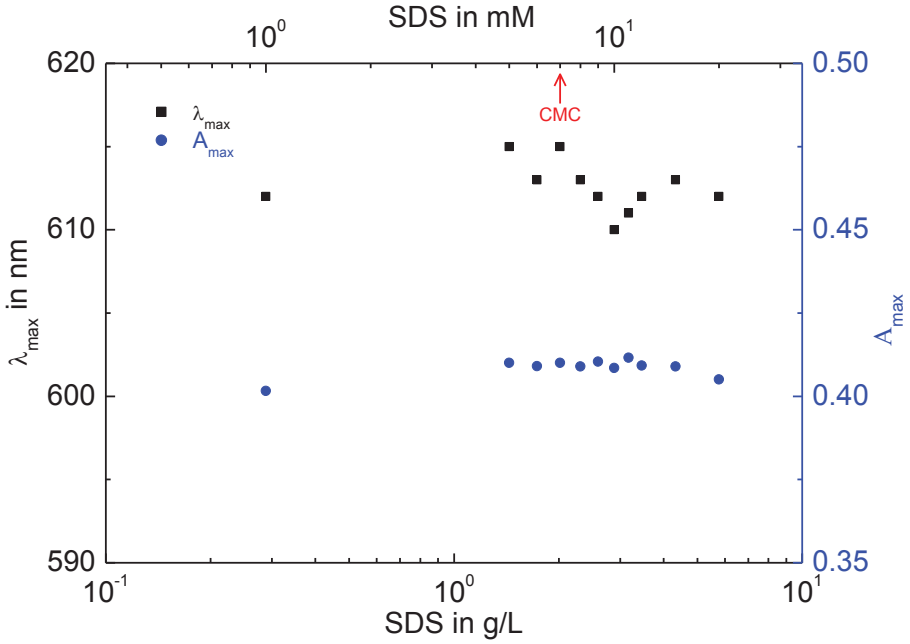

Figure 4-9 Plotting of the maximal absorbance values (A_{max}) and corresponding wavelengths (λ_{max}) for the ternary system Acid blue 113 + PVPVI + SDS in dependence of SDS concentrations. The concentration of Acid blue 113 is 0.009 mM and of PVPVI $1 \cdot 10^{-2}$ mM in all solutions. The concentration of SDS varies from 0 mM to 20 mM. The solutions of mixtures were equilibrated for 24 h before UV-Vis measurements. The λ_{max} for the three-component system is in the range of 610−615 nm and the A_{max} varies from 0.40 to 0.41, which are comparable with those of the two-component system of Acid blue 113 + PVPVI. This implies the dominant dye-polymer complex in the three-component system due to the stronger dye-polymer interaction than that between dye and surfactant at high polymer concentrations.

Oakes and Dixon[25] found that SDS has a higher affinity for the polymer PVP-NO than the dye DR80 and can displace the dye from the polymer at high surfactant concentrations, forming surfactant-polymer complexes, which lowers the efficacy of polymer for inhibiting the deposition of dyes on cotton. This influence of SDS was not observed in the system of Acid blue 113 + PVPVI + SDS, since the values of λ_{max} and A_{max} are much greater than those of Acid blue 113-SDS mixtures (ref. Fig. 4-4) in all studied SDS concentrations. Moreover, it was found that the result of this system was not influenced by the order of the addition of PVPVI and SDS in the dye. This implies the stronger interaction between the dye and polymer than that between the dye and surfactant at high polymer concentrations.

In the presence of $1 \cdot 10^{-3}$ mM PVPVI (Fig. 4-10), the λ_{max} for the ternary system is in the range of 605−611 nm and the A_{max} differs from 0.35 to 0.38.

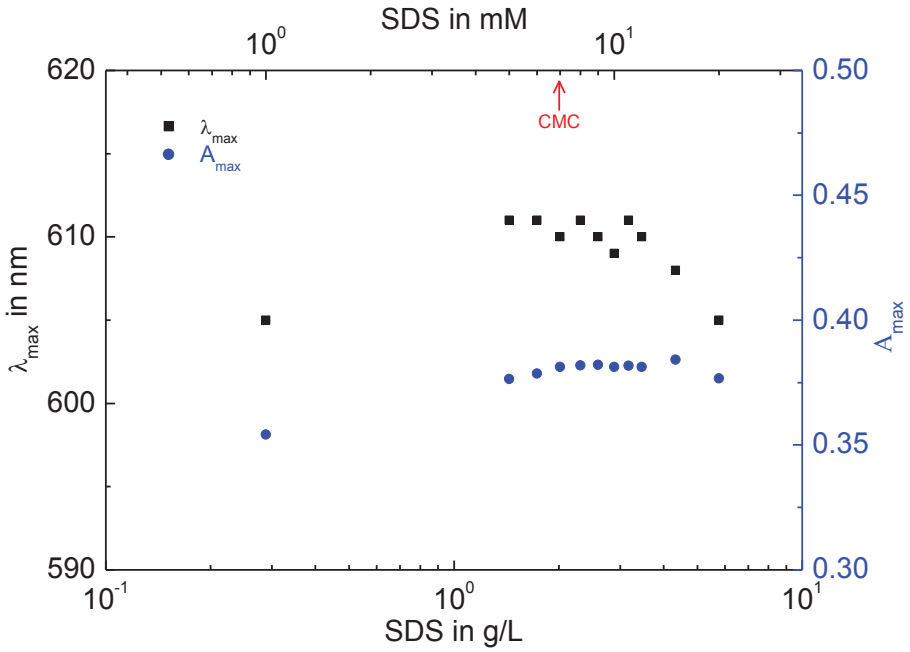

Figure 4-10 Plotting of the maximal absorbance values (A_{max}) and corresponding wavelengths (λ_{max}) for the ternary system Acid blue 113 + PVPVI + SDS in dependence of SDS concentrations. The concentration of Acid blue 113 is 0.009 mM and of PVPVI $1 \cdot 10^{-3}$ mM in all solutions. The concentration of SDS varies from 0 mM to 20 mM. The solutions of mixtures were equilibrated for 24 h before UV-Vis measurements. The λ_{max} for the three-component system is in the range of 605−611 nm and the A_{max} varies from 0.35 to 0.38, which indicate neither the dye-polymer nor the dye-surfactant complex alone. This phenomenon may be attributed to the interaction between SDS and PVPVI resulting in dye-polymer-surfactant complexes at relatively low polymer concentrations.

In the absence of SDS the averaged λ_{max} for the binary system of Acid blue 113 + PVPVI is 598 nm and the A_{max} 0.33 (ref. Fig. 4-6). As it is shown in Figure 4-4, in the two-component system of Acid blue 113 + SDS the absorption maximum (λ_{max}) shifts from 566 nm to 584 nm

as the surfactant concentration increases from 7 mM to 11 mM. Therefore, the values of λ_{max} and A_{max} for the three-component system indicate neither the dye-polymer nor the dye-surfactant complex alone. This phenomenon may be attributed to the interaction between SDS and PVPVI. As known in Section 4.1.3, at the polymer concentration of $1 \cdot 10^{-3}$ mM the binding of dye-polymer is not saturated yet, which means that there are still free dyes not bound to the polymer. In the presence of SDS, SDS may interact with PVPVI forming surfactant-polymer complexes, which can further bind with the dye by new binding sites[25] of surfactant-polymer complexes in addition to the dye-polymer interaction.

According to the UV-Vis spectroscopic studies of three-component systems in solution, it was found that the binding of dye with the DTI polymer and with surfactants are competitive. In the presence of the polymer of high concentrations, the dye-polymer complex is dominant and not affected by surfactants at a large concentration range of surfactants even above the CMC. In the presence of the polymer of low concentrations, the dye-polymer complex is obviously influenced by the anionic surfactant SDS, which may be due to the interaction between the polymer PVPVI and SDS. This surfactant-polymer interaction may result in new bindings of the dye in the dye-polymer-surfactant mixture.

4.2 Particle size analysis by DLS

To further evaluate the interactions between surfactant, polymer and dye in solution observed in UV-Vis spectroscopic studies, the size of particles of single components and binary mixtures were analyzed by DLS. Intensity-weighted size distributions and parameters containing the hydrodynamic diameter (Z-average, $D_{h,z}$) and peak size $D_{h,i}$ (i=1, 2) are shown. For single components there is only one peak in the size distribution, both Z-average ($D_{h,z}$) and peak size ($D_{h,i}$) correspond to the size of particle in water. For binary mixtures showing more than one peak, the particle size is described by the peak size $D_{h,i}$ with respect to the corresponding component in solution.

In a size distribution by intensity for multicomponent systems, the intensity presented for each component can be affected by the fraction of component. This makes the quantitative analysis of such systems complex in terms of one system with components of various quantities or mole ratios. That means the change in intensity of the respective component in a binary system can be attributed on the one hand to the interaction between components and on the other hand to the change in composition of the studied mixture. Therefore, the results for binary mixtures are

analyzed by the changes in intensity and size of respective components, to give an interpretation of the interaction between two components.

4.2.1 DLS studies of single components

$C_{12\text{-}18}E_7$

At the concentrations above 1 mM, the nonionic surfactant $C_{12\text{-}18}E_7$ shows a monomodal size distribution (Fig. 4-11). It was observed that the size of the surfactant micelles increases with increasing $C_{12\text{-}18}E_7$ concentrations, as shown in Table 4-3.

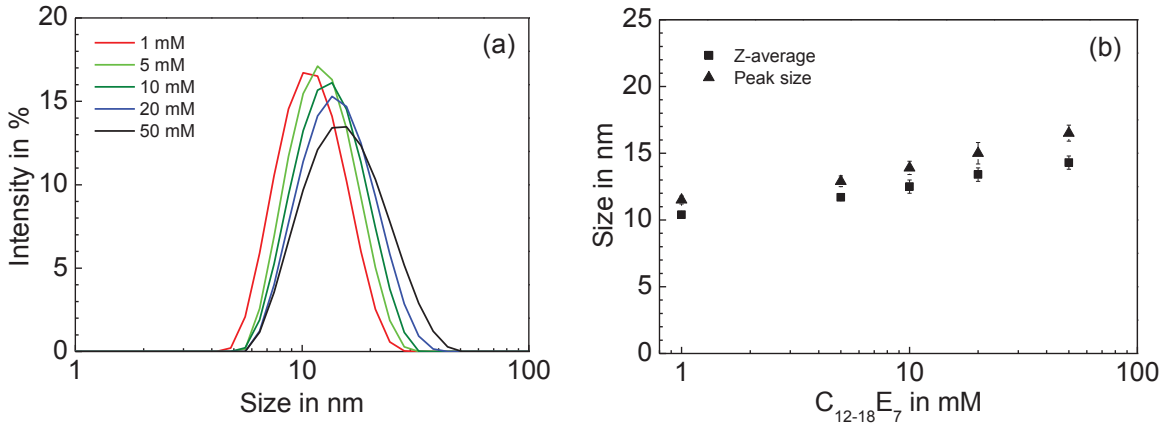

Figure 4-11 (a) Intensity-weighted size distributions of $C_{12\text{-}18}E_7$ at the concentrations of 1−50 mM. (b) Size of $C_{12\text{-}18}E_7$ micelles presented as the Z-average and peak size depending on $C_{12\text{-}18}E_7$ concentrations. $C_{12\text{-}18}E_7$ shows a monomodal distribution at the concentrations above 1 mM. The $D_{h,z}$ value is in the range of 10−14 nm and the peak size 12−17 nm. The size of surfactant micelles increases with increasing $C_{12\text{-}18}E_7$ concentrations, which may be attributed on the one hand to the decreased proportion of small micelles containing alcohol or surfactants of low molecular weight and on the other hand to the reduced diffusion of micelles due to the intermicellar interaction[80].

Table 4-3 Hydrodynamic diameter $D_{h,z}$ (Z-average), PDI and peak size of $C_{12\text{-}18}E_7$ micelles in the size distribution analyzed by DLS measurements.

$C_{12\text{-}18}E_7$ in mM	Z-average ($D_{h,z}$) in nm	PDI	Peak size in nm
1	10.4 ± 0.2	0.118 ± 0.037	11.5 ± 0.3
5	11.7 ± 0.2	0.085 ± 0.014	12.9 ± 0.4
10	12.5 ± 0.5	0.092 ± 0.003	13.9 ± 0.5
20	13.4 ± 0.5	0.105 ± 0.011	15.0 ± 0.8
50	14.3 ± 0.5	0.129 ± 0.001	16.5 ± 0.6

It is known that technical polyoxyethylene-based surfactants usually contain unethoxylated fatty alcohol and ethoxylated species with different molecular weight.[87] The increase in hydrodynamic size related to the concentration can result from the decreased proportion of small micelles containing alcohol or surfactants of low molecular weight. At low surfactant concentrations, the number of small micelles is not negligible compared to the total number of micelles. Nevertheless, with increasing total surfactant concentrations the proportion of small aggregates decreases, resulting in an increase of averaged size of surfactant micelles. In addition to this, according to the study of self-diffusion coefficients depending on surfactant concentrations, an attractive interaction between micelles may exist,[80] which reduces the diffusion of surfactant micelles. Considering the dependence of hydrodynamic radius on diffusion coefficient by the Stokes-Einstein equation (Equation 2-19 and 2-22), this intermicellar interaction can result in an increase in the hydrodynamic size as well.

The hydrodynamic diameter ($D_{h,z}$) of $C_{12\text{-}18}E_7$ varies from 10 nm to 14 nm and the peak size from 12 nm to 17 nm. The PDI values are less than 0.13 at all concentrations, corresponding to a narrow size distribution range. The hydrodynamic radius of $C_{12}E_7$ micelle reported is about 3 nm,[80,82,88] which is smaller than the size presented here. However, it was found that $C_{14}E_7$ micelle has a size (diameter) of 12−18 nm at the concentrations of 10−40 mM.[89] This size is in coincidence with the presented results for $C_{12\text{-}18}E_7$, since the used $C_{12\text{-}18}E_7$ contains homologues with hydrophobic chains of C_{12}−C_{18}.

SDS

Figure 4-12 shows the size distributions for the anionic surfactant SDS at concentrations above the CMC. As can be seen in Figure 4-12, the peaks at lower concentrations ($\leq$ 50 mM) are nearly symmetrical, corresponding to a spherical micellar form of most surfactant aggregates. At very high concentrations ($\geq$100 mM), there are steep slopes as the size is less than 0.5 nm. This is because the particle size in this range is very near or out of the limitation of size analyzer of the used apparatus (0.3 nm).

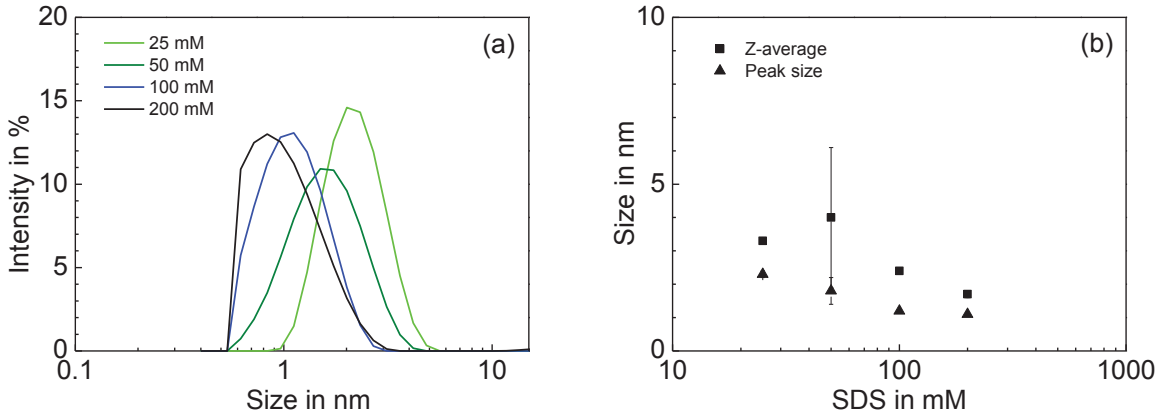

Figure 4-12 (a) Intensity-weighted size distributions of SDS at the concentrations of 25−200 mM. (b) Size of SDS micelles presented as the Z-average and peak size depending on SDS concentrations. SDS shows a monomodal distribution at the concentration range studied. The $D_{h,z}$ value is in the range of 2−4 nm and the peak size 1−2 nm.

Table 4-4 Hydrodynamic diameter $D_{h,z}$ (Z-average), PDI and peak size in the size distribution of SDS micelles analyzed by DLS measurements.

SDS in mM	Z-average ($D_{h,z}$) in nm	PDI	Peak size in nm
25	3.3 ± 0.1	0.205 ± 0.008	2.3 ± 0.1
50	4.0 ± 2.1	0.250 ± 0.115	1.8 ± 0.4
100	2.4 ± 0.1	0.166 ± 0.006	1.2 ± 0
200	1.7 ± 0.1	0.129 ± 0.006	1.1 ± 0

As seen in Table 4-4, the size of SDS micelles is much smaller than that of the nonionic surfactant $C_{12\text{-}18}E_7$. Because of the repulsive interaction caused by the ionic headgroups, SDS has generally a smaller aggregation number than $C_{12\text{-}18}E_7$, corresponding to a smaller micelle size. The hydrodynamic diameter ($D_{h,z}$) of SDS varies in the range of 2−4 nm and the peak size differs from 1 nm to 2 nm. This agrees well with the results obtained by molecular dynamics simulation[81,83].

Acid blue 113

The size distribution of the dye Acid blue 113 shows a peak in the size range over 100 nm at the concentrations of 0.004 − 0.073 mM (Fig. 4-13). This indicates that Acid blue 113 forms aggregates in aqueous solution. Unlike certain organic dyes which show shifts or splitting of dye absorption spectrum owing to dye aggregation in solution[90], no such spectral change was observed in aqueous solution of Acid blue 113 at all concentrations studied in the DLS

measurements. Therefore, despite that shown by the DLS study the dye is at least not completely molecular solubilized in water, the Lambert-Beer law was still applied in this case.

Although it is suggested that a range of dye molecules prefer to stack in one dimension prominently driven by the π-π interaction between aromatic rings forming dimers and/or trimers,[91,92] it was found that some ionic azo dyes can form aggregates with high aggregation numbers[93] or colloidal aggregates with a diameter more than 100 nm determined by inelastic light scattering[94]. Comparing to these dyes where large aggregates are present at concentrations in the range of ~0.1−10 mM,[93] the aggregates of Acid blue 113 are detected at surprisingly low concentrations.

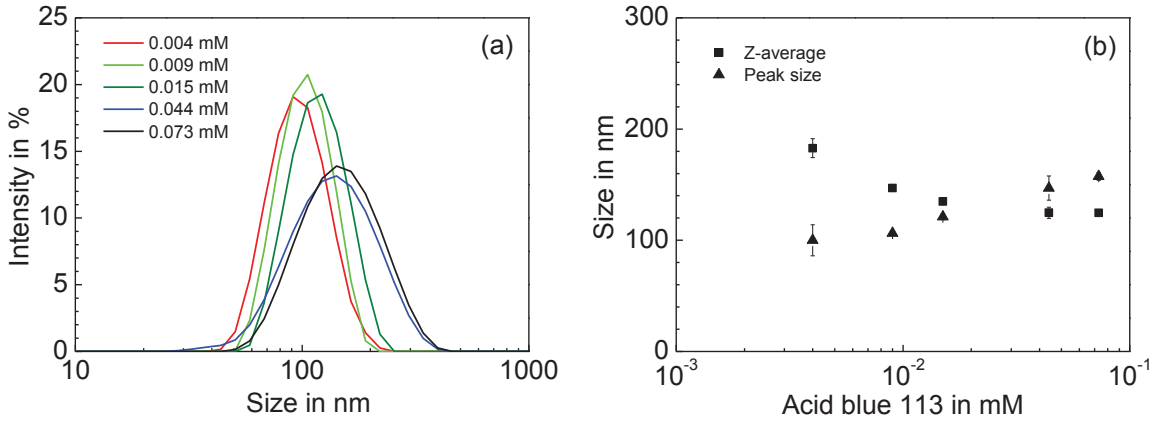

Figure 4-13 (a) Intensity-weighted size distributions of Acid blue 113 at the concentrations of 0.004−0.073 mM. (b) Size of dye aggregates presented as the Z-average and peak size depending on dye concentrations. Acid blue 113 shows one peak in the size range over 100 nm, indicating dye aggregates in aqueous solution.

Table 4-5 Hydrodynamic diameter $D_{h,z}$ (Z-average), PDI and peak size in the size distribution of Acid blue 113 analyzed by DLS measurements.

Acid blue 113 in mM	Z-average ($D_{h,z}$) in nm	PDI	Peak size in nm
0.004	182.8 ± 8.5	0.238 ± 0.027	100.0 ± 13.9
0.009	147.0 ± 3.1	0.232 ± 0.020	106.3 ± 2.0
0.015	134.9 ± 2.2	0.227 ± 0.027	121.2 ± 2.7
0.044	124.8 ± 5.0	0.253 ± 0.025	146.9 ± 10.9
0.073	124.7 ± 1.2	0.231 ± 0.013	157.4 ± 3.5

As shown in Table 4-5, there is a great difference between the $D_{h,z}$ value and the peak size at low dye concentrations. This may be due to that the shape of dye aggregate is not ideally

spherical. If the dye aggregation results from the one-dimensional growth by the molecular stacking, the difference of radii of dye aggregate in two directions, which are parallel and perpendicular to the centered molecule plane, can be significant. The Z-averaged diameter ($D_{h,z}$) is a calculated value on the assumption that the particle has an ideal sphere structure with the same translational diffusion in all directions. Otherwise, the apparent size ($D_{h,z}$) may be over- or underestimated by the DLS analysis.

PVPVI

Figure 4-14 shows the intensity-weighted size distribution of PVPVI dissolved in water. It was found that, up to a concentration of 0.01 mM PVPVI shows a single peak in the size distribution. The hydrodynamic diameter ($D_{h,z}$) determined from the size distribution for PVPVI is not much changed with increasing polymer concentrations, as presented in Table 4-6.

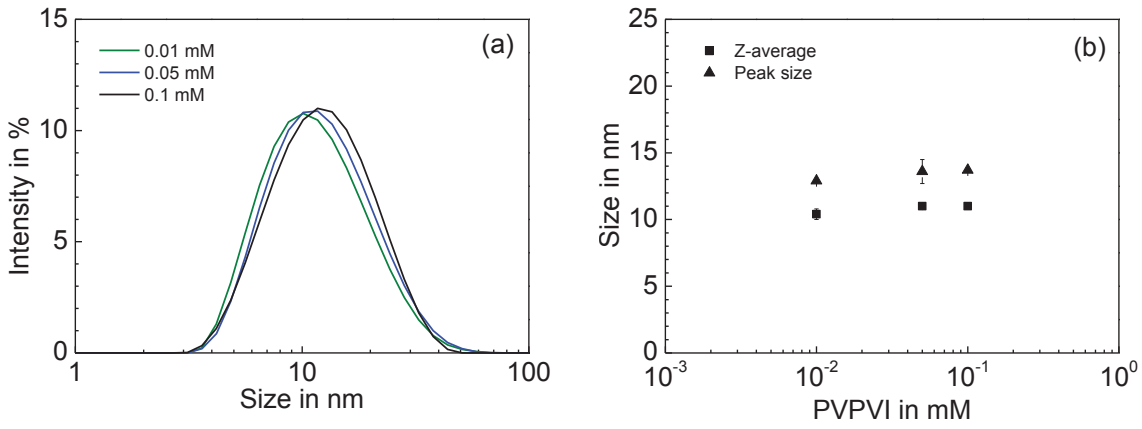

Figure 4-14 (a) Intensity-weighted size distributions of PVPVI at the concentrations of 0.01−0.1 mM. (b) Size of PVPVI presented as the Z-average and peak size depending on PVPVI concentrations. PVPVI shows a monomodal distribution at the concentration above 0.01 mM. The $D_{h,z}$ value is in the range of 10−11 nm and the peak size 13−14 nm.

Table 4-6 Hydrodynamic diameter $D_{h,z}$ (Z-average), PDI and peak size in the size distribution of PVPVI analyzed by DLS measurements.

PVPVI in mM	Z-average ($D_{h,z}$) in nm	PDI	Peak size in nm
0.01	10.4 ± 0.4	0.214 ± 0.008	12.9 ± 0.1
0.05	11.0 ± 0.2	0.202 ± 0.013	13.6 ± 0.9
0.1	11.0 ± 0	0.181 ± 0.004	13.7 ± 0.1

It can be observed that the shape of the peak becomes more symmetrical with increased PVPVI concentrations, indicating that the sample becomes more uniform with increasing polymer

concentrations[95]. This may be attributed to the change in conformation of polymer molecules with respect to the concentration.[39(p. 141-144)] The symmetrical peak reveals that there are substantial polymers in the globular form with a similar size.

The DLS data shows that PVPVI has a $D_{h,z}$ value of 10−11 nm and peak size of 13−14 nm. Guettari reported that in a comparable study, PVP (M_w=3.6 · 10^5 g/mol) has a hydrodynamic radius (R_h) of 36 nm in water.[96] As known in the Flory theory[97], there is a relationship between the size and the molecular weight of polymer in solution. The relationship is described with the equation $R_h \sim M^a$, where M is the molecular weight of polymer and a is a constant depending on the property of polymer and solvent.[98–100] In practice, a is usually in the range of 0.5−0.8.[99,100] According to this relationship in the similar behavior, the hydrodynamic diameter of PVPVI (M_w=7 · 10^4 g/mol) derived from DLS study corresponds to one polymer molecule.

4.2.2 Acid blue 113 + $C_{12\text{-}18}E_7$

The intensity-weighted size distributions of the mixtures of Acid blue 113 and $C_{12\text{-}18}E_7$ are shown in Figure 4-15. The concentration of dye remained unchanged in all solutions. Two peaks in different size ranges were observed in the mixture of the dye with $C_{12\text{-}18}E_7$, which are indicated as peak 1 (on the right) and peak 2 (on the left). The peak 1 relates to the dye aggregate. The peak 2 corresponding to surfactant micelles was observed as the concentration of $C_{12\text{-}18}E_7$ is above the CMC (0.03 mM).

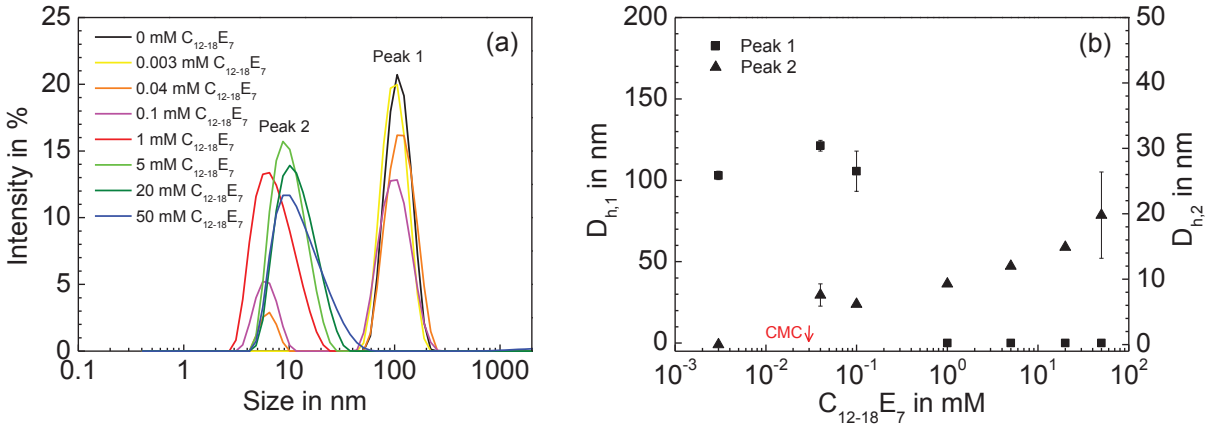

Figure 4-15 (a) Intensity-weighted size distributions of the mixtures of Acid blue 113 with $C_{12\text{-}18}E_7$ at different surfactant concentrations. (b) Peak size for the peak 1 ($D_{h,1}$) and peak 2 ($D_{h,2}$) displayed in (a) depending on $C_{12\text{-}18}E_7$ concentrations. The concentration of Acid blue 113 is 0.009 mM in all solutions. The peaks in the size distribution are indicated as peak 1 (right) and peak 2 (left), which relate to the dye aggregate and the surfactant micelle respectively. At surfactant concentrations of more than 1 mM, the peak of dye aggregate could not be observed, indicating that the dye aggregates are dissolved in surfactant solutions due to incorporation of the dye into surfactant micelles.

Table 4-7 Hydrodynamic diameter $D_{h,z}$ (Z-average), PDI and peak sizes $D_{h,i}$ in the size distribution for the system Acid blue 113-$C_{12\text{-}18}E_7$ analyzed by DLS measurements.

$C_{12\text{-}18}E_7$/Acid blue 113 in mM/mM	Z-average ($D_{h,z}$) in nm	PDI	Peak 1 ($D_{h,1}$) in nm	Peak 2 ($D_{h,2}$) in nm
0/0.009	146.8 ± 12.3	0.238 ± 0.032	110.3 ± 2.3	-
0.003/0.009	148.2 ± 10.3	0.223 ± 0.016	103.0 ± 2.6	-
0.04/0.009	116.5 ± 0.8	0.181 ± 0	121.3 ± 3.3	7.6 ± 1.7
0.1/0.009	109.7 ± 21.4	0.159 ± 0.003	105.6 ± 12.3	6.2 ± 0
1/0.009	7.9 ± 0	0.157 ± 0.010	-	9.3 ± 0.1
5/0.009	10.9 ± 0.1	0.087 ± 0	-	12.0 ± 0.1
20/0.009	13.1 ± 0	0.117 ± 0.009	-	14.9 ± 0.1
50/0.009	14.8 ± 1.1	0.226 ± 0.020	-	19.8 ± 6.6

In Table 4-7, the particle size analysis data including the Z-averaged hydrodynamic diameter ($D_{h,z}$), peak size ($D_{h,1}$ and $D_{h,2}$) and polydispersity index (PDI) are summarized for the mixtures. The hydrodynamic diameter and peak size of dye aggregate without additives are 146.8 nm and 110.3 nm respectively. Generally speaking, the size of surfactant micelles ($D_{h,2}$) increases with increasing surfactant concentrations. The size of dye aggregate ($D_{h,1}$) shows a small increase as the concentration of $C_{12\text{-}18}E_7$ is slightly higher than the CMC. At high surfactant concentrations of more than 1 mM, the peak of dye aggregate could not be observed. That means the dye aggregates may be dissolved in surfactant micelles due to the dye-surfactant interaction.

In the presence of 1 mM $C_{12\text{-}18}E_7$ there are 0.97 mM surfactants interacting with the dye (1 mM−CMC). Considering the aggregation number of 110 for $C_{12\text{-}18}E_7$,[80] at 1 mM of $C_{12\text{-}18}E_7$ it gives a ratio of surfactant micelle to dye molecule determined by DLS, namely ~1:1. This is in agreement with the result from the UV-Vis spectroscopic study giving a comparable ratio of 1:2−3. The DLS study indicates that Acid blue 113 interacts with $C_{12\text{-}18}E_7$ above the CMC by incorporation of the dye into surfactant micelles. Because the amount of dyes bound to one surfactant micelle is low, the size of surfactant micelle in the presence of dye has no great change compared to that without dyes, which is 14.0 ± 4.5 nm averaged for 1−50 mM $C_{12\text{-}18}E_7$.

4.2.3 Acid blue 113 + SDS

Figure 4-16 shows the size distributions of the mixtures of Acid blue 113 with SDS. At the SDS concentrations of 0.1−0.8 mM, only the peak corresponding to dye aggregates (peak 1) can be

observed. However, from a concentration of 10 mM (above the CMC), it shows a bimodal distribution, where the scattered intensity of dye aggregates has an obvious decrease. The peak 2 indicating the surfactant micelle appears in a size range of 1−5 nm (Tab. 4-8). The DLS results indicate that Acid blue 113 interacts with SDS above the CMC.

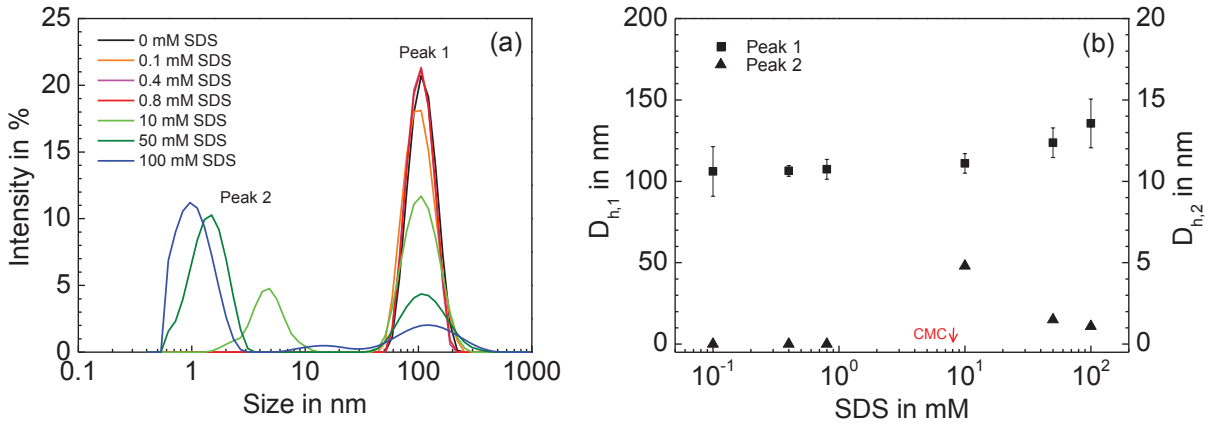

Figure 4-16 (a) Intensity-weighted size distributions of the mixtures of Acid blue 113 with SDS at different surfactant concentrations. (b) Peak size for the peak 1 ($D_{h,1}$) and peak 2 ($D_{h,2}$) displayed in (a) depending on SDS concentrations. The concentration of Acid blue 113 is 0.009 mM in all solutions. The peaks in the size distribution are indicated as peak 1 (right) and peak 2 (left), which relate to the dye aggregate and the surfactant micelle respectively. At surfactant concentrations above the CMC, the size of dye aggregate increases with increasing SDS concentrations but the intensity of dye aggregate decreases.

Table 4-8 Hydrodynamic diameter $D_{h,z}$ (Z-average), PDI and peak sizes $D_{h,i}$ in the size distribution for the system Acid blue 113-SDS analyzed by DLS measurements.

SDS/Acid blue 113 in mM/mM	Z-average ($D_{h,z}$) in nm	PDI	Peak 1 ($D_{h,1}$) in nm	Peak 2 ($D_{h,2}$) in nm
0/0.009	152.8 ± 1.3	0.225 ± 0.002	118.1 ± 0.1	-
0.1/0.009	124.1 ± 1.0	0.205 ± 0.011	106.1 ± 15.2	-
0.4/0.009	146.1 ± 11.2	0.232 ± 0.027	106.4 ± 3.3	-
0.8/0.009	138.6 ± 7.1	0.226 ± 0.026	107.4 ± 6.2	-
10/0.009	87.5 ± 8.8	0.146 ± 0.032	111.0 ± 6.0	4.8 ± 0.1
50/0.009	22.0 ± 22.2	0.251 ± 0.117	123.7 ± 9.1	1.5 ± 0.1
100/0.009	4.4 ± 0.1	0.239 ± 0.071	135.6 ± 15.0	1.1 ± 0

As it can be seen in Figure 4-16 (b), below the CMC of SDS (~8 mM) the size of dye aggregate is independent of the concentration of SDS. Above the CMC, the size of dye aggregate increases with increasing SDS concentrations and the intensity of dye aggregate decreases. As it can be seen, the aggregate in the range of more than 100 nm was still detected even at the SDS

concentrations of above 50 mM. It is known from the UV-Vis spectroscopic study that, at such high SDS concentrations the interaction of dye with surfactant is saturated and the high molar ratio of SDS to the dye (444:1) indicates the weak dye-surfactant interaction (see Section 4.1.2).

Hence, the aggregate over 100 nm at high SDS concentrations may relate to the dye aggregate or large nonspherical SDS micelle. Because of the weak dye-surfactant interaction, the dye aggregates may be not completely dissolved in surfactant micelles. On the other hand, it was found that the formation of SDS micelles shows different phases with increasing concentrations, exhibiting various shapes of surfactant micelles such as cylindrical surfactant aggregates.[101] This nonspherical structure of micelles at high SDS concentrations can result in an increased or overestimated micelle size determined by DLS, corresponding to the peak 1. Therefore, the interaction between SDS and Acid blue 113 needs to be further studied and quantified by other methods.

4.2.4 Acid blue 113 + PVPVI

The intensity-weighted size distributions of the mixtures of Acid blue 113 and PVPVI are shown in Figure 4-17. As seen, the intensity of peak 1 for dye aggregate decreases with increasing polymer concentrations. Until to a polymer concentration of 0.1 mM peak 1 was not observed in the size distribution.

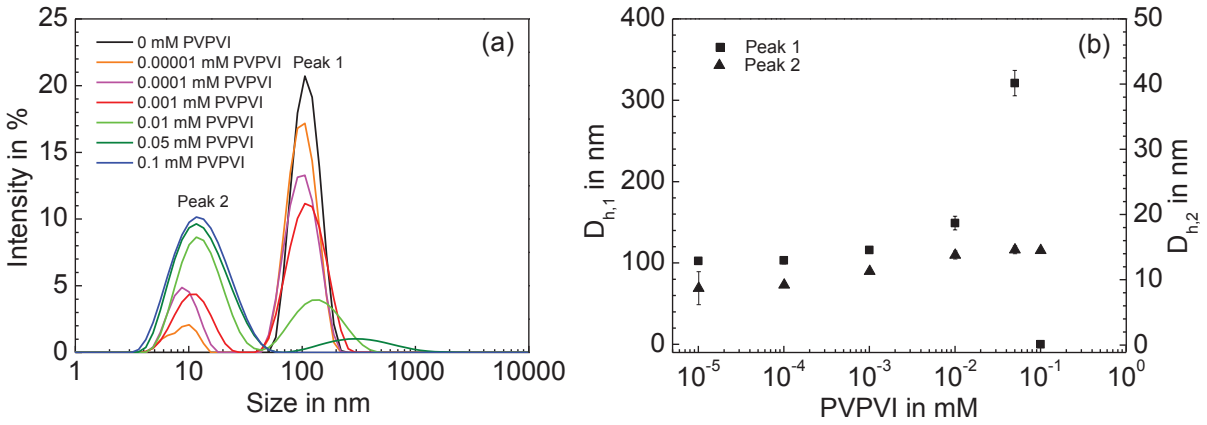

Figure 4-17 (a) Intensity-weighted size distributions of the mixtures of Acid blue 113 with PVPVI at different polymer concentrations. (b) Peak size for the peak 1 ($D_{h,1}$) and peak 2 ($D_{h,2}$) displayed in (a) depending on PVPVI concentrations. The concentration of Acid blue 113 is 0.009 mM in all solutions. The peaks in the size distribution are indicated as peak 1 (right) and peak 2 (left), which relate to the dye aggregate and the polymer respectively. From a polymer concentration of 0.001 mM, the size of dye aggregate increases with increasing polymer concentrations. Until to a polymer concentration of 0.1 mM the peak for dye aggregates was not observed, indicating the formation of dye-polymer complexes.

Table 4-9 Hydrodynamic diameter $D_{h,z}$ (Z-average), PDI and peak sizes $D_{h,i}$ in the size distribution for the system Acid blue 113-PVPVI analyzed by DLS measurements.

PVPVI/Acid blue 113 in mM/mM	Z-average ($D_{h,z}$) in nm	PDI	Peak 1 ($D_{h,1}$) in nm	Peak 2 ($D_{h,2}$) in nm
0/0.009	150.8 ± 6.1	0.225 ± 0.008	111.4 ± 1.0	-
0.00001/0.009	128.9 ± 21.4	0.200 ± 0.034	102.6 ± 2.5	8.7 ± 2.5
0.0001/0.009	94.4 ± 3.2	0.176 ± 0.032	103.2 ± 4.4	9.2 ± 0.3
0.001/0.009	82.3 ± 23.0	0.196 ± 0.050	115.9 ± 1.6	11.3 ± 0
0.01/0.009	18.1 ± 0.1	0.526 ± 0.002	149.1 ± 8.3	13.8 ± 0.6
0.05/0.009	12.7 ± 0	0.297 ± 0.004	321.1 ± 15.6	14.6 ± 0.6
0.1/0.009	11.7 ± 0	0.223 ± 0.007	-	14.5 ± 0.3

As shown in Table 4-9, from a polymer concentration of 0.001 mM, the size of dye aggregate (peak 1, $D_{h,1}$) increases with increasing polymer concentrations. The size change of dye aggregate may be due to the binding of the dye with the polymer, resulting in the change of conformation of the dye aggregate. In the presence of Acid blue 113 the size of PVPVI (peak 2, $D_{h,2}$) increases with increasing polymer concentrations. From 0.05 mM of PVPVI, the polymer size is not changed with increasing polymer concentrations. The size of polymer in the presence of dye is slightly greater than that in the absence of dye for $0.01-0.1$ mM (peak size: $12.9-13.7$ nm).

At 0.1 mM of PVPVI the peak for dye aggregate cannot be seen in the size distribution, indicating the dissolution of dye aggregates in polymer solution due to the dye-polymer interaction, where the molecular ratio of the polymer to the dye is about 11:1. This mole ratio of the polymer to dye is greater than that determined in the UV-Vis spectroscopic study by one order of magnitude. On the one hand, the ratio of the polymer to dye obtained by UV-Vis spectroscopy implies the binding property at an initial saturation, which can be changed depending on dye and polymer concentrations. On the other hand, because there may be a correlation between the decreased amount of dye aggregates remaining in solution and the formation of dye-polymer complex, all resulting in the decrease of intensity of the peak 2 in the binary system. Hence, the quantitative analysis of the system in DLS study is considered more complicated in comparison with that by UV-Vis spectroscopy.

4.2.5 $C_{12\text{-}18}E_7$ + PVPVI

The result of the DLS measurement on the mixtures of PVPVI and $C_{12\text{-}18}E_7$ is shown in Figure 4-18. The mixture of PVPVI with the nonionic surfactant $C_{12\text{-}18}E_7$ shows a monomodal distribution. At the concentration near to the CMC of $C_{12\text{-}18}E_7$, there is a small increase of size. From the point of 1 mM $C_{12\text{-}18}E_7$ the size keeps growing with increasing surfactant concentrations.

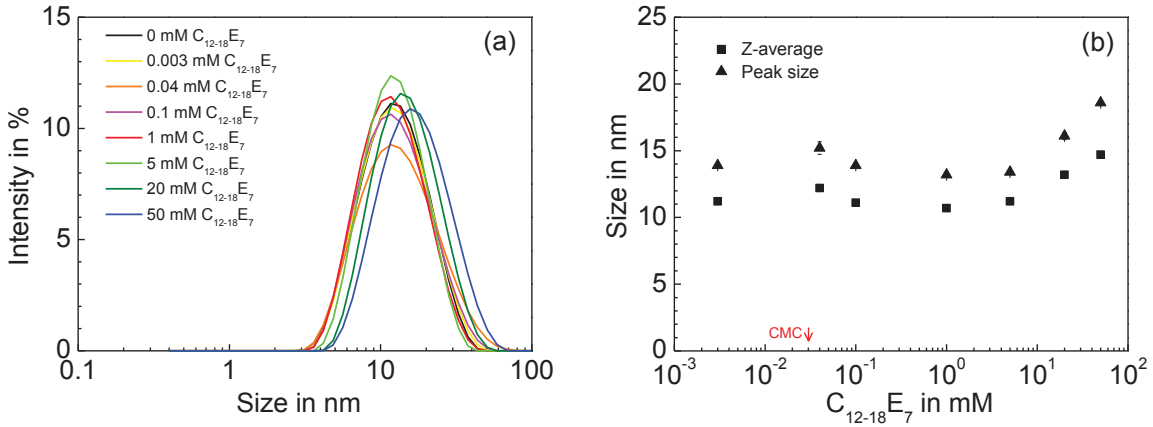

Figure 4-18 (a) Intensity-weighted size distributions of the mixtures of PVPVI with $C_{12\text{-}18}E_7$ at different surfactant concentrations. (b) Size of the mixture presented as the Z-average and peak size depending on $C_{12\text{-}18}E_7$ concentrations. The concentration of PVPVI is 0.1 mM in all solutions. There was only one peak observed at all surfactant concentrations. The $D_{h,z}$ and peak size value below the CMC are related to the polymer and those above the CMC correspond mostly to surfactant micelles. Therefore, no interaction between $C_{12\text{-}18}E_7$ and PVPVI in solution was observed in the DLS study.

Table 4-10 Hydrodynamic diameter $D_{h,z}$ (Z-average), PDI and peak size in the size distribution for the system $C_{12\text{-}18}E_7$-PVPVI analyzed by DLS measurements.

$C_{12\text{-}18}E_7$/PVPVI in mM/mM	Z-average ($D_{h,z}$) in nm	PDI	Peak size in nm
0/0.1	11.0 ± 0	0.181 ± 0.004	13.7 ± 0.1
0.003/0.1	11.2 ± 0.2	0.192 ± 0.023	13.9 ± 0.1
0.04/0.1	12.2 ± 0	0.275 ± 0.025	15.2 ± 0.5
0.1/0.1	11.1 ± 0	0.194 ± 0.011	13.9 ± 0.1
1/0.1	10.7 ± 0.2	0.171 ± 0.003	13.2 ± 0.2
5/0.1	11.2 ± 0	0.148 ± 0	13.4 ± 0
20/0.1	13.2 ± 0.1	0.168 ± 0.005	16.1 ± 0.3
50/0.1	14.7 ± 0	0.188 ± 0.001	18.6 ± 0.1

It is known that the size ($D_{h,z}$) of $C_{12\text{-}18}E_7$ micelles in the absence of polymer increases from 10.4 nm to 14.3 nm with increasing concentrations from 1 mM to 50 mM. The $D_{h,z}$ value of 0.1 mM PVPVI is 11 nm, which is in the size range of surfactant micelles of $C_{12\text{-}18}E_7$ alone. Below the CMC of $C_{12\text{-}18}E_7$, the peak detected with the size of about 11 nm is related to the polymer. As the concentration of $C_{12\text{-}18}E_7$ is above the CMC, surfactant micelles form and the size of micelle increases with increasing surfactant concentrations. Because the size of 0.1 mM PVPVI and of $C_{12\text{-}18}E_7$ above the CMC are in the same size range, one may expect that the size distribution of the mixture of $C_{12\text{-}18}E_7$ with PVPVI shows a monomodal distribution (one peak). Therefore, if there is an interaction between $C_{12\text{-}18}E_7$ and PVPVI, it was not seen by DLS measurements.

4.2.6 SDS + PVPVI

In contrast to the size distribution for the system of $C_{12\text{-}18}E_7$-PVPVI, the mixture of PVPVI with the anionic surfactant SDS shows a bimodal distribution (Fig. 4-19). The right peak (peak 1) in the size distribution indicates the polymer and the left (peak 2) the surfactant micelle. As presented in Table 4-11, 0.1 mM PVPVI has a peak size of 13.7 nm (peak 1, $D_{h,1}$). At low SDS concentrations far below the CMC (0.1 – 0.8 mM), the peak size of polymer has a slight increase to 15.3 nm. As the SDS concentration increases to 6 mM, an obvious size growth of the polymer to about 32 nm was observed.

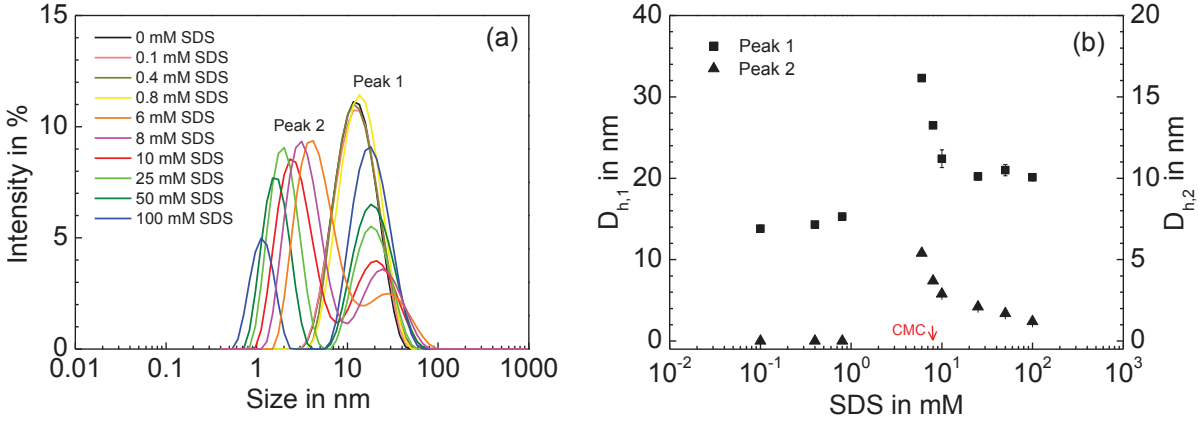

Figure 4-19 (a) Intensity-weighted size distributions of the mixtures of PVPVI with SDS at different surfactant concentrations. (b) Peak size for the peak 1 ($D_{h,1}$) and peak 2 ($D_{h,2}$) displayed in (a) depending on SDS concentrations. The concentration of PVPVI is 0.1 mM in all solutions. The peaks in the size distribution are indicated as peak 1 (right) and peak 2 (left), which relate to the polymer and the surfactant micelle respectively. At low SDS concentrations (< CMC), the polymer may have an expanded conformation with bound surfactants corresponding to an increased polymer size. With further increasing surfactant concentrations to above the CMC, surfactants bound with the polymer form micelles resulting in the size decrease of the surfactant-polymer complex. At saturation the size of surfactant-polymer complex is not changed by increasing surfactant concentrations, which is greater than that of polymer alone.

Table 4-11 Hydrodynamic diameter $D_{h,z}$ (Z-average), PDI and peak sizes $D_{h,i}$ in the size distribution for the system SDS-PVPVI analyzed by DLS measurements.

SDS/PVPVI in mM/mM	Z-average ($D_{h,z}$) in nm	PDI	Peak 1 ($D_{h,1}$) in nm	Peak 2 ($D_{h,2}$) in nm
0/0.1	11.0 ± 0	0.181 ± 0.004	13.7 ± 0.1	-
0.1/0.1	11.1 ± 0.2	0.178 ± 0.006	13.8 ± 0.4	-
0.4/0.1	11.6 ± 0.1	0.184 ± 0.003	14.3 ± 0.3	-
0.8/0.1	12.4 ± 0.1	0.175 ± 0.002	15.3 ± 0.2	-
6/0.1	5.3 ± n.a.	0.275 ± n.a.	32.3 ± n.a.	5.4 ± n.a.
8/0.1	4.7 ± n.a.	0.271 ± n.a.	26.5 ± n.a.	3.7 ± n.a.
10/0.1	4.4 ± 0.1	0.272 ± 0.001	22.4 ± 1.1	2.9 ± 0.1
25/0.1	4.5 ± 0.1	0.291 ± 0.003	20.2 ± 0.4	2.1 ± 0.1
50/0.1	5.8 ± 0.2	0.343 ± 0.006	21.0 ± 0.7	1.7 ± 0
100/0.1	9.3 ± 0.1	0.412 ± 0.004	20.1 ± 0.2	1.2 ± 0

At the SDS concentrations above the CMC, the size of polymer begins to decrease with increasing surfactant concentrations, where the SDS micelles can also be detected (peak 2, $D_{h,2}$). At high surfactant concentrations (25−100 mM) the polymer size is not dependent on surfactant concentrations, corresponding to a size of about 20 nm.

The DLS study shows that SDS interacts with PVPVI in solution, which further evidences the SDS-PVPVI interaction in solution confirmed by UV-Vis spectroscopic studies for ternary systems (see Section 4.1.5). The dependence of the polymer size on surfactant concentrations may originate from a change in the conformation of the surfactant-polymer complex, as reported by Liu et al.[102] using coarse-grained molecular dynamics simulations. It is suggested that SDS begins to interact with PVPVI at low SDS concentrations (< CMC), corresponding to a relative expanded polymer chain with bound surfactant monomers, the size of which increases with increasing surfactant concentrations. As the SDS concentration reaches the CMC, surfactants bound to the polymer chain form micelles resulting in a size decrease to some extent. Until to the saturation of surfactant-polymer complexes, the size of the complex is not changed with increasing surfactant concentrations, which is greater than that of the polymer alone. In the comparable system of SDS-PVP (PVP: 40000 g/mol and 360000 g/mol), a molecular ratio of SDS to PVP of 120−150:1 studied by fluorescence probe techniques[103] and a ratio of about 61:1 by surface tension measurements[104] are found respectively. That means one PVP polymer

chain may be bound with up to 2 surfactant micelles in solution, with the aggregation number[81] of 60 for SDS.

4.3 Interaction at the air-solution interface by surface tension measurement

In solution, an interaction between the anionic surfactant SDS and the DTI polymer PVPVI was found both in the UV-Vis spectroscopic and DLS study. To confirm the interaction between surfactant and polymer, studies of the surfactant-polymer interaction at the air-solution interface by surface tension measurements were carried out. In addition, the surface activity of the DTI polymer and the dye was also evaluated by surface tension measurements.

4.3.1 Single components at the air-solution interface

Figure 4-20 shows the surface tension as a function of concentration for single surfactants, DTI polymer and dye dissolved in water.

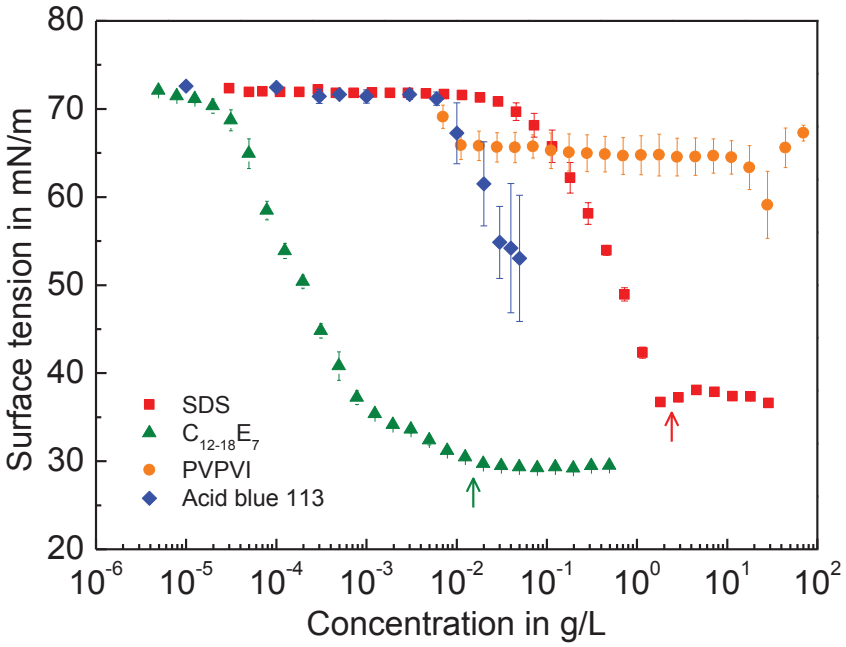

Figure 4-20 Surface tension as a function of the concentration for single surfactants, the DTI polymer and dye. SDS and $C_{12\text{-}18}E_7$ are surface-active and have well-defined CMC as indicated by arrows, which are 8 mM and 0.03 mM respectively. PVPVI is not surface-active and Acid blue 113 is weakly surface-active at high concentrations.

The anionic surfactant SDS has a well-defined CMC of 8 mM as indicated in the surface tension curve (red arrow), which agrees well with the literature value[105]. The nonionic surfactant $C_{12\text{-}18}E_7$ gives a CMC value of 0.03 mM (green arrow), which is lower than that of pure $C_{12}E_7$ reported by other authors (0.07−0.08 mM)[82,87]. This may be due to the homologues

with the alkyl chains of more than 12 C in the used $C_{12\text{-}18}E_7$, since B. Folmer[87] found that the technical surfactant $C_{12\text{-}15}E_7$ has a lower CMC of 0.016 mM than that of pure $C_{12}E_7$. The surface tension reduction can obviously be seen in both surfactants with increase of surfactant concentrations. The minimal surface tensions of SDS and $C_{12\text{-}18}E_7$ are 36 mN/m and 29 mN/m respectively.

In contrast, the DTI polymer PVPVI is not surface-active, where the surface tension is generally in the range of 63 − 69 mN/m. The surface tension of the aqueous dye solution begins to decrease at the concentration up to 0.01 g/L (0.015 mM). At the highest dye concentration measured, the surface tension is lowered to about 53 mN/m. Hence, Acid blue 113 is weakly surface-active at high concentrations. Such weak surface-activity was also observed in the study of some azo dyes with sulfonate groups.[106] If it is not otherwise stated in this work, the concentration of the dye in binary systems is 0.006 g/L (0.009 mM), at which the dye is considered not surface-active.

The surface tension curve of surfactants allows the determination of the molecular area (see Section 2.2.1). The molecular area of SDS and $C_{12\text{-}18}E_7$ at the air-water interface are 79 $Å^2$ and 63 $Å^2$ respectively, as presented in Table 4-12. These results are in very good agreement with the value for SDS determined by Adane[107] (~80 $Å^2$) and that for monodisperse $C_{12}E_7$ by Folmer et al.[87] (66 $Å^2$). The CMC values obtained from surface tension measurements are compared with those from the UV-Vis spectroscopic study (see Section 4.1.1 and 4.1.2), as seen in Table 4-12. For both surfactants, the CMC value from the surface tension measurement is in good agreement with that from the UV-Vis spectroscopic study.

Table 4-12 The CMC and molecular area of SDS and $C_{12\text{-}18}E_7$ determined by surface tension measurements and the CMC of SDS and $C_{12\text{-}18}E_7$ determined by UV-Vis spectroscopic studies.

Surfactant	Surface tension measurement		UV-Vis spectroscopic study
	CMC in mM	Molecular area in $Å^2$	CMC in mM
SDS	8	79	7
$C_{12\text{-}18}E_7$	0.03	63	0.02

4.3.2 $C_{12\text{-}18}E_7$-PVPVI at the air-solution interface

Figure 4-21 shows the surface tension curve of the mixture of $C_{12\text{-}18}E_7$ and PVPVI compared with the curve of $C_{12\text{-}18}E_7$ alone. In mixture of $C_{12\text{-}18}E_7$ with 0.5 mg/L PVPVI, the surface

tension curve of the mixture is almost overlapped with the curve of single $C_{12\text{-}18}E_7$. Based on the surface tension measurement, it suggests that there is no interaction between $C_{12\text{-}18}E_7$ and PVPVI at the air-solution interface.

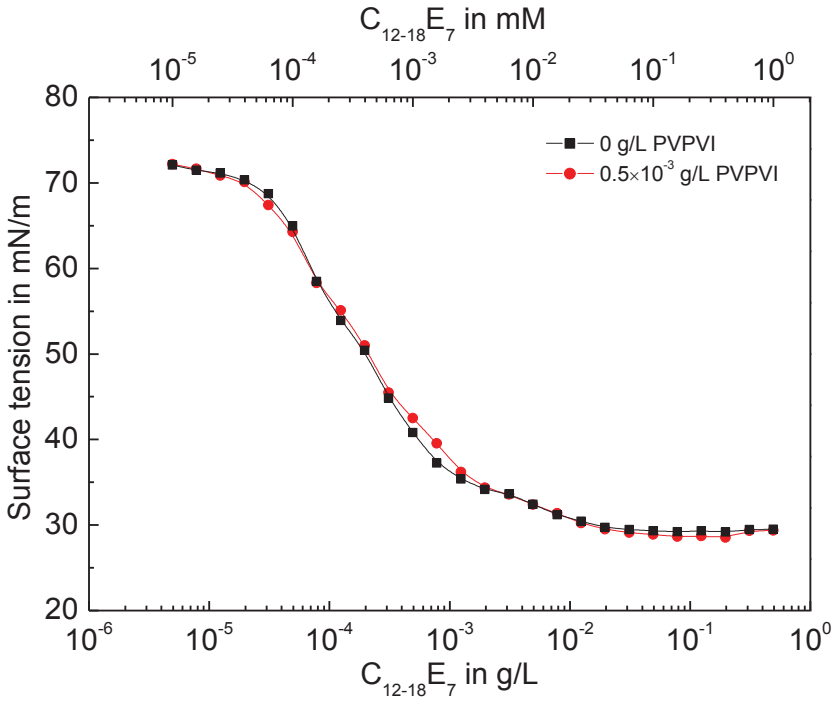

Figure 4-21 Surface tension as a function of $C_{12\text{-}18}E_7$ concentrations with and without PVPVI. All solid lines are referred to as guidelines. The surface tension curve for the mixture is almost overlapped with that of $C_{12\text{-}18}E_7$ alone, indicating no interaction between $C_{12\text{-}18}E_7$ and PVPVI at the air-solution interface.

As is known, the association of ionic surfactants with oppositely charged polyelectrolytes is considered to stabilize the formation of surfactant micelles by lowering the unfavorable repulsive interaction between the headgroups of ionic surfactants.[108] Therefore, this surfactant-polymer interaction is generally not observed between the nonionic surfactant and polymer electrolyte, because the stabilization of micelles by addition of polyelectrolytes is not effective for nonionic surfactants, which exhibit no unfavorable electrostatic repulsion between headgroups upon micellization.

4.3.3 SDS-PVPVI at the air-solution interface

The surface tension curves of SDS-PVPVI mixtures are shown in Figure 4-22 in dependence of SDS concentrations, where the curve of SDS alone is also presented. Compared with the SDS, the behavior of SDS in mixture with 0.1 mg/L PVPVI is not markedly changed. In the presence of 0.3 mg/L PVPVI, the surface tension of the mixture drops at a low SDS concentration (0.025 mM). From a point of 0.1 mM SDS, the surface tension is not so much dependent on

surfactant concentrations. As the surfactant concentration is above 0.6 mM, the surface tension decreases again with increasing surfactant concentrations until to the CMC of SDS (8 mM).

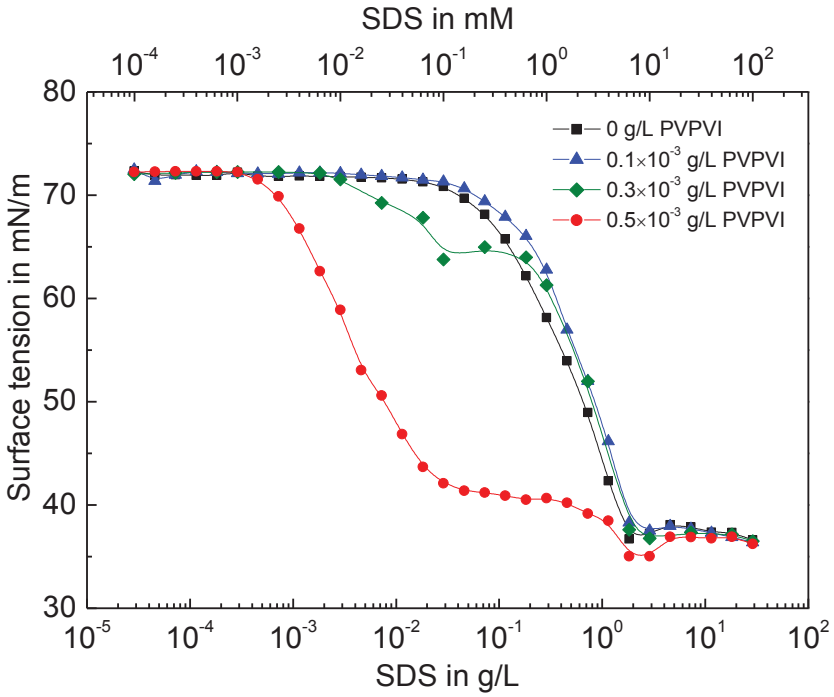

Figure 4-22 Surface tension as a function of SDS concentrations with and without PVPVI. All solid lines are referred to as guidelines. In the mixture of SDS with 0.1 mg/L PVPVI, no obvious change in the surface tension curve was observed in comparison with SDS alone. In the presence of 0.3 mg/L and 0.5 mg/L PVPVI, the surface tension decreases at low SDS concentrations, which may result from the association of the surfactant and the polymer at the air-water interface. Additionally, at high SDS concentrations (> CMC) no influence of the polymer on surface tension of the surfactant-polymer mixture was observed.

In the presence of 0.5 mg/L PVPVI, a substantial decrease of surface tension of the mixture begins at the very low SDS concentration of about 0.0025 mM. From an SDS concentration of approximately 0.16 mM, the surface tension curve shows a plateau region, where a distinguishable change in surface tension was not observed with increased surfactant concentrations. At the SDS concentration of more than 1 mM, the surface tension decreases again until to a minimum. Above the CMC of SDS the surface tension remains almost constant at the same level as in SDS alone.

The studies of surface tension for the SDS-PVPVI mixtures indicate a surfactant-polymer interaction at the air-solution interface. In the presence of the polymer, the surface tension reduction at very low surfactant concentrations may be due to the initial adsorption of surfactant-polymer complex at the air-water interface.[108–113] Additionally, no influence of the polymer on surface tension at high SDS concentrations (> CMC) was observed in the SDS-

PVPVI mixtures. Unlike other studies of surfactant-polymer interactions,[108,109,114] no phase separation (precipitation) was observed in surface tension measurements for the SDS-PVPVI system. This may be due to the very low polymer concentration in the studied SDS-PVPVI mixtures.

Nagarajia[115] gave different models for the surfactant-polymer interaction, which is dependent on the structure of surfactant and polymer as well as on the interaction between the solute and solvent. On the other hand the composition of the surfactant-polymer complex is affected by the charge ratio of the system (electroneutrality).[102] This indicates that each polymer may be bound with a specific amount of surfactants, resulting in the charge balance of the polyelectrolyte by bound surfactants. Therefore, the electrostatic interaction may play a very important role in the surfactant-polymer interaction.

It is therefore assumed that the association of SDS with PVPVI at the air-water interface is induced by the electrostatic attraction, which causes the surface tension reduction of the mixture at lower surfactant concentrations, in comparison with that of SDS alone. In addition, the DLS study of the mixture of SDS and PVPVI implies that at high SDS concentrations above the CMC the surfactant-polymer complex is mainly driven by the hydrophobic interaction between surfactants (see Section 4.2.6). Hence, besides the electrostatic interaction the hydrophobic interaction may also contribute to the surfactant-polymer association for the SDS-PVPVI system.

4.4 Adsorption of Acid blue 113 at the carbon black-solution interface

In order to understand the interaction between the dye Acid blue 113 and a solid surface from aqueous solutions, the adsorption of the dye on the nonpolar carbon black surface was studied. The adsorbed amounts of the dye and the dye in mixture with surfactant on carbon black are determined to provide quantitative information about the adsorption of the dye at the solid-liquid interface, supplementing the study of adsorption structures on graphite by AFM.

4.4.1 Adsorption isotherm of Acid blue 113 on carbon black

To evaluate the influence of the amount of adsorbent on the adsorption isotherm of Acid blue 113 at carbon black-water interfaces, two adsorption isotherms for different amounts of carbon black are shown in Figure4-23. The amount of adsorbent is 0.3 g/L and 0.4 g/L respectively and

the contact time is 2 h. The original dye concentration varies from 0.002 g/L (~0.003 mM) to 0.06 g/L (~0.088 mM).

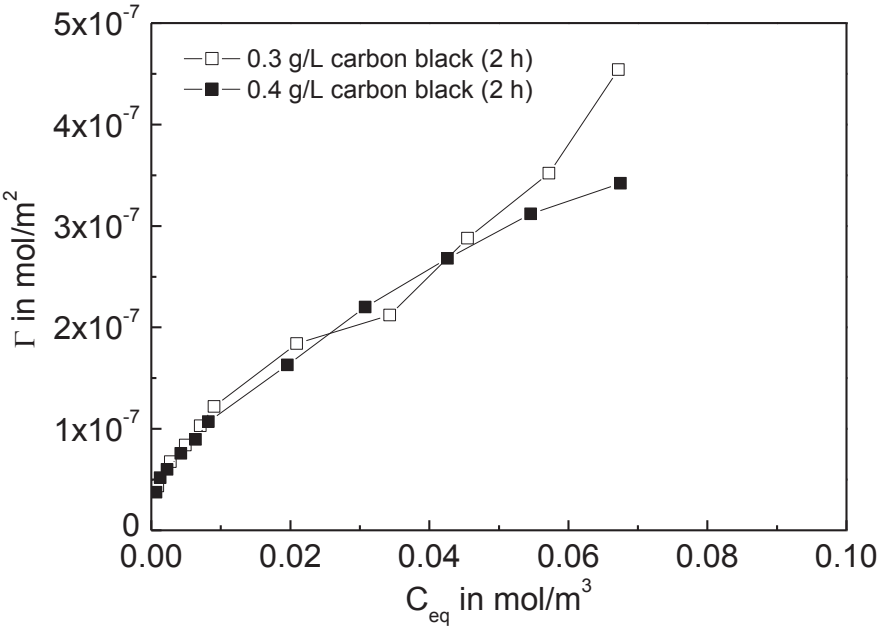

Figure 4-23 Adsorbed amounts Γ of Acid blue 113 on carbon black as a function of the equilibrium dye concentration C_{eq} with respect to different amounts of adsorbent as indicated. Generally, the adsorbed amount of dye increases with increasing dye concentrations until to the solubility limit of the dye in water.

In general, the adsorbed amount of dye on carbon black increases with increasing original dye concentrations. The adsorption curve is not simply linear and shows no distinguishing saturation (plateau) at certain equilibrium. This can be attributed to the solubility of the dye in water, which is considered to be less than 0.08 g/L through the observation of the dye absorption spectrum by UV-Vis spectroscopy. That means the determination of the adsorbed amount of the dye at a higher original dye concentration cannot be achieved in this measurement. The amount of adsorbent of 0.4 g/L was used for further studies of dye adsorption at the carbon black-solution interface.

As seen in Figure 4-24, the adsorbed amount of Acid blue 113 at the carbon black-water interface increases with increasing equilibrium concentrations of the dye. It was observed that the obvious variation of experimental data was found at the equilibrium concentration above 0.01 mol/m^3 (0.01 mM). This can be due to the dispersion effect for the carbon black caused by the dye, since the dye does show surface activity at concentrations above 0.015 mM in surface tension measurements (ref. Fig. 4-20). In order to evaluate the adsorption isotherm, two adsorption isotherm models (ref. Section 2.2.2) are applied to fit the experimental data. The

fitting parameters for the Langmuir and Freundlich model are presented in Table 4-13 respectively.

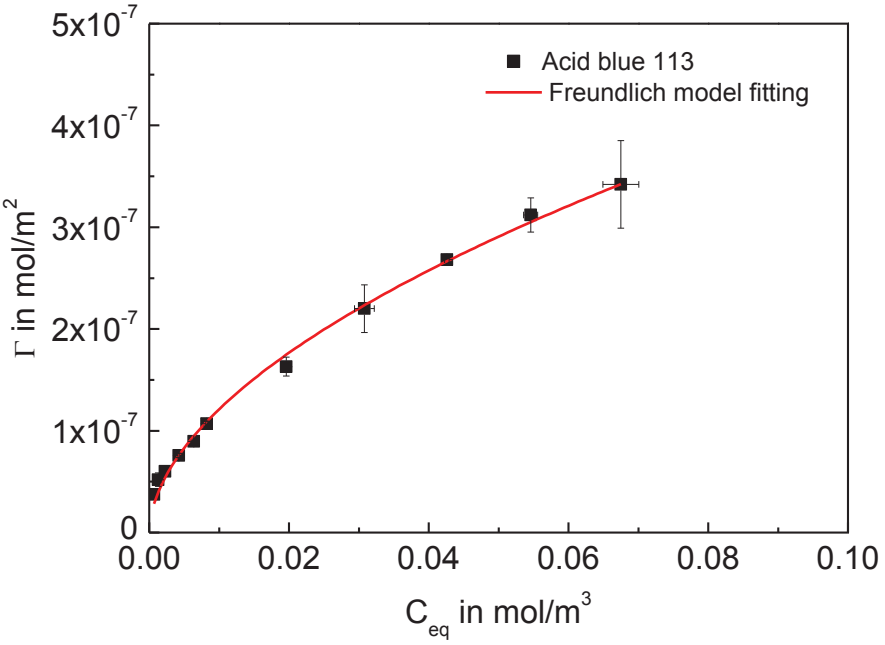

Figure 4-24 Plot of the adsorbed amount Γ of Acid blue 113 on carbon black versus the equilibrium dye concentration C_{eq}. The dye was dissolved in water. The carbon black was 0.4 g/L and the contact time was 2 h. Fitting of the adsorption isotherm by the Freundlich model is completed using Origin, indicated as the red curve.

Table 4-13 Fitting parameters obtained by the Langmuir and Freundlich isotherm model for the adsorption of Acid blue 113 at the carbon black-water interface.

Isotherm model	**Parameter**		**R^2**
Langmuir	Γ_{max} in mol/m^2	$1.7 \cdot 10^{-7}$	0.8652
	k in m^3/mol	354	
	A_{ad} in nm^2	9.6	
Freundlich	k_F	$1.5 \cdot 10^{-6}$	0.9955
	n	0.54	

Γ_{max}: the maximal adsorbed amount per unit area at a monolayer.

A_{ad}: the molecular area of the adsorbate at a monolayer.
k: the Langmuir constant.
k_F and n: the Freundlich constants.
R^2: the coefficient of determination.

As seen in Table 4-13, the coefficient of determination R^2 for the Langmuir and Freundlich isotherm is 0.8652 and 0.9955 respectively. Obviously, the experimental data are more suitably described by the Freundlich model, which is a purely empirical model indicating a heterogeneous adsorption. Additionally, the constant n describing the intensity of adsorption is less than 1, which indicates a favorable adsorption process where the heat of adsorption decreases in magnitude with increasing adsorbed amounts on surface.[116–120] Moreover, the high value of the Langmuir constant k also predicts a high affinity of the dye for the carbon black.

Acid blue 113 forms aggregates in aqueous solution, which was verified by the study using DLS as presented in Section 4.2.1. The adsorption of Acid blue 113 on carbon black may take place in two ways: the one-step adsorption and the two-step adsorption. In one-step adsorption, the substrate surface is adsorbed by dye aggregates, which diffuse directly from the bulk phase onto the surface. In this case, the adsorbed amount of dye is dependent on the aggregate size and mass with respect to dye concentrations. The DLS study suggests that the size of dye aggregates increases with increasing dye concentrations, as a result, one may expect that the adsorbed amount of dye also increases with increasing original dye concentrations. In two-step adsorption, it is assumed that the dye molecules adsorb firstly on the surface at specific energetically favorable sites, from which dye aggregates form due to the intermolecular interaction. Therefore, in this case the adsorption in the first step is only due to the dye-substrate interaction and in the second step to the dye-dye interaction. Both assumptions reflect an interaction between the dye and the carbon black.

The adsorption process of dye on surfaces can be affected by the nature of substrates. Porter[121] found that the adsorption of direct and acid dyes on the cellulose and cotton implies the Langmuir model. The adsorption of Acid blue 113 on waste rubber tire and activated carbon is better described by the Langmuir model,[28] while the adsorption isotherm of Acid blue 113 on activated red mud[122] indicates the Freundlich adsorption model. However, in these reports no interpretation for the adsorption mechanism of dyes was given. It can be assumed that the adsorption of dyes on surfaces is specific dependent on the interaction between the dye and the substrate, showing different adsorption isotherm models.

4.4.2 Adsorption isotherm of Acid blue 113 in mixture with SDS on carbon black

To know the influence of surfactants on the adsorption of the dye on surfaces, the adsorption of the mixture of the dye with surfactant was studied. It is known that both the nonionic surfactant

$C_{12\text{-}18}E_7$ and the anionic surfactant SDS can adsorb on the carbon black, whose adsorption isotherms were shown by M. Jabnoun as seen in Figure 4-25 respectively.[13(p. 53)]

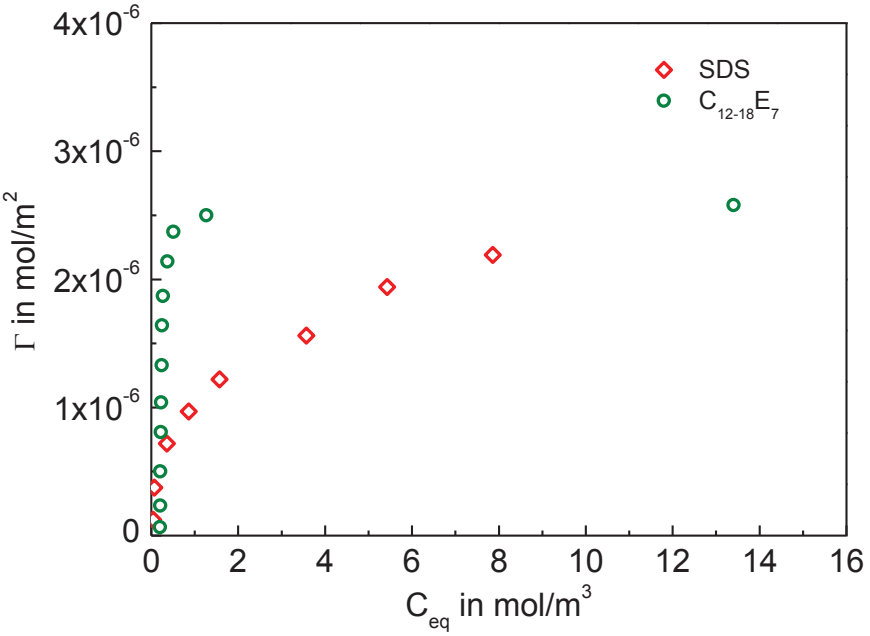

Figure 4-25 Adsorption isotherms of the anionic surfactant SDS and nonionic surfactant $C_{12\text{-}18}E_7$ at the carbon black-water interface.[13(p. 53)]

The adsorption isotherms indicate that $C_{12\text{-}18}E_7$ adsorbs much more strongly and at lower surfactant concentrations on the carbon black than SDS.[13(p. 102)] Furthermore, it was found in AFM studies that $C_{12\text{-}18}E_7$ has a higher affinity to graphite surface than SDS.[13(p. 127)] Therefore, in order to better evaluate the influence of surfactants on the adsorption of the dye on solid surfaces and compare the results on carbon black with AFM studies on graphite, the binary system of Acid blue 113 and SDS was selected for the further study of adsorption of the dye in mixture with surfactants.

Adsorption of dye in mixture with 10 mM (> CMC) SDS on carbon black

The adsorption isotherm of the dye in mixture with the anionic surfactant SDS at the carbon black-water interface was investigated. Acid blue 113 was dissolved in the SDS solution of 10 mM (> CMC) and the measurement was conducted under the same condition as stated in Figure 4-24. As can be seen in Figure 4-26, the adsorption behavior of Acid blue 113 on carbon black is changed in the presence of SDS. The adsorption isotherm of the dye in mixture with SDS implies the Langmuir adsorption model.

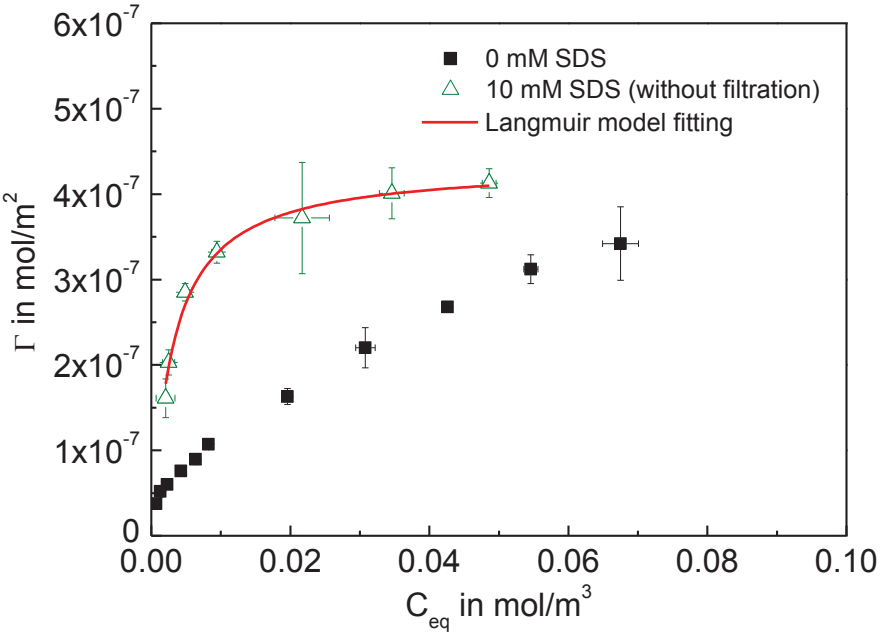

Figure 4-26 Plot of the adsorbed amount Γ of Acid blue 113 on carbon black versus the equilibrium dye concentration C_{eq}. The dye was dissolved in 10 mM SDS (above the CMC) solution. The carbon black was 0.4 g/L and the contact time was 2 h. Fitting of the adsorption isotherm by the Langmuir model is completed using Origin, indicated as the red curve.

In order to diminish the variation of experimental data of repeated measurements as seen in Figure 4-26, the adsorption experiments of dye in mixture with SDS were conducted with filtration, where all solutions were filtered after reaction with carbon black prior to centrifugation (see Section 3.2.5). In Figure 4-27, it can be confirmed that filtration has almost no influence on the adsorption isotherm of the dye in mixture with 10 mM SDS, while the variation of the experimental data is greatly decreased compared to that without filtration. This is because most carbon black dispersed was filtrated out of the solution and the remaining dispersion of carbon black was much better separated from the remaining dye solution after centrifugation, resulting in the decreased variation for each data point in the UV-Vis measurement.

In mixture with 10 mM SDS with filtration, the adsorption isotherm of the dye on carbon black remains the Langmuir model as indicated fitting curve in Figure 4-27. The maximal adsorbed amount of the dye is $4.2 \cdot 10^{-7}$ mol/m^2 and the area per dye molecule adsorbed is 4.0 nm^2 (Tab. 4-14). In the mixture of the dye with 10 mM SDS, at low dye concentrations the adsorption increases evidently with increasing dye concentrations. As the dye equilibrium concentration is above 0.01 mol/m^3, the adsorbed amount increases to a less extent and tends to reach a maximum. For all original dye concentrations, the adsorption of dye in the presence of SDS is

greater than that of the dye alone. The high value of the Langmuir constant k (522 m^3/mol) indicates a strong interaction between the dye and the surface.

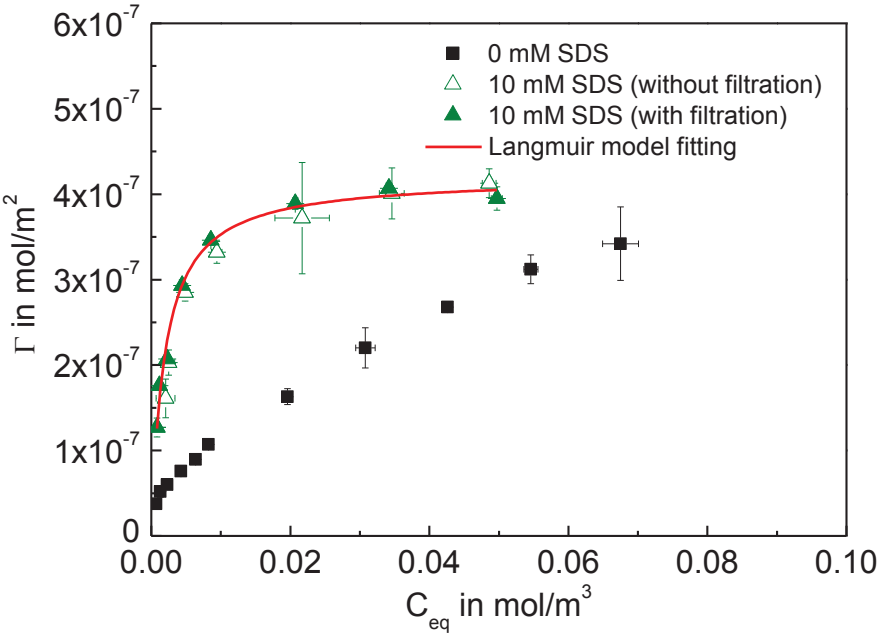

Figure 4-27 Plot of the adsorbed amount Γ of Acid blue 113 on carbon black versus the equilibrium dye concentration C_{eq}. The dye was dissolved in 10 mM SDS (above the CMC) solution. The carbon black was 0.4 g/L and the contact time was 2 h. The remaining dye solution was filtrated prior to centrifugation. Fitting of the adsorption isotherm for the mixture with filtration by the Langmuir model is completed using Origin, indicated as the red curve.

Table 4-14 Fitting parameters obtained by the Langmuir and Freundlich isotherm model for the adsorption of Acid blue 113 at the carbon black-water interface in the presence of 10 mM SDS (above the CMC) with filtration.

Isotherm model	**Parameter**		**R^2**
Langmuir	Γ_{max} in mol/m^2	$4.2 \cdot 10^{-7}$	0.9865
	k in m^3/mol	522	
	A_{ad} in nm^2	4.0	
Freundlich	k_F	$1.0 \cdot 10^{-6}$	0.8809
	n	0.27	

Adsorption of dye in mixture with 1.7 mM (< CMC) SDS on carbon black

As stated above, the adsorption isotherm of Acid blue 113 at the carbon black-water interface is changed in the presence of SDS above the CMC. In solution, the interaction of Acid blue 113 with SDS was only observed above the CMC. In order to clarify the adsorption of the dye in mixture with SDS below the CMC, a study of the adsorption for the mixture of the dye with 1.7 mM SDS was performed. The original dye concentrations are the same as those in Figure 4-27.

Figure 4-28 shows the adsorption isotherm for the mixture of the dye with 1.7 mM SDS. The adsorption capacity of dye in the presence of 1.7 mM SDS is also greater than that of the dye in water. The parameters obtained by the Langmuir and Freundlich isotherm equation are displayed in Table 4-15. The experimental data can be well fitted by the Langmuir equation. The maximal adsorbed amount of the dye at saturation is $5.1 \cdot 10^{-7}$ mol/m^2, from which the calculated area occupied per dye molecule is 3.3 nm^2. The Langmuir constant in the presence of 1.7 mM SDS is similar to that of 10 mM SDS. This indicates that the adsorption mechanism of the dye in mixture with SDS is not changed in the presence of SDS of different concentrations.

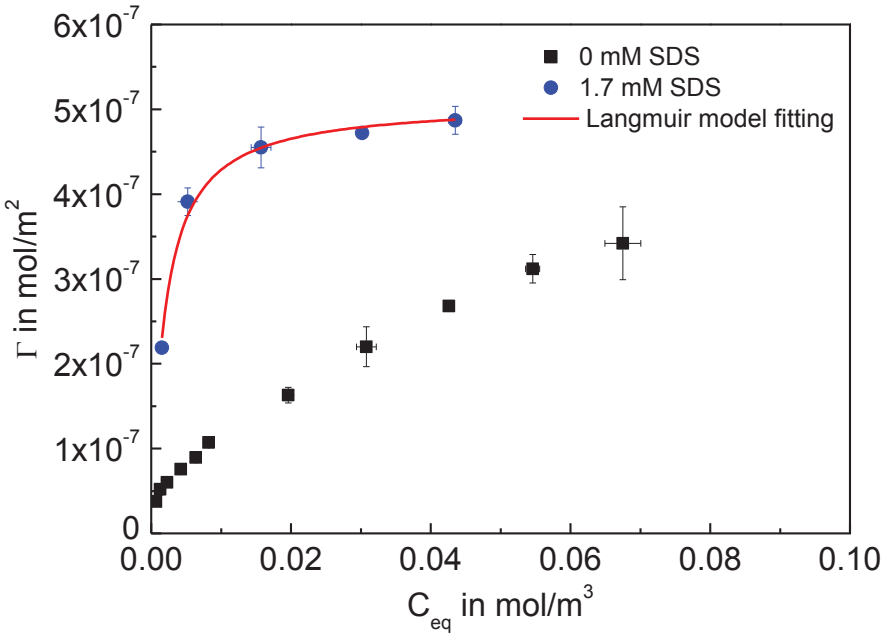

Figure 4-28 Plot of the adsorbed amount Γ of Acid blue 113 on carbon black versus the equilibrium dye concentration C_{eq}. The dye was dissolved in 1.7 mM SDS (below the CMC) solution. The carbon black was 0.4 g/L and the contact time was 2 h. The remaining dye solution was filtrated prior to centrifugation. Fitting of the adsorption isotherm by the Langmuir model is completed using Origin, indicated as the red curve.

Table 4-15 Fitting parameters obtained by the Langmuir and Freundlich isotherm model for the adsorption of Acid blue 113 at the carbon black-water interface in the presence of 1.7 mM SDS (below the CMC) with filtration.

Isotherm model	Parameter		R^2
Langmuir	Γ_{max} in mol/m^2	$5.1 \cdot 10^{-7}$	0.9873
	k in m^3/mol	535	
	A_{ad} in nm^2	3.3	
Freundlich	k_F	$1.1 \cdot 10^{-6}$	0.8133
	n	0.23	

To give an overview of the adsorption isotherms of the dye on carbon black in the absence and presence of surfactant, the adsorption curves of the dye dissolved in water and in SDS solutions of 1.7 mM as well as 10 mM are displayed in Figure 4-29. The corresponding parameters obtained by suitable adsorption isotherm models are summarized in Table 4-16. The adsorbed amounts of the dye in the absence and presence of SDS are compared for corresponding original dye concentrations, as shown in Table 4-17.

Acid blue 113 alone adsorbs on carbon black obeying the Freundlich adsorption model, showing a high affinity for the carbon black surface. In the presence of SDS, on the one hand, the adsorption of Acid blue 113 onto carbon black is promoted and, on the other hand, the adsorption of the dye shows a different adsorption mechanism, namely the Langmuir adsorption model. As seen in Table 4-16, the high Langmuir constants for the adsorption of the dye in mixture with SDS imply also a high adsorption preference of the dye for the carbon black. In addition, the Langmuir constant for the adsorption of the dye in the presence of SDS is not much influenced by the concentration of the surfactant. This indicates that the adsorption behavior of the dye at low dye concentrations is not changed due to different surfactant concentrations. At high dye concentrations the adsorbed amounts of the dye are decreased as the surfactant concentration is increased.

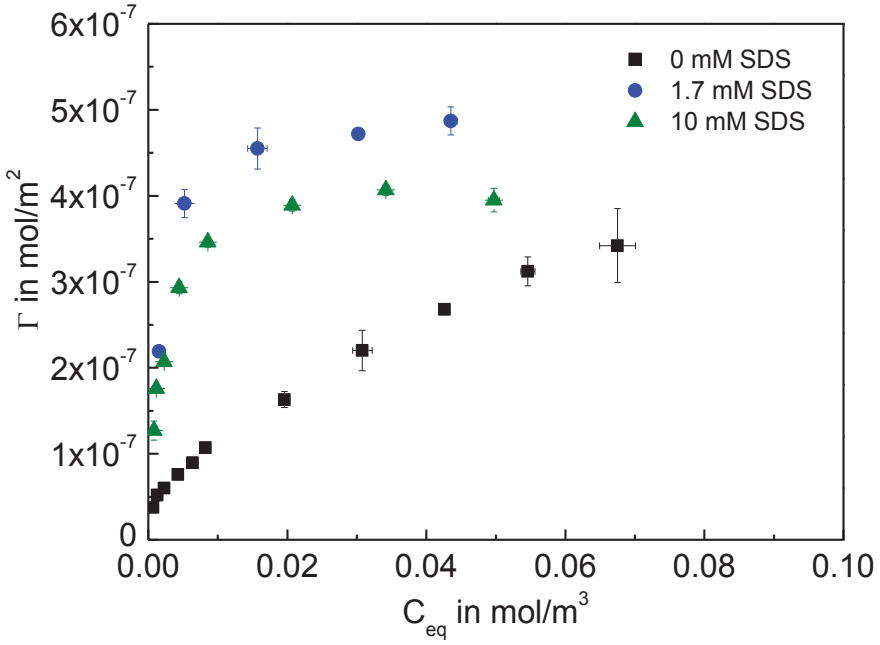

Figure 4-29 Plot of the adsorbed amount Γ of Acid blue 113 on carbon black versus the equilibrium dye concentration C_{eq}. The dye was dissolved in water, 1.7 mM (< CMC) and 10 mM (> CMC) SDS solution. The carbon black was 0.4 g/L and the contact time was 2 h. The remaining dye solution in the mixture with SDS was filtrated prior to centrifugation. The adsorption of Acid blue 113 alone obeys the Freundlich model. The adsorption of the dye in mixture with SDS follows the Langmuir model. The promotion of dye adsorption in the presence of SDS may be attributed to the improved dispersion of carbon black by surfactants. The change in adsorption mechanism of the dye in the presence of SDS can be explained by the improved dispersion of the dye by surfactants, resulting in finely divided dye adsorption. The decrease of the adsorption of the dye in mixture with SDS of higher concentration may result from the increased adsorbed amount of SDS on carbon black and the stabilization of partial dyes in solution above the CMC.

Table 4-16 Fitting parameters obtained by suitable adsorption isotherm models for the adsorption of Acid blue 113 dissolved in water, 1.7 mM (< CMC) and 10 mM (> CMC) SDS solution at the carbon black-solution interface. The remaining dye solution in the mixture with SDS was filtrated prior to centrifugation.

	Isotherm model						
	Langmuir				**Freundlich**		
Solvent	Γ_{max} in mol/m^2	k in m^3/mol	A_{ad} in nm^2	R^2	k_F	n	R^2
Water					$1.5 \cdot 10^{-6}$	0.54	0.9955
1.7 mM SDS	$5.1 \cdot 10^{-7}$	535	3.3	0.9873			
10 mM SDS	$4.2 \cdot 10^{-7}$	522	4.0	0.9865			

Table 4-17 Comparison of the adsorbed amount of Acid blue 113 on carbon black for different original dye concentrations. The dye was dissolved in water, 1.7 mM (< CMC) and 10 mM (> CMC) SDS solution. The original data are displayed in Table 1 (water), Table 2 (1.7 mM SDS) and Table 3 (10 mM SDS), as seen in Appendix.

C_0	C_0	Increased dye adsorption(1)	Increased dye adsorption(2)	Decreased dye adsorption(3)
in g/L	in mol/L	water→1.7 mM SDS	water→10 mM SDS	1.7 mM→10 mM SDS
0.006	$8.80 \cdot 10^{-6}$	-	68%	-
0.008	$1.17 \cdot 10^{-5}$	-	97%	-
0.01	$1.47 \cdot 10^{-5}$	105%	93%	5%
0.02	$2.93 \cdot 10^{-5}$	140%	112%	12%
0.03	$4.40 \cdot 10^{-5}$	107%	77%	15%
0.04	$5.87 \cdot 10^{-5}$	76%	52%	14%
0.05	$7.34 \cdot 10^{-5}$	56%	27%	19%

C_0: the original dye concentration applied in the adsorption measurement.
(1): the increased adsorption of the dye in mixture with 1.7 mM SDS compared to the adsorption of the dye dissolved in water.
(2): the increased adsorption of the dye in mixture with 10 mM SDS compared to the adsorption of the dye dissolved in water.
(3): the decreased adsorption of the dye in mixture with 10 mM SDS compared to the adsorption of the dye in mixture with 1.7 mM SDS.

It is known that SDS can also adsorb on hydrophobic carbon black.[12,13] Therefore, compared to that in water, the active surface of carbon black dispersed in surfactant solution can be increased owing to a better wetting of the surface by the adsorption of surfactants at the carbon black-water interface, resulting in increased small carbon black aggregates, i.e., increased total surface area per unit mass. As a result, in the presence of SDS the amount of adsorbed dye will generally increase. The increased dye adsorption in the presence of SDS is quantified for different original dye concentrations respectively, as seen in Table 4-17.

The increase of the active surface area of the carbon black should result in the increase of adsorbed amount of the dye but not change the adsorption mechanism of the dye. There are two assumptions to explain the change in the adsorption model.

One is that the change in adsorption behavior of the dye in mixture with surfactant can result from the weak interaction between the dye and SDS on carbon black. It was found that the adsorption of SDS on the same carbon black shows a Langmuir-type isotherm model.[13(p. 100)] This can interpret the adsorption isotherms of Acid blue 113 in mixture with SDS both below

and above the CMC, indicating the similar adsorption isotherm model on carbon black. Under this assumption, because the adsorbed amounts of surfactant increase with increasing surfactant concentrations[13(p. 53)], it is expected that the adsorbed dyes in the presence of 10 mM SDS should be more than those of 1.7 mM SDS, which however seems to not coincide with the experimental results. Additionally, the UV-Vis spectroscopic study (see Section 4.1.2) implies that there is a weak interaction between the dye and SDS. Hence, it is considered that the weak interaction between the dye and SDS is not responsible for the change in adsorption model of the dye in the presence of SDS.

The other explanation for the change of adsorption model from Freundlich to Langmuir originates from the improved dispersion of the dye in the presence of SDS, which results in much more homogenous dye adsorption due to the finer form of the dye in surfactant solution, corresponding to a Langmuir adsorption model. In this assumption, the adsorption of the dye and SDS on carbon black is coexistent. Actually, the Langmuir constant for the adsorption of the dye on carbon black ($522 - 535\ m^3/mol$) is much higher than that of SDS ($\sim 1\ m^3/mol$)[13(p. 101)], which predicts that the dye has a stronger interaction with the surface than SDS. Therefore, the decreased adsorption of the dye in mixture with 10 mM SDS may result from the increased adsorption of SDS on carbon black in the presence of 10 mM SDS compared to the dye adsorption in the presence of 1.7 mM SDS.

It is known that the adsorption of SDS on the same carbon black shows a maximal adsorbed amount of about $2 \cdot 10^{-6}\ mol/m^2$ at the surfactant concentration above the CMC (6.8 mM), indicating a horizontal orientation of adsorption.[13(p. 57)] The adsorbed amount of SDS for an original SDS concentration of 1.7 mM is estimated to be about $1 \cdot 10^{-6}\ mol/m^2$ (see Fig. 4-25).[13(p. 53)] That means in the presence of 1.7 mM SDS only 50% of the carbon black surface is covered by SDS molecules even with a horizontal orientation. Consequently, the available adsorption sites for the dye in mixture with 1.7 mM SDS are more than those with 10 mM SDS, corresponding to a higher adsorbed amount of the dye on carbon black. The decreased dye adsorption for 10 mM SDS compared to the dye adsorption for 1.7 mM SDS is shown in Table 4-17. In addition, this decrease of dye adsorption may also be due to the stabilization of the dye in the bulk phase at the SDS concentration above the CMC. As the UV-Vis spectroscopic and DLS study show, Acid blue 113 interacts with surfactants above the CMC, where the dye may be incorporated into surfactant micelles. Therefore, at an SDS concentration of 10 mM the dyes are partially solubilized in the micellar surfactant solution, which also accounts for the decrease of adsorbed dyes on carbon black. Based on the spectroscopic study shown in Table 4-2 (see

Section 4.1.3), at 10 mM of SDS the dye solubilized in surfactant micelles is estimated to be $4.5 \cdot 10^{-6}$ mol/L, which is about 6% of the highest original dye concentration.

According to the van der Waals molecular surface area (2D) given by the software MarvinSketch (Version 18.21.0), Acid blue 113 has a molecular area of about 2 nm^2. Considering this molecular area of the dye, the maximal adsorbed amount of the dye in the absence of SDS corresponds to a coverage of about 40% for the total carbon black surface. In the same way, the maximal adsorption of the dye in the presence of SDS refers to a coverage of about 60% for 1.7 mM SDS and 50% for 10 mM SDS. Therefore, at such coverages the adsorption of the dye on carbon black is expected to relate to averagely a monomolecular adsorption.

Acid blue 113 in aqueous solution shows a high affinity for the nonpolar carbon black surface, where the adsorbed amounts of the dye increase with increasing dye concentrations until to its solubility limit. In mixture with the anionic surfactant SDS, the adsorption of the dye becomes much more homogeneous compared to that in the absence of surfactant. In addition, because of the competitive adsorption of the surfactant, the adsorption of the dye on carbon black has a maximum in the presence of surfactant. In mixture with SDS, the adsorption of the dye at low dye concentrations is not influenced by surfactant concentrations and the adsorbed amounts of the dye at high dye concentrations decrease in the presence of SDS above the CMC, indicating the inhibition of dye adsorption by the surfactant of high concentrations ($>$ CMC).

4.5 Adsorption structures at the graphite-solution interface by AFM

In order to further understand the influence of surfactants and the DTI polymer on the adsorption of the dye on surface at a molecular level, the adsorption structures of single components and their binary mixtures at the graphite-solution interface were investigated by AFM. Through optimization of the AFM setup (see Section 3.2.4), the resolution of colloidal structures in nanometers was achieved by measurements directly in solution. In the AFM study, the force applied should enable the highest resolution of the soft structures, thus, at which the underlying graphite cannot be observed. Hence, it is necessary to continuously change the force load (set point) during imaging, in order to have a better contrast (resolution) in topographic images. Under these conditions, all deflection images (topography) were captured with the feedback gain (Z Gain) not more than 1 and the scan rate of 1−2 Hz. In this section, the morphology (topography) of adsorption structures at the interface and the force-distance (F-D) curves of selected points are presented.

In AFM studies, every F-D curve indicates the force interaction of only one point. Furthermore, the F-D profile is greatly impacted by the set point of the single measurement. Therefore, it is difficult to give precise quantities of the force interaction for an entire system. The feature displayed in the F-D curve can be considered as a qualitative analysis for the force interaction yet.

4.5.1 $C_{12\text{-}18}E_7$ at the graphite-solution interface

Structure of $C_{12\text{-}18}E_7$ adsorbed on graphite

The nonionic surfactant $C_{12\text{-}18}E_7$ adsorbed on graphite forms an ordered structure at concentrations above the CMC (0.03 mM). As seen in Figure 4-30, aggregates of $C_{12\text{-}18}E_7$ appear as parallel stripes with a certain separation. This periodic aggregate structure relates to a hemicylindrical surfactant structure as interpreted in other reports.[8,10] It was found that the surfactant aggregates are generally oriented in two directions, which close an angle of about 60°. This preference of orientations may be attributed to the lattice symmetry of the underneath graphite. The template influence of graphite on aggregation of $C_{12}E_x$ (x=5, 8−10) has been observed before by Patrick et al..[8]

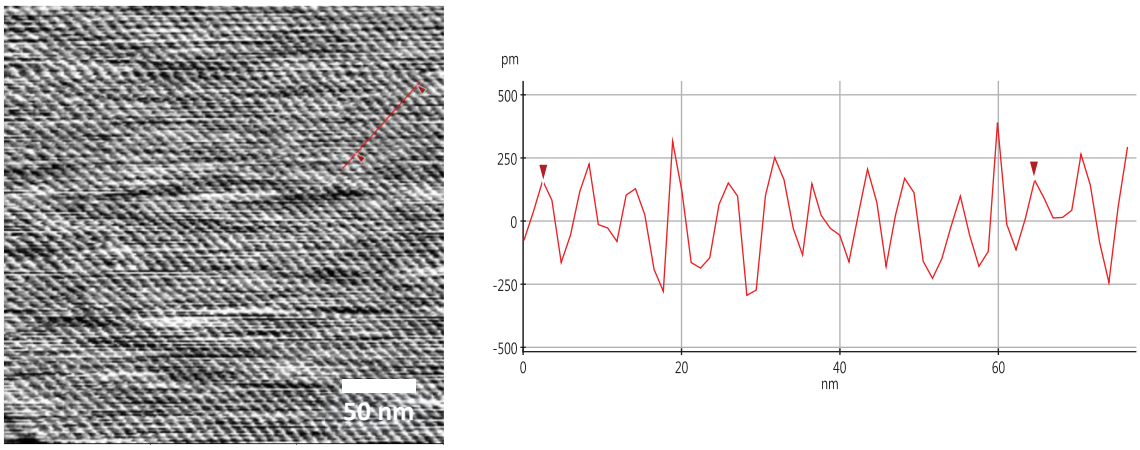

Figure 4-30 AFM image and height profile of 0.1 mM $C_{12\text{-}18}E_7$ adsorbed at the graphite-solution interface. $C_{12\text{-}18}E_7$ forms hemicylindrical aggregate structures,[8] which appear as periodic parallel stripes in the AFM image. The periodicity of aggregate structure is 5.7−6.4 nm at the concentrations of 0.1−50 mM. The height of aggregate structure is in the range of 250−500 pm.

The distance between two adjacent stripes perpendicular to the long axis of the aggregate structure is described as the periodicity of the surfactant structure. The distance was valued

from separation of the selected maxima (stripes) in the height profile (Fig. 4-30), with respect to the orientation of stripes to the fast-scan line (x-axis). Otherwise, in the case where the stripes align perpendicular to the fast-scan line, the separation of two maxima will directly be referred as the periodic spacing of stripes. For each AFM image, 2−4 positions involving 4−10 stripes were measured and the average of which corresponds to the period of the aggregate structure. The periodicity of the aggregate structure was determined by 2−3 images for each system investigated.

Figure 4-30 also shows a height profile of the indicated line in the presented AFM image. In such a profile, the height between peak and valley is related to the height of the surfactant aggregate. It was found that the height of the aggregate structure of $C_{12\text{-}18}E_7$ varies in a range of 250 − 500 pm. Unsurprisingly, this height is not really consistent with a height of the hemicylindrical aggregate of $C_{12\text{-}18}E_7$, because the dimension of structures given by AFM images is very dependent on the shape and geometry of the used tip and the specimen[123]. In the case of surfactant structures at graphite-solution interfaces, the curvature radius of the tip is much larger than that of the hemicylinder aggregate, i.e. the tip cannot "touch" the bottom of the groove between hemicylindrical structures. Hence, the morphology presented in AFM images gives precisely the lateral dimension (here the periodicity) but usually decreased height of the adsorbed structure.

In this study, two typical periods for $C_{12\text{-}18}E_7$ at the graphite-solution interface were observed, which are 5.7 nm and 6.3 nm as shown in Table 4-18.

Table 4-18 Periodicity of hemicylindrical aggregate structures of $C_{12\text{-}18}E_7$ adsorbed at the graphite-solution interface at different surfactant concentrations.

$C_{12\text{-}18}E_7$ in mM	**Surface**	**Periodicity in nm**
0.1	hemicylindrical structure	5.7 ± 0.4
10	hemicylindrical structure	5.7 ± 0.2
20	hemicylindrical structure	5.7 ± 0.5 and 6.4 ± 0.1
50	hemicylindrical structure	5.6 ± 0.2 and 6.2 ± 0.3

The periodicity of 5.7 nm was found at all measured concentrations. Thus, the higher periodicity of 6.3 nm was observed at high surfactant concentrations. The characterized

periodicity of 5.7 nm is well consistent with the result reported by Patrick et al..[8] They found a periodicity for $C_{12}E_x$ (x=5, 8−10) in the range of 5.3−5.8 nm at the surfactant concentrations less than 1 mM. The larger spacing observed at much higher concentrations can be attributed to larger surfactant aggregates formed by the surfactants with longer alkyl chains and ethylene oxide chains in the used $C_{12\text{-}18}E_7$.

F-D measurement of $C_{12\text{-}18}E_7$ adsorbed on graphite

The force-distance (F-D) curves for graphite in water and 10 mM $C_{12\text{-}18}E_7$ at the graphite-solution interface are shown in Figure 4-31. In F-D measurements, the deflection of the cantilever is recorded in dependence of the displacement of the scanner, which is referred to as the force-distance (F-D) curve. An F-D measurement consists of two parts, the trace curve (red) and the retrace curve (blue). The trace means that the tip is driven to approach the surface, in turn, during the retraction the tip will be lifted off the surface. Figure 4-31 (a) shows F-D curves for graphite in water. As the tip-graphite distance is beyond the interactive range, there is no force that can be detected (zero line in the trace curve). With further approach of the tip toward the sample, a repulsive interaction occurs (positive part in the trace curve). The repulsive force increases with decreasing tip-sample distance. During retraction of the tip, an adhesive attraction forms resulting in the negative force in the retrace curve. The maximal adhesive force corresponding to the peak in the retrace curve is 1.089 nN at the graphite-water interface.

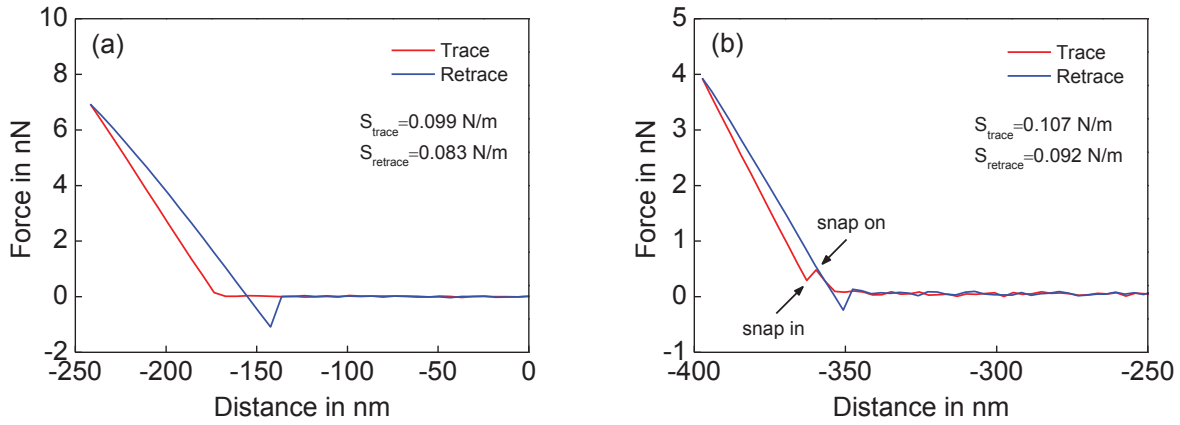

Figure 4-31 F-D curves for graphite in water (a) and 10 mM $C_{12\text{-}18}E_7$ (b) at the graphite-solution interface. (a): The set point is 0.52 V, the maximal adhesive force is 1.089 nN. (b): The set point is 0.041 V. The tip jumps to contact with the graphite surface at a force of 0.483 nN. The maximal adhesive force is 0.242 nN. The thickness of adsorbed surfactant layer determined from the approach curve is 3.1 nm, corresponding to a monolayer of hemicylindrical $C_{12\text{-}18}E_7$ aggregates. The slope of curve in the contact region for $C_{12\text{-}18}E_7$ is slightly larger than that for graphite due to the adsorbed surfactant layer.

Figure 4-31 (b) shows F-D curves for 10 mM $C_{12\text{-}18}E_7$ on graphite. The red curve indicates the trace measuring and the blue the retrace measuring. As shown in the trace path (red curve), there are two break points, where a change of slope takes place in the repulsion region. As the tip gets so close to adsorbates, there is firstly a repulsive interaction between the tip and surfactant. With further approaching, the tip jumps into contact with the graphite surface at a point, where the attractive interaction between the tip and graphite is dominant. Until the tip gets closer to the graphite, the repulsive interaction between the tip and graphite occurs. These discontinuities are presented in an approach curve as a "snap on" and "snap in" appearance. These effects are considered as an evidence of an adsorbed layer of surfactants on the graphite surface.[8] The tip jumps to contact with the graphite surface at a force of about 0.483 nN.

In withdrawing of the tip (blue curve), because of the adhesion of the surface to the tip the deflection of cantilever points downwards (negative part in the F-D curve). Until some point, the tip jumps off contact with the surface, where a force minimum below the zero line can be seen in the retrace curve, which corresponds to the maximal pull-off force or the maximal adhesion. The maximal adhesive force is 0.242 nN for 10 mM $C_{12\text{-}18}E_7$ at the graphite-solution interface.

The F-D curve allows determination of the thickness of the adsorbed structures. It is related to the distance from the point of jumping to contact with the adsorbates to the point where the graphite surface is detected[7], which equals the distance between the "snap on" and "snap in" point. The thickness of the adsorbed surfactant structure determined by the approach curve in Figure 4-31 (b) is 3.1 nm. Patrick et al.[8] reported that $C_{12}E_3$ forms an adsorbed layer on graphite with a thickness of 2.5 nm and the lamellar spacing in the bulk phase is 4 nm. Therefore, it can be concluded that the thickness of the structure determined here is related to a monolayer of hemicylindrical $C_{12\text{-}18}E_7$ micelles adsorbed on graphite.

4.5.2 SDS at the graphite-solution interface

Structure of SDS adsorbed on graphite

Figure 4-32 shows an AFM image of 100 mM SDS at the graphite-solution interface. The SDS structure also appears as periodic parallel stripes in AFM images. In some AFM images the stripes are very wavy. That may be because, in general, the SDS aggregate structure was difficult to maintain in a large range, the set point was therefore frequently changed during imaging, which can affect the appearance of the resolved structure in AFM images[7].

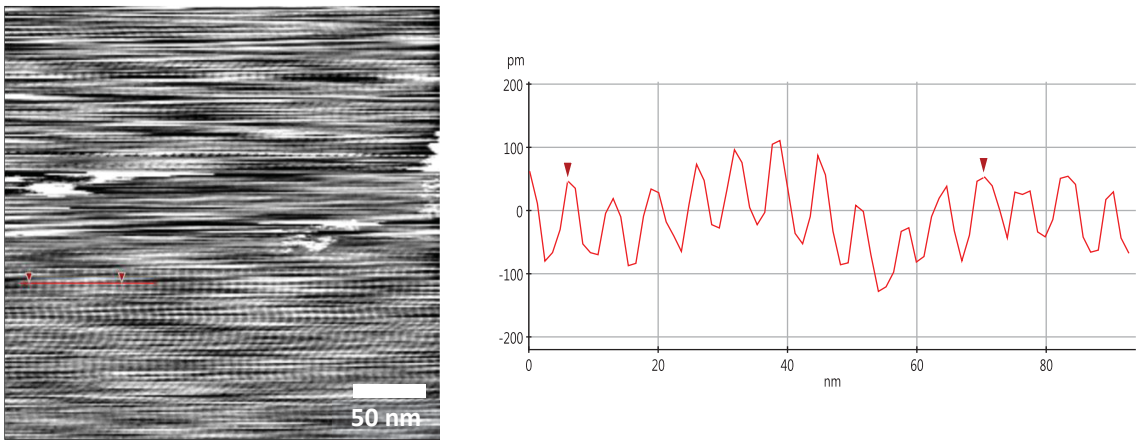

Figure 4-32 AFM image and height profile of 100 mM SDS adsorbed at the graphite-solution interface. SDS forms hemicylindrical aggregate structures,[7] which appear as periodic parallel stripes in AFM images. The periodicity of aggregate structure is 5.2−5.5 nm at the concentrations of 50−100 mM. The height of aggregate structure is in the range of 100−200 pm.

The period of SDS structures is about 5.2−5.5 nm (Tab. 4-19), which is slightly smaller than that of $C_{12\text{-}18}E_7$ structures. This period of SDS structures agrees very well with that studied by Wanless et al.[43] for 80 mM SDS (5.2 nm) and by M. Jabnoun[13(p. 79)] for 50 mM SDS (5.6 nm). The height of SDS aggregates at graphite-solution interfaces is typically in the range of 100−200 pm, as displayed in the height profile in Figure 4-32. As stated in 4.5.1, the height measured in AFM images does not reflect the real height of SDS aggregates. A comparable height for SDS aggregates on graphite has also been observed in other AFM studies.[7]

An AFM image for the SDS solution of 50 mM after pH adjustment to 8.3 is presented in Figure 4-33. The pH of SDS solution was adjusted with 0.1 M NaOH before measurements. As can be seen, the SDS aggregates show still the hemicylindrical structure. Additionally, there is a domain in the middle of the image, which has a different orientation. The periodicity of surfactant aggregate structure is 5.3 ± 0.5 nm and the height of aggregate structure is about 200 pm. The addition of ions into the surfactant solution did not change the aggregate structure but increased the variation of the spacing of surfactant aggregates (Tab. 4-19).

Structure of SDS adsorbed on graphite at pH=8.3

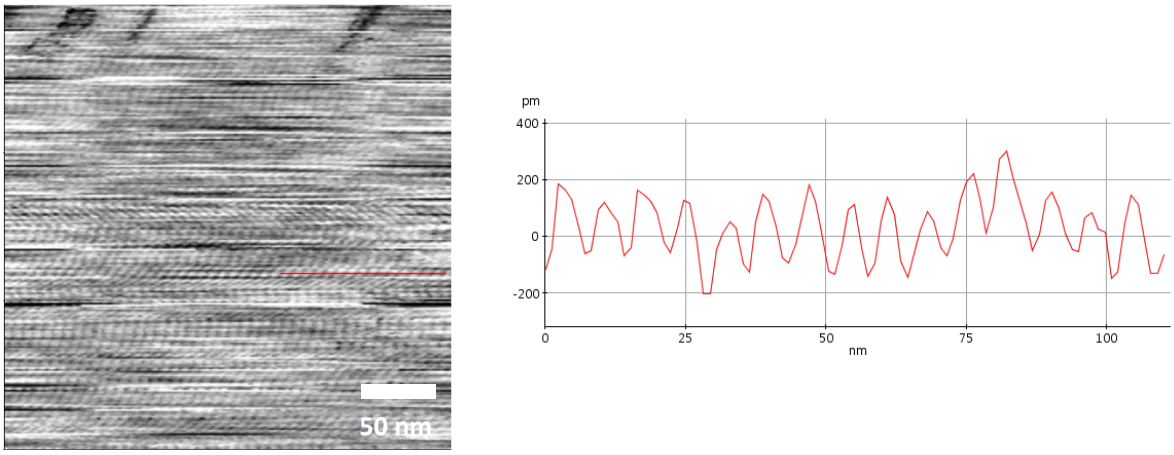

Figure 4-33 AFM image and height profile of 50 mM SDS adsorbed at the graphite-solution interface after pH adjustment (pH=8.3). SDS maintains the hemicylindrical aggregate structure in the presence of NaOH. The periodicity of aggregate structure is not changed. The height of aggregate structure is in the range of 200−300 pm.

Wanless et al. found that, in addition of monovalent or divalent ions the period of SDS below the CMC decreases with increasing ion concentrations, however, above the CMC the period has a limit of 5 nm.[43] The SDS concentration studied here is much higher than the CMC, therefore the influence of added ions on the surfactant aggregates may be not significant. Additionally, it was found that the imaging was less noisy in the presence of NaOH compared to that of SDS alone. This may be explained by the weakening of the electrostatic interaction between headgroups of the anionic surfactants due to the added ions[124], conversely, which stabilizes the surfactant aggregates adsorbed. On the other hand, NaOH may cause the change in the potential of the surface (electrolyte effect), which influences the imaging at the interface.

Table 4-19 Periodicity of hemicylindrical aggregate structures of SDS adsorbed at the graphite-solution interface.

SDS in mM	**Surface**	**Periodicity in nm**
50	hemicylindrical structure	5.5 ± 0.1
100	hemicylindrical structure	5.2 ± 0.2
50 (pH=8.3, with NaOH)	hemicylindrical structure	5.3 ± 0.5

4.5.3 Acid blue 113 at the graphite-solution interface

Structure of Acid blue 113 adsorbed on graphite

Figure 4-34 shows AFM images of Acid blue 113 adsorbed on graphite at different concentrations. Generally, Acid blue 113 adsorbs on graphite in an unstructured way, showing as white spots in AFM images.

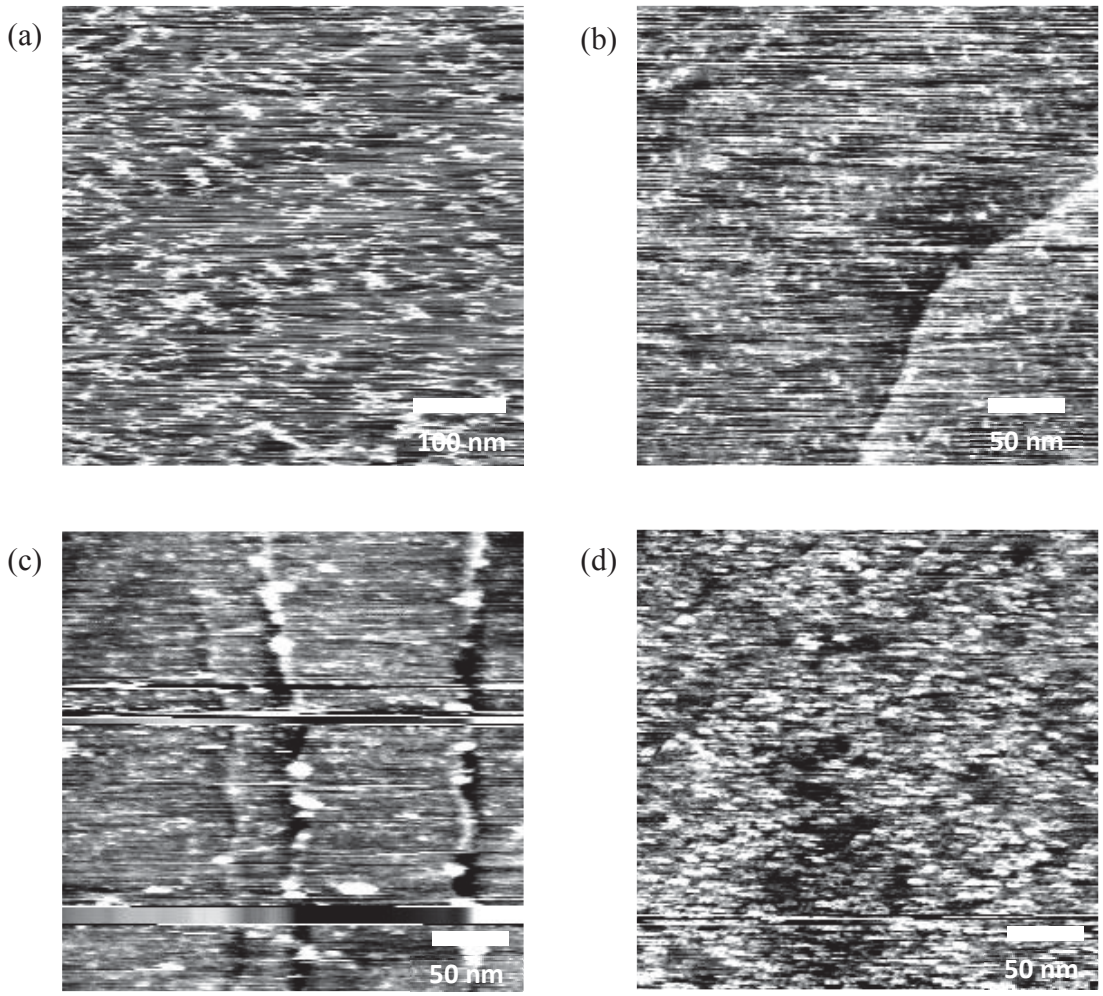

Figure 4-34 AFM images of Acid blue 113 of different concentrations adsorbed at the graphite-solution interface. (a) 0.009 mM, (b) 0.015 mM, (c) 0.044 mM and (d) 0.073 mM. Generally, Acid blue 113 adsorbs on graphite in an unstructured way (white spots in images), forming structures with a size (lateral dimension) of 1−13 nm by considering the geometry of the AFM tip. Taking into account the dimension of the dye molecule, the adsorbed dye structures may refer to single dye molecules and small dye aggregates. The roughness of surface with adsorbed dyes increases with increasing dye concentrations, corresponding to the increase in adsorbed amount of the dye on the surface.

At high dye concentrations some globular structures are seen at the steps of graphite, as shown in Figure 4-34 (c). The size (lateral dimension) of the dye structures observed is in the range of 10−40 nm, corresponding to a size range of 1−13 nm corrected by considering the geometry of the AFM tip as described in Section 2.4.4 (see Equation 2-33). According to the dimension of the dye molecule (length × width: 2.5 nm × 1.4 nm) given by the software MarvinSketch (Version 18.21.0), the structures of adsorbed dyes may refer to single dye molecules and small dye aggregates. It can be seen in Figure 4-34 (d) that the adsorbed amount of the dye is obviously increased at high dye concentrations, which is in agreement with the study of the dye adsorption on carbon black. Additionally, it was found that the adsorbed dyes of low concentrations (Fig. 4-34 (a) and (b)) tend to be scratched by the AFM tip during imaging.

The roughness of surface with dyes was analyzed and is shown in Figure 4-35, where the roughness of graphite in water is also given. The roughness of surface is given by the software XEI of the used AFM (Park Systems), calculated by the standard definition as shown in Equation 2-34 and 2-35. The roughness values S_q (the root mean square height of the surface) and S_a (the arithmetic mean height of the surface) for each concentration were calculated from 5−6 AFM images with the scan size of 500×500 nm^2 and the average value was taken.

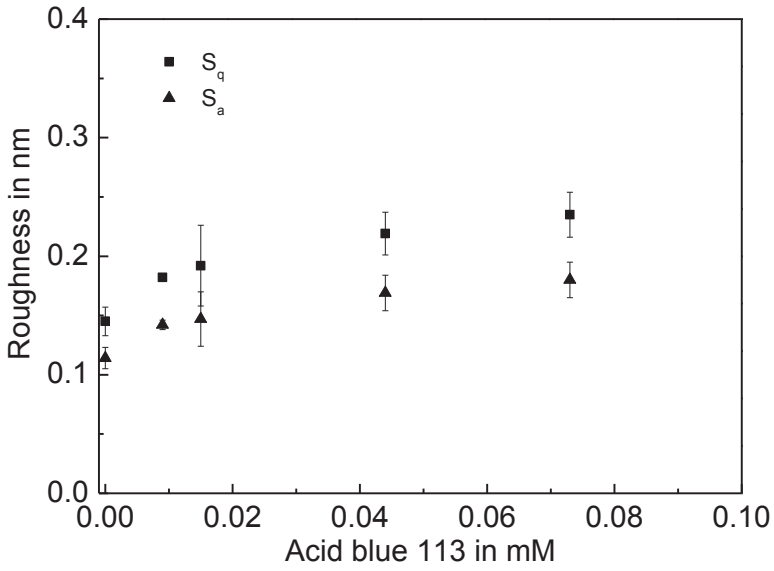

Figure 4-35 Roughness S_q and S_a of the surface upon adsorption of Acid blue 113 on graphite with respect to different dye concentrations. The roughness S_q (the root mean square height of the surface) and S_a (the arithmetic mean height of the surface) increases with increasing dye concentrations respectively.

As shown here, the roughness of surface with adsorbed dyes increases with increasing dye concentrations. The S_q value increases from about 0.180 nm to 0.240 nm and the S_a value from

0.142 nm to 0.180 nm. At the low dye concentration of 0.009 mM the deviation (ref. Equation 1 in Appendix) of roughness is very small. However, above 0.01 mM the deviation of roughness is obviously greater than that at low dye concentrations. This may be due to the agglomeration of dyes by dye aggregation on graphite, corresponding to the increased amount of adsorbed dyes.

F-D measurement of Acid blue 113 adsorbed on graphite

The approach and retraction curves of F-D measurements for different dye concentrations are shown in Figure 4-36. The slopes of curves in the contact region are given for each concentration. The slope of the approach and retraction curve of 0.009 mM Acid blue 113 are 0.121 N/m and 0.094 N/m respectively, which are higher than those of higher dye concentrations. From 0.015 mM the slope of the approach curve increases from 0.095 N/m to 0.116 N/m and the slope of the retraction curve from 0.075 N/m to 0.092 N/m.

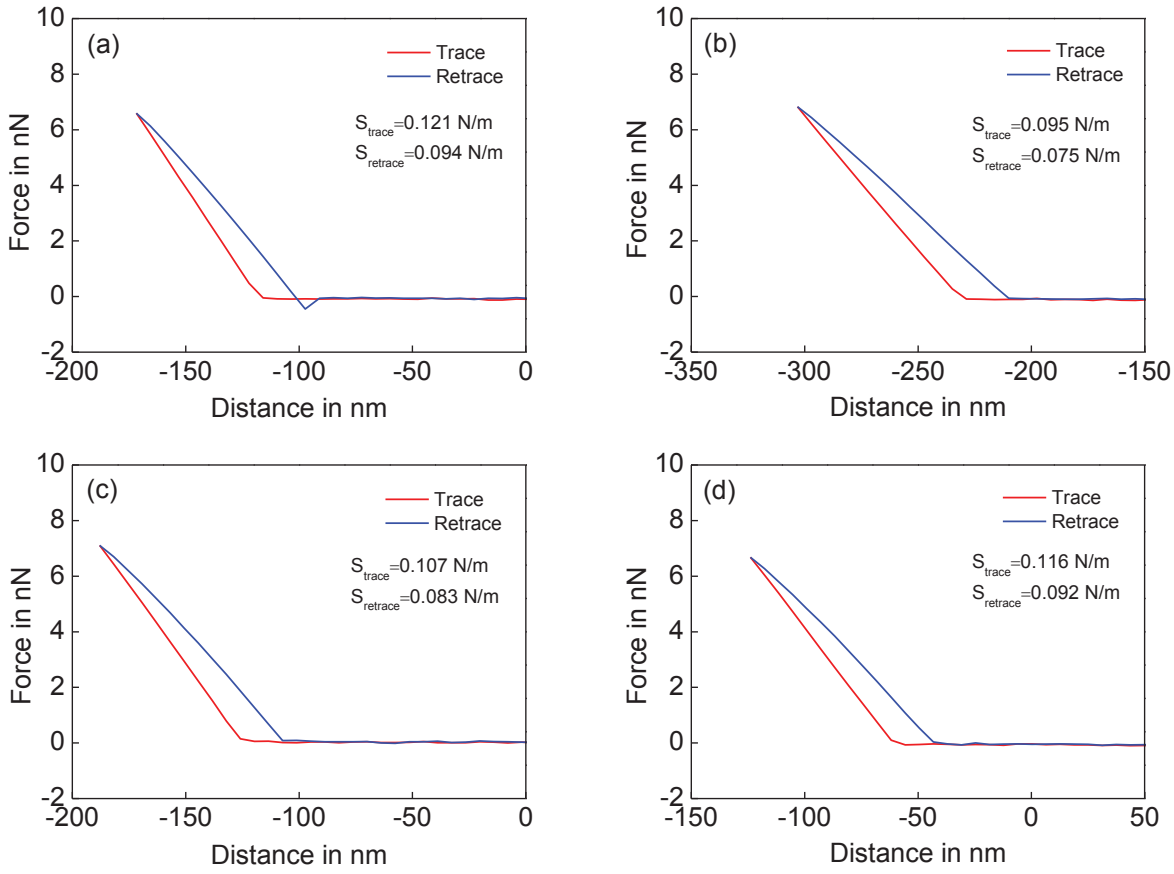

Figure 4-36 F-D curves for Acid blue 113 at different concentrations as indicated in Figure 4-34. (a) 0.009 mM, set point 0.09 V, the maximal adhesive force 0.445 nN, (b) 0.015 mM, set point 0.36 V, (c) 0.044 mM, set point 0.23 V and (d) 0.073 mM, set point 0.34 V.

As can be seen in Figure 4-36, no pull-off force is shown in the F-D curves in (b)−(d). This indicates that the repulsive force is dominant between the tip and adsorbed layer, which originates from the charged headgroups of the dye. As is known, the dye molecule may adsorb both on the tip and on the graphite. During imaging, there may be always repulsive interactions between the tip and the adsorbed layer. If the adsorbed layer is a continuous film, the F-D curve may therefore show a continuous repulsive force.[43,125] Hence, the higher slope and the adhesion at the low dye concentration of 0.009 mM may be due to the uncompleted discrete adsorption of Acid blue 113 on the graphite surface, corresponding to a stiffer interface and showing an obvious adhesive force as shown in Figure 4-36 (a).

4.5.4 PVPVI at the graphite-solution interface

Structure of PVPVI adsorbed on graphite

The adsorption structure of the DTI polymer PVPVI on graphite was investigated at the concentration of 0.01 mM, 0.05 mM and 0.1 mM. Figure 4-37 shows the AFM images of PVPVI at the graphite-solution interface with respect to different concentrations. As can be seen in Figure 4-37 (a) for 0.01 mM PVPVI, there is no adsorbed polymer structure that can be observed in the AFM image. At a higher polymer concentration of 0.05 mM, the surface is covered with a polymer layer after exposure of the polymer solution for 1 h (Fig. 4-37 (b)). The S_q and S_a values concerning the roughness of surface in the scan size of $1 \times 1\ \mu m^2$ are 0.348 ± 0.056 nm and 0.272 ± 0.04 nm respectively, which are averaged from 3 AFM images. The roughness of the surface was not changed after 24 h, indicating a strong interaction between PVPVI and graphite. Except for the dominant rough regions, few globular structures were observed as indicated with the arrow. At the concentration of 0.1 mM, single globular structures of polymer were found over the surface after exposure time of 4 h (Fig. 4-37 (c) and (d)). By an appropriate set point less than 0.4 V the rough underlayer can still be seen in the image (Fig. 4-37 (d)). The roughness S_q and S_a of the underlayer surface are 0.316 ± 0.016 nm and 0.251 ± 0.014 nm respectively. Both the rough underlayer and the globular structures did not significantly alter over several hours.

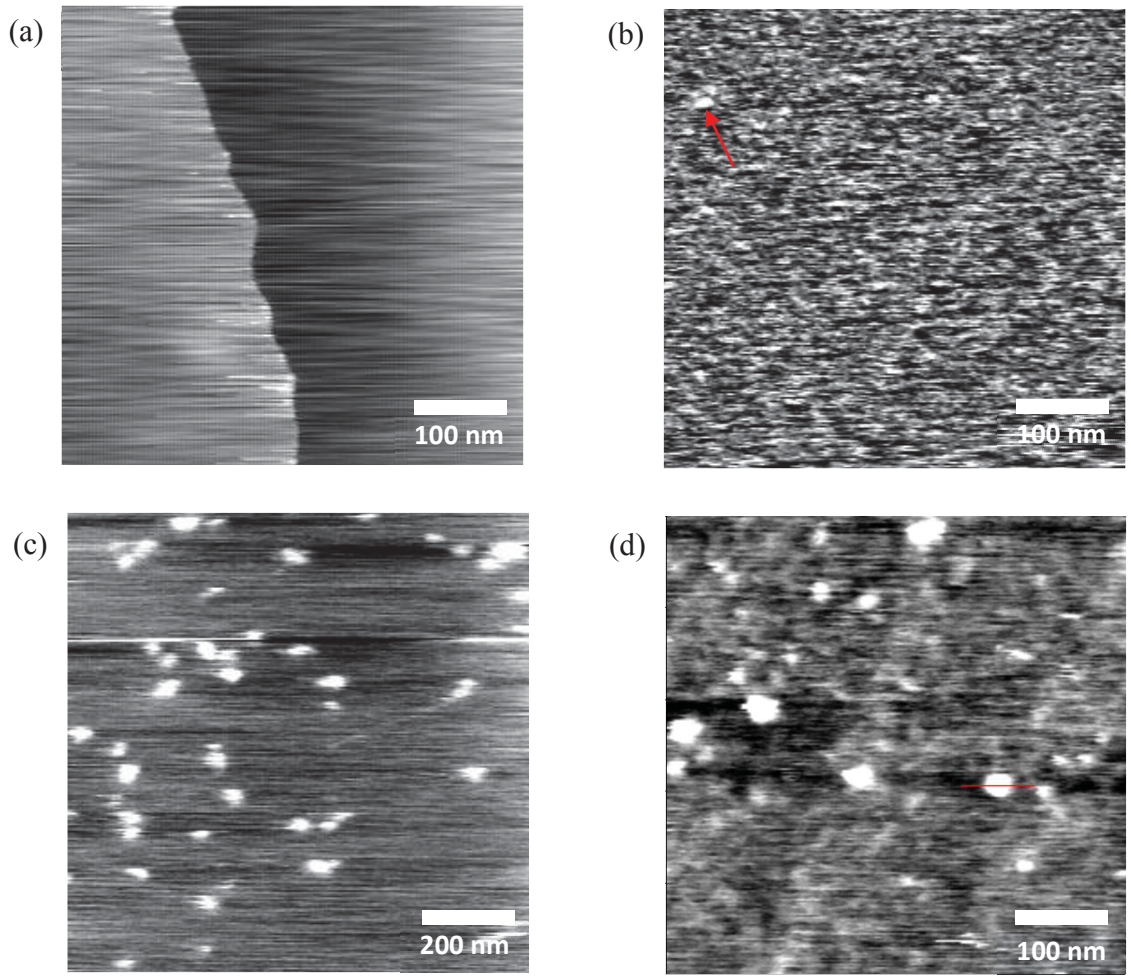

Figure 4-37 AFM images of PVPVI at the graphite-solution interface depending on PVPVI concentrations. The concentration of PVPVI is 0.01 mM (a), 0.05 mM (b) and 0.1 mM (c and d). At the PVPVI concentration of 0.01 mM, no adsorbed polymer can be seen in AFM images. At 0.05 mM of PVPVI, the graphite is covered by an adsorbed polymer layer with a roughness S_q of 0.348 nm and S_a of 0.272 nm. At the high polymer concentration of 0.1 mM, single globular structures were observed over the graphite surface. The roughness S_q and S_a of the underlayer surface in (d) are 0.316 nm and 0.251 nm respectively.

Stipp[126] investigated the dynamic process of the adsorption of poly(acrylic acid) (PAA) on muscovite by AFM in solution and found that the structure of adsorbed polymers changes after an exposure time of more than 20 h, from a rough layer to aggregates with the diameter of 30−50 nm in AFM images. Nevertheless, the structure change of adsorbed polymers with time was not seen for PVPVI on graphite. Therefore, the formation of globular structures of PVPVI may be completed mainly in terms of polymer concentrations.

Size of PVPVI globules adsorbed on graphite

The size of the globular structure of the polymer can be determined by height profiles (Fig. 4-38). Two AFM images in the scan size of 1×1 μm^2 were chosen. The diameters (widths) of 66 single globules in the images were measured by the software XEI (Park Systems). The diameter of globular structures without consideration of the tip geometry differs from 29 nm to 80 nm, as shown in the size distribution in Figure 4-38 (black solid lines). The radius of the used tip is 15 nm and the diameter of globules in AFM images can be corrected by Equation 2-33 (see Section 2.4.4). Considering the geometry of the tip, the diameter of globules presented in AFM images is corrected as displayed by orange dashed lines in the size distribution.

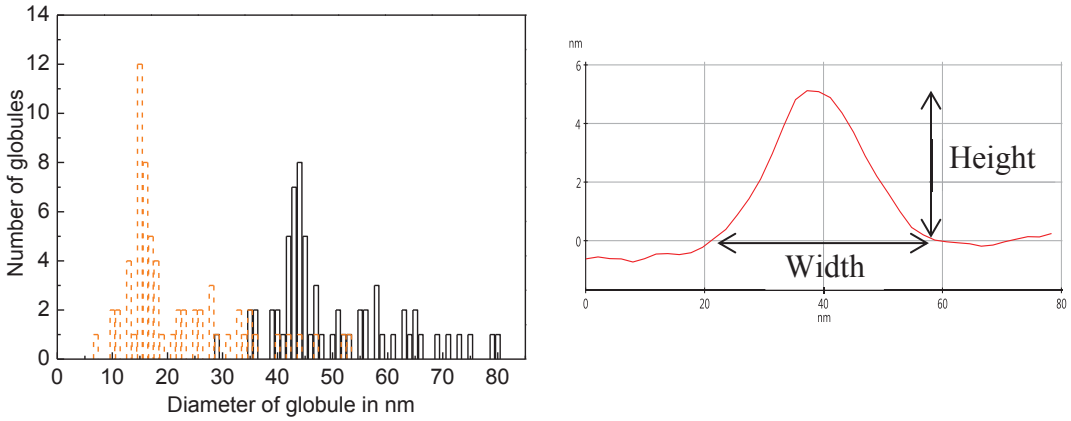

Figure 4-38 Size distribution of globules observed in AFM images for 0.1 mM PVPVI (left) and height profile of the indicated globule in Figure 4-37 (d) (right). The diameter (width) was measured according to the height profile of each globule. The diameter of globular structure without consideration of the tip geometry differs from 29 nm to 80 nm, as indicated by black solid lines in the size distribution. Taking the tip geometry into account, the diameter of globules is in the range of 7−53 nm (orange dashed lines), most of which appear in the range of 15−17 nm, which is consistent with the result by DLS. The observed single globules correspond to polymer molecules adsorbed. The broad range of diameter may be attributed to the scratch of AFM tip on the polymer during imaging, resulting in the change of polymer conformation.

As can be seen in the size distribution, the diameter of globules corrected is in the range of 7−53 nm, where the globules mostly appeared have a diameter of 15−17 nm. In comparison with the hydrodynamic diameter ($D_{h,z}$) and peak size of PVPVI obtained by the DLS study, which is 11 nm and 14 nm respectively, the single globule corresponds to one polymer molecule adsorbed on graphite. Thus, the result from the AFM study is in good agreement with that from the DLS study, which indicates that the structure of the polymer on graphite is in coincidence with that in the bulk phase.

The height of globule is not consistent with the diameter of globule, which is in the range of 1−6 nm. This can be caused by the geometry effect of tip, as described in Section 4.5.1. Additionally, it was found that the tip tends to scratch the adsorbed polymer during imaging. As a result, the polymer globules might be compressed or deformed by the tip during imaging to some extent, resulting in a decreased height of globule, which also explains a wide size range of polymer globules in AFM images.

Table 4-20 Structures of PVPVI adsorbed at the graphite-solution interface.

PVPVI in mM	Surface	Diameter in nm
0.01	no adsorbed polymer	-
0.05	polymer layer	-
0.1	globular structure	15−17*

*: the globules mostly appeared in the size distribution as presented in Figure 4-38.

F-D measurement of PVPVI adsorbed on graphite

Figure 4-39 shows the F-D curves for PVPVI solutions presented in Figure 4-37 (a)−(d). At 0.01 mM of PVPVI, the F-D curves are very similar to the curves for the water-graphite interface (ref. Fig. 4-31 (a)). The maximal pull-off force here is 1.085 nN (Fig. 4-39 (a)), corresponding to an adhesive force at the water-graphite interface. This further confirms that there is no adsorbed polymer in a large range. At the PVPVI concentration of 0.05 mM (Fig. 4-39 (b)), the negative peak in the retrace curve is much smaller than that in Figure 4-39 (a), indicating a decreased adhesion interaction between the tip and surface. At 0.1 mM of PVPVI no remarked adhesion can be seen in the F-D curves for both the polymer globules (Fig. 4-39 (c)) and the underlying layer (Fig. 4-39 (d)). The maximal adhesive force of the underlayer is slightly greater than that of single polymer globule.

The slope of F-D curves for approach and retraction are very similar at the polymer concentration of 0.01 mM (Fig. 4-39 (a)) and 0.1 mM (Fig. 4-39 (c) and (d)). The F-D curves for 0.05 mM PVPVI have a higher slope both in the approach and retraction curve, which may be caused by the homogeneous completely adsorbed polymer layer resulting in the continuous greater tip-sample force interaction. The adhesion observed for 0.05 mM PVPVI in Figure 4-39

(b) and for 0.1 mM PVPVI in Figure 4-39 (c) and (d) occurs in two different distances, indicating the increase of thickness of the adsorbed layer with increased polymer concentrations.

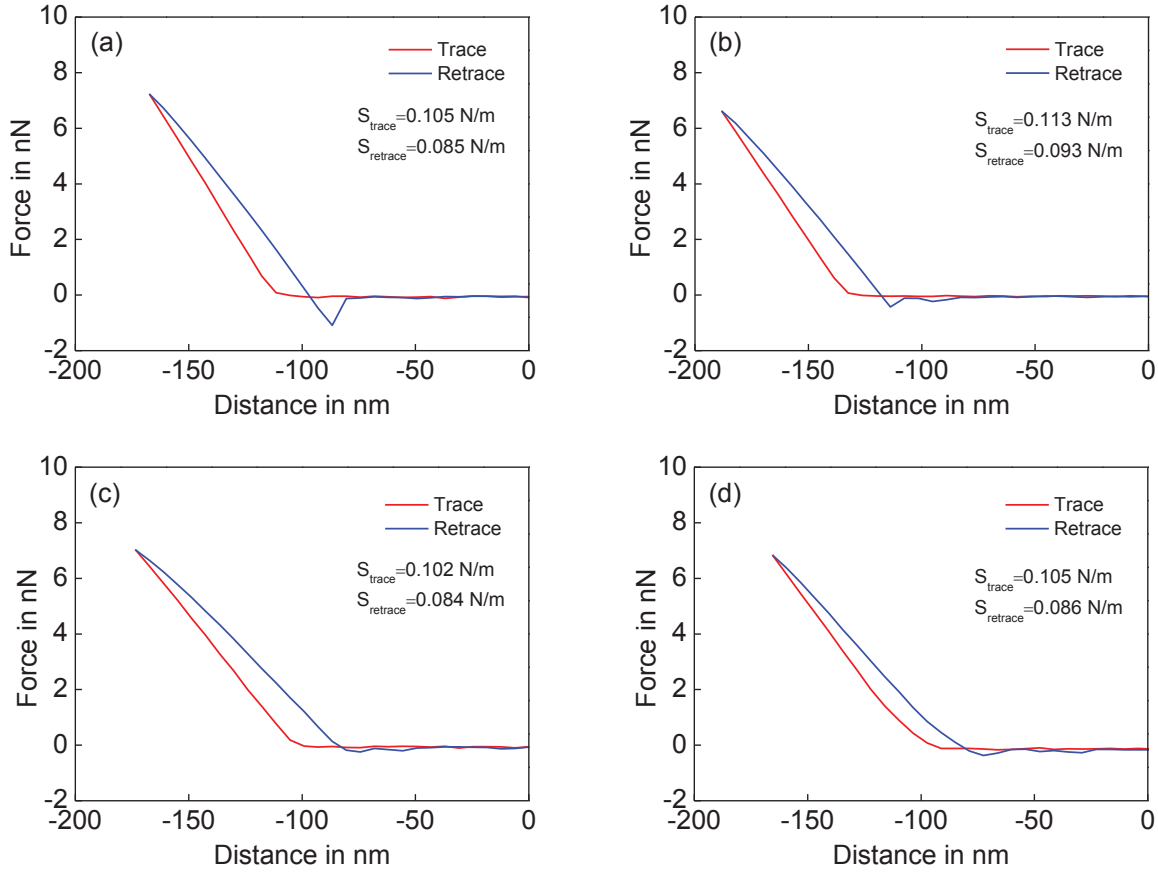

Figure 4-39 F-D curves for PVPVI at different concentrations as presented in Figure 4-37. (a) 0.01 mM PVPVI, set point 0.33 V, the maximal adhesive force 1.085 nN. (b) 0.05 mM PVPVI, set point 0.19 V, the maximal adhesive force 0.425 nN. (c) 0.1 mM PVPVI with the force load on the globular structure, set point 0.12 V, the maximal adhesive force 0.244 nN. (d) 0.1 mM PVPVI with the force load on the underlayer, set point 0.30 V, the maximal adhesive force 0.369 nN.

4.5.5 Acid blue 113-$C_{12\text{-}18}E_7$ at the graphite-solution interface

Figure 4-40 shows the images of mixtures of 0.009 mM Acid blue 113 with the nonionic surfactant $C_{12\text{-}18}E_7$ of different concentrations. At 0.003 mM of $C_{12\text{-}18}E_7$ (Fig. 4-40 (a)), the typical dye structure adsorbed on graphite as shown in Figure 4-34 (a) could not be seen. This indicates that the adsorption of the dye onto the surface is inhibited in the presence of the surfactant of even a low concentration below the CMC. The adsorption of the dye can be inhibited by the adsorption of $C_{12\text{-}18}E_7$ on graphite due to the higher affinity of the nonionic surfactant for graphite compared to the dye Acid blue 113.

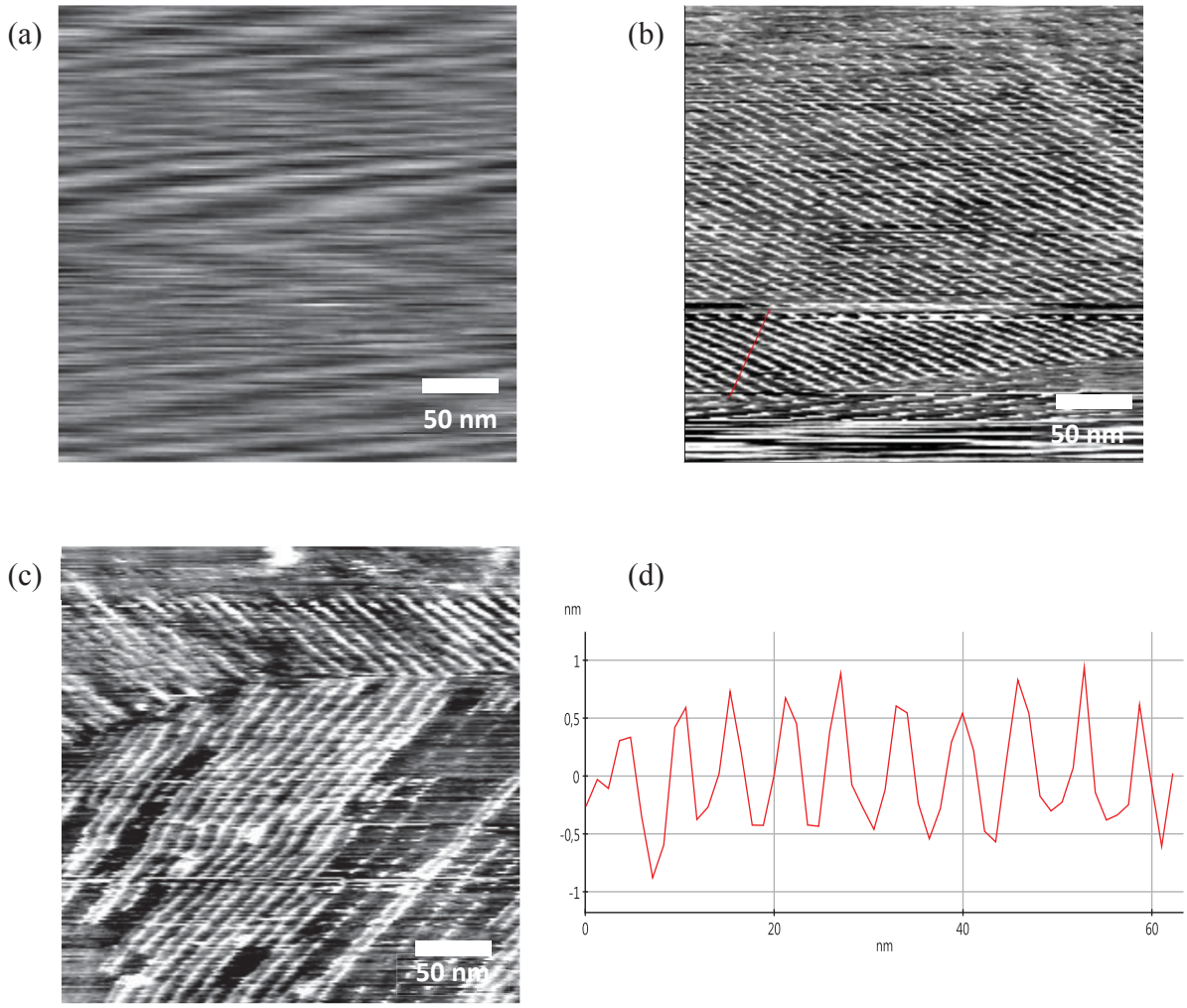

Figure 4-40 AFM images for the mixtures of 0.009 mM Acid blue 113 with (a) 0.003 mM, (b) 0.1 mM and (c) 50 mM $C_{12\text{-}18}E_7$ at the graphite-solution interface. (d) Height profile of the indicated line in (b). At 0.003 mM of $C_{12\text{-}18}E_7$ (below the CMC), no dye structure can be observed on graphite, indicating the inhibition of the dye adsorption due to the adsorption of surfactants. At the surfactant concentrations of 0.1 mM and 50 mM (above the CMC), it shows periodic parallel stripes implying the hemicylindrical surfactant aggregates. The periodicity of the surfactant structure is about 7.2 nm, which is higher than that of surfactants alone. This indicates that adsorbed $C_{12\text{-}18}E_7$ keeps the hemicylindrical aggregate structure with incorporated dyes in small amounts into surfactant aggregates.

At very low $C_{12\text{-}18}E_7$ concentrations (< CMC), $C_{12\text{-}18}E_7$ may adsorb on graphite in the form of monomers, i.e., forming a vertical or horizontal lamellar adlayer as mentioned in Section 2.3. In AFM topographical images, this continuous layer usually appears as featureless structures. According to the study of dye-surfactant interaction in solution phase (see Section 4.1.1 and 4.2.2), it is known that the dye interacts with $C_{12\text{-}18}E_7$ above the CMC by incorporation of the dye into surfactant micelles, thus an adsorption of the dye-surfactant complex is also not expected here.

As the concentration of $C_{12\text{-}18}E_7$ increases above the CMC, only periodic parallel stripes are seen (Fig. 4-40 (b) and (c)) on the surface. There are two domains in (c), where the long axes of aggregates have different orientations about 90° to each other. The periodicity of aggregate structures of $C_{12\text{-}18}E_7$ at 0.1 mM and 50 mM is 7.0 nm and 7.3 nm respectively (Tab. 4-21). The periodicity for mixtures of the dye with $C_{12\text{-}18}E_7$ is greater than that of $C_{12\text{-}18}E_7$ alone. Furthermore, the height of the aggregate structures is also increased compared to that in the absence of dye (Fig. 4-40 (d)). The increases in both lateral and vertical directions indicate an increase in the size of aggregates. It is suggested that the aggregate structure maintains the hemicylindrical structure as the surfactant alone adsorbed on graphite and the dye is incorporated into the hemicylindrical surfactant aggregates, resulting in the size increase of surfactant aggregates. It was found in UV-Vis spectroscopic studies that in solution one $C_{12\text{-}18}E_7$ micelle can bind 2−3 dye molecules at saturation (see Table 4-2).

Therefore, two effects were observed here for the mixture of the dye with the nonionic surfactant on graphite. On the one hand, at very low surfactant concentrations below the CMC the adsorption of the dye on graphite is inhibited due to the strong adsorption of surfactants. On the other hand, the dye may be incorporated into surfactant aggregates adsorbed in small amounts at surfactant concentrations above the CMC.

Table 4-21 Structures of the mixtures of Acid blue 113 (0.009 mM) with $C_{12\text{-}18}E_7$ at different surfactant concentrations adsorbed at the graphite-solution interface.

$C_{12\text{-}18}E_7$ in mM	**Surface**	**Periodicity in nm**
0.003	no dye structure	-
0.1	hemicylindrical structure	7.0 ± 0.5
50	hemicylindrical structure	7.3 ± 1

4.5.6 Acid blue 113-SDS at the graphite-solution interface

In general, the imaging for the mixture of Acid blue 113 and the anionic surfactant SDS was very noisy, where neither the dye structure nor the surfactants adsorbed could be recognized in AFM images at low SDS concentrations. This may be due to a considerable amount of

counterions in this system, which makes the force interaction between the tip and adsorbates complicated. At the high SDS concentration of 100 mM the periodic parallel stripes can partially be seen as indicated by arrows in Figure 4-41. The periodic structure indicates the hemicylindrical aggregate structure, which is characteristic for surfactants adsorbed on graphite.

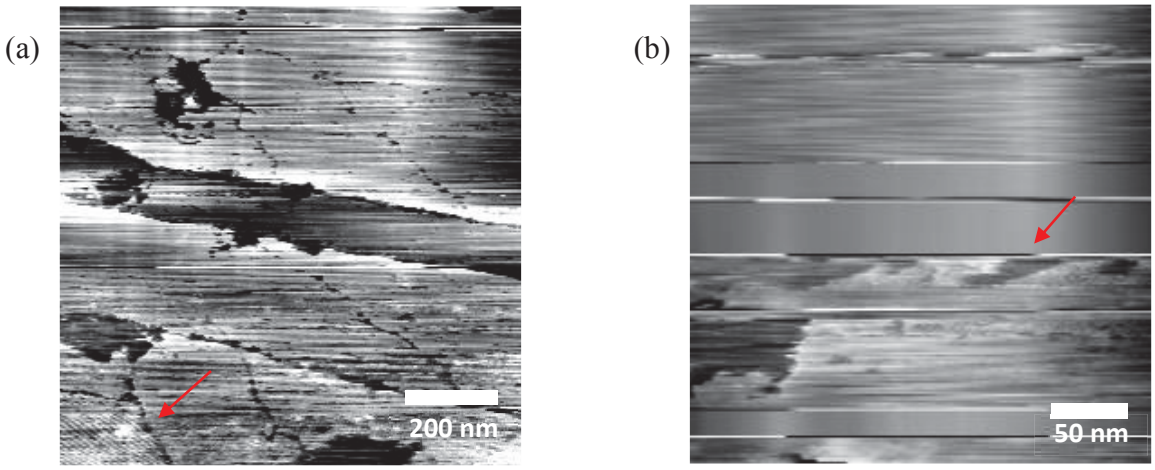

Figure 4-41 AFM images for the mixtures of 0.009 mM Acid blue 113 with 100 mM SDS at the graphite-solution interface. At the high SDS concentration (above the CMC) the periodic parallel stripes can partially be seen in the images (red arrows), indicating the hemicylindrical aggregate structure of surfactants. However, the imaging for the system was generally very noisy, the dimension of the structure could not be determined.

As seen in Section 4.4.2, the adsorption of the dye on carbon black can be inhibited by SDS of high concentrations above the CMC. One may expect that SDS can also compete with the dye during adsorption on the similar nonpolar graphite surface. In solution, the dye shows a weak interaction with SDS above the CMC, where on average 7−8 SDS micelles can bind only one dye molecule (see Table 4-2) at saturation. Because the contrast of the SDS structure in AFM images is too low, the dimension of the hemicylindrical surfactant structure cannot be determined. Therefore, it cannot be concluded whether there is also an interaction between the dye and SDS on graphite by incorporation of the dye in surfactant aggregates adsorbed, since the change in the surfactant aggregate structure cannot be confirmed in this case.

4.5.7 Acid blue 113-PVPVI at the graphite-solution interface

The structures of the mixtures of 0.009 mM Acid blue 113 with the DTI polymer PVPVI varying from $1 \cdot 10^{-6}$ mM to 0.1 mM and the mixture of 0.073 mM Acid blue 113 with 0.01 mM PVPVI were studied by AFM. Figure 4-42 shows four AFM images of the mixtures containing different polymer and dye concentrations. As seen here, unordered structures were observed for

all studied systems. It was found that in AFM images the surface becomes more homogeneous with increasing polymer concentrations. In addition, it is to note that at the high polymer concentration of 0.1 mM no polymer globule can be seen on the surface (Fig. 4-42 (c)). This indicates that Acid blue 113 has a higher affinity for graphite than PVPVI.

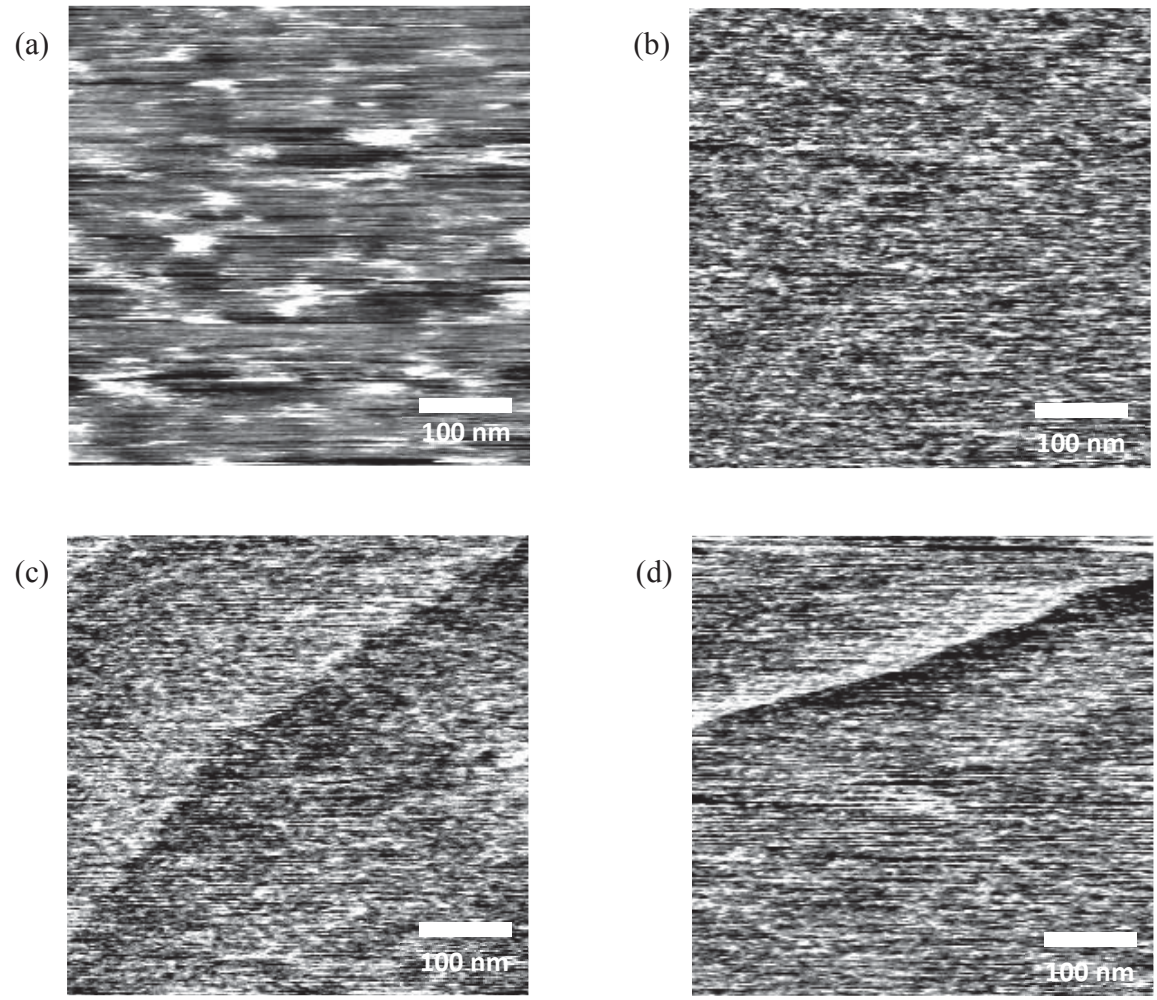

Figure 4-42 AFM images for mixtures of Acid blue 113 with PVPVI of different concentrations at the graphite-solution interface. The moles of PVPVI to Acid blue 113 are (a) $1 \cdot 10^{-4}$ mM/0.009 mM, (b) 0.01 mM/0.009 mM, (c) 0.1 mM/0.009 mM and (d) 0.01 mM/0.073 mM. The mixtures of Acid blue 113 with PVPVI show an unstructured layer adsorbed on graphite. Acid blue 113 shows a higher affinity for graphite than the DTI polymer. Above the CAC of the polymer, the dye forms a dye-polymer complex with the polymer on the surface.

In order to further understand the adsorbed structures for the mixture of the dye with the DTI polymer, the roughness of the surface for each system was investigated, as is shown in Table 4-22. At the very low polymer concentration of $1 \cdot 10^{-6}$ mM, the roughness of surface is similar to that of dye without the polymer. At the polymer concentration of $1 \cdot 10^{-4}$ mM the roughness S_q

increases to 0.503 nm and then decreases to 0.303 nm as the polymer concentration reaches 0.005 mM. From a polymer concentration of 0.01 mM, the roughness keeps almost constant and is independent of polymer concentrations. In addition, with an increased dye concentration to 0.073 mM the roughness of the surface is still not greatly changed.

Table 4-22 Surface roughness of adsorbed structures for the mixtures of Acid blue 113 with PVPVI with respect to various dye and polymer concentrations. The roughness values for each mixture are averaged from 3 to 6 AFM images with the scan size of 500×500 nm^2.

PVPVI/Acid blue 113	Roughness			
	S_q	S_q deviation	S_a	S_a deviation
in mM/mM	in nm	in nm	in nm	in nm
$1 \cdot 10^{-6}$/0.009	0.180	0.004	0.137	0.004
$1 \cdot 10^{-5}$/0.009	0.227	0.045	0.175	0.028
$1 \cdot 10^{-4}$/0.009	0.503	0.160	0.360	0.113
0.001/0.009	0.347	0.064	0.263	0.036
0.005/0.009	0.303	0.015	0.237	0.008
0.01/0.009	0.288	0.019	0.224	0.014
0.05/0.009	0.288	0.019	0.224	0.017
0.1/0.009	0.289	0.019	0.226	0.010
0.01/0.073	0.262	0.020	0.204	0.016

S_q: the root mean square height of the surface (see Section 2.4.4, Equation 2-35).
S_a: the arithmetic mean height of the surface (see Section 2.4.4, Equation 2-34).
Deviation: see Equation 1 in Appendix.

The change in roughness of the surface for the mixtures can be interpreted by the interaction of the dye with the polymer. According to the UV-Vis spectroscopic study for the mixture of 0.009 mM Acid blue 113 with PVPVI (see Section 4.1.3), it is known that Acid blue 113 interacts with PVPVI above the critical aggregation concentration (CAC) of about $1 \cdot 10^{-4}$ mM of the polymer. Until to about 0.01 mM PVPVI the interaction reaches an initial saturation, forming the (1:1) dye-polymer complex.

Acid blue 113 has a higher affinity for graphite than the DTI polymer. At very low polymer concentrations, only dye adsorbs on graphite. When the CAC of the polymer is reached, the adsorbed dyes begin to bind with the polymer forming the dye-polymer complex at the graphite-solution interface, which results in a significant increase in roughness of the surface.

With further increasing polymer concentrations, the roughness is decreased. That may be because if more and more dye-polymer complexes form on the surface, the complex may be more compacted, corresponding to a less rough surface. As all adsorbed dyes are bound with polymers, the adsorption of mixtures reaches saturation. From this point, the roughness is not changed any more, even at the high polymer concentration of 0.1 mM. On the other hand, a great increase in dye concentration did not make the surface rougher as well. It seems that neither the polymer nor the dye in the bulk phase tends to bind further with the dye-polymer complexes preadsorbed on the graphite. This effect is interesting for the influence of DTI polymer on the adsorption of dyes onto surfaces. That means the adsorption of the dye may be inhibited by addition of the polymer due to the formation of the dye-polymer adlayer. The inhibition of further dye adsorption may be attributed on the one hand to occupancy of the active adsorption sites for the dye and on the other hand to the change of the surface property due to adsorbed dye-polymer complexes.

4.5.8 $C_{12\text{-}18}E_7$-PVPVI at the graphite-solution interface

Structure of $C_{12\text{-}18}E_7$-PVPVI adsorbed on graphite

Figure 4-43 shows three AFM images of the mixtures of 0.1 mM PVPVI with $C_{12\text{-}18}E_7$ at different surfactant concentrations. At 0.003 mM of $C_{12\text{-}18}E_7$ the adsorption of PVPVI on graphite is markedly inhibited, where few polymer globules can be seen (Fig. 4-43 (a)). At the surfactant concentration of 0.1 mM the parallel stripes can be seen on the graphite surface (Fig. 4-43 (b)). The periodicity of stripes for the mixture is 6.1 ± 0.7 nm, which is in agreement with that for $C_{12\text{-}18}E_7$ alone at the same concentration (see Table 4-18). It was found that the height of the periodic structure of the mixture is still in the range of 250−500 pm (Fig. 4-43 (d)), which was also observed in $C_{12\text{-}18}E_7$ alone. After 24 h the aggregate structure remained unchanged and the periodicity increased slightly to 6.7 nm. This may result from contamination of the tip with time.

At 50 mM of $C_{12\text{-}18}E_7$ the periodic structure is still dominant, as shown in Figure 4-43 (c). The periodicity of the structure is about 6.2 nm. Therefore, it can be concluded that the hemicylindrical aggregate structure of $C_{12\text{-}18}E_7$ is not changed in the presence of PVPVI. At the high $C_{12\text{-}18}E_7$ concentration of 50 mM, the aggregate structure was found to be more fragile than that at lower surfactant concentrations. The instability of aggregates at high surfactant concentrations is related to the enhanced diffusion of surfactants between the interface and the bulk phase.

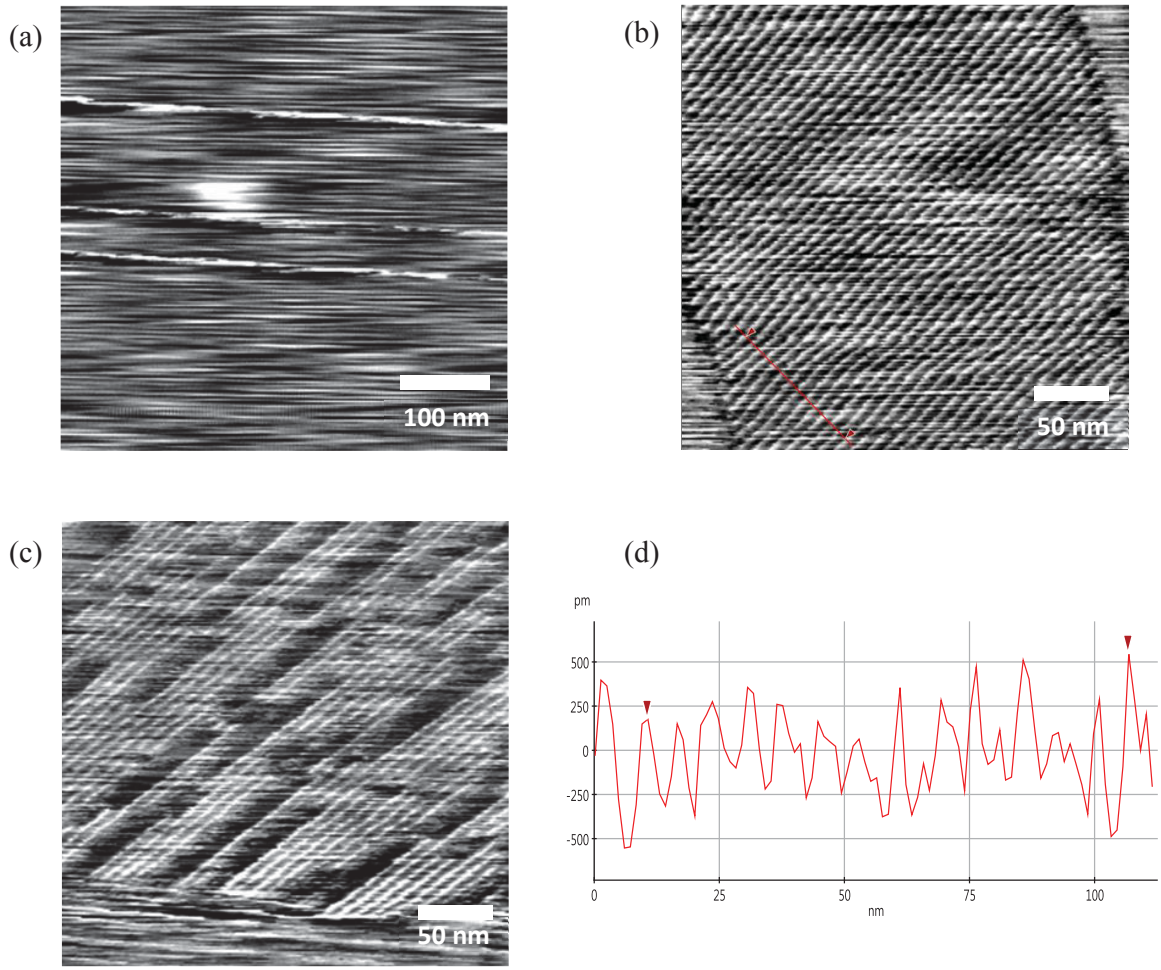

Figure 4-43 AFM images of mixtures of 0.1 mM PVPVI with (a) 0.003 mM, (b) 0.1 mM and (c) 50 mM $C_{12\text{-}18}E_7$ at the graphite-solution interface. (d) Height profile of the indicated line in (b). At a low surfactant concentration of 0.003 mM (below the CMC), the adsorption of polymer is markedly inhibited, where few adsorbed globular polymers can be observed. At the surfactant concentrations of 0.1 mM and 50 mM (above the CMC), it shows periodic parallel stripes. The periodicity and height of the structure agree with that of surfactants alone. This indicates that the hemicylindrical aggregate structure of $C_{12\text{-}18}E_7$ is not changed in the presence of PVPVI.

Table 4-23 Structures of the mixtures of PVPVI (0.1 mM) with $C_{12\text{-}18}E_7$ at different surfactant concentrations adsorbed at the graphite-solution interface.

$C_{12\text{-}18}E_7$ in mM	**Surface**	**Periodicity in nm**	**After 24 h**
0.003	few polymer globules	-	-
0.1	hemicylindrical surfactant structure	6.1 ± 0.7	6.7 ± 0.6
50	hemicylindrical surfactant structure	6.2 ± 0.8	-

F-D measurement of $C_{12\text{-}18}E_7$-PVPVI adsorbed on graphite

Figure 4-44 shows the F-D measurements on the mixtures of PVPVI and $C_{12\text{-}18}E_7$ as presented in Figure 4-43. By contrast with the system of 50 mM $C_{12\text{-}18}E_7$ + 0.1 mM PVPVI (Fig. 4-44 (d)), the systems at lower surfactant concentrations (Fig. 4-44 (a)−(c)) represent higher stiffness, corresponding to greater slope of the curves in the contact region.

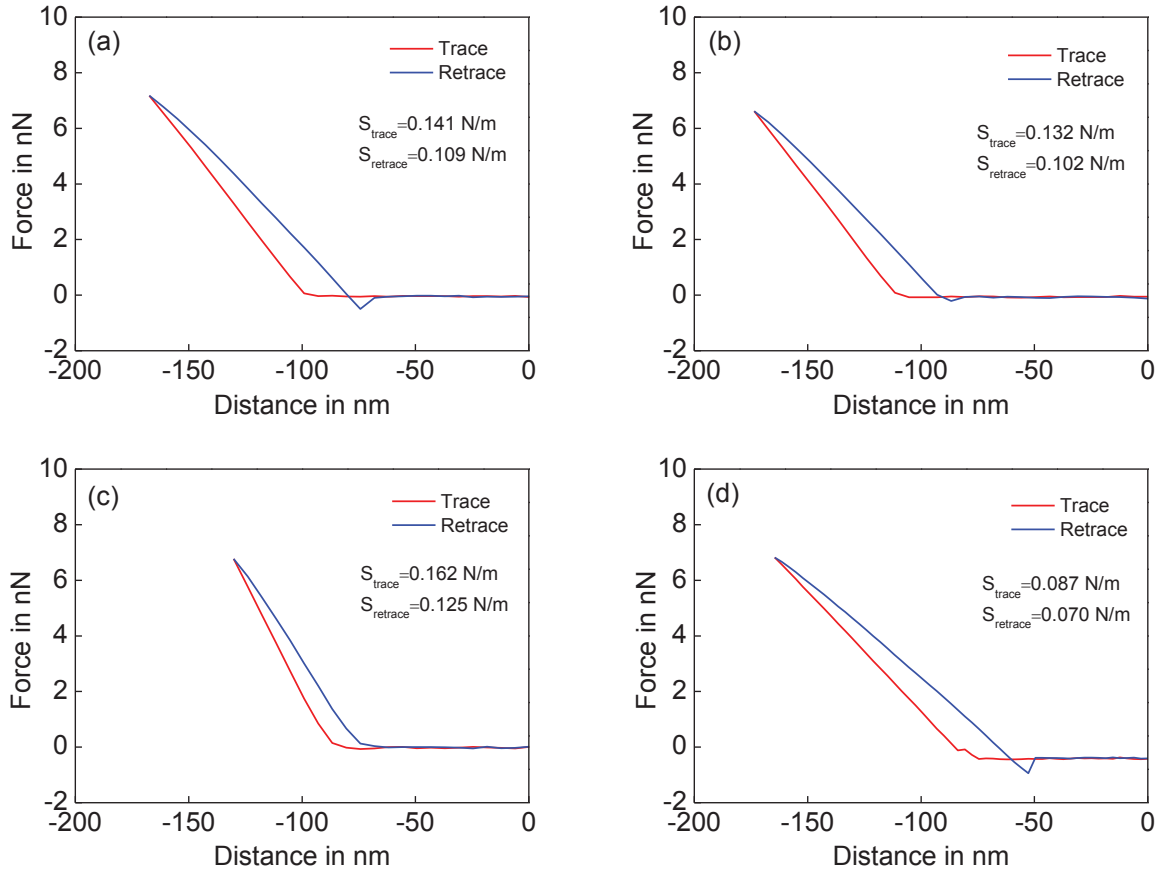

Figure 4-44 F-D curves for mixtures of 0.1 mM PVPVI and $C_{12\text{-}18}E_7$ at different surfactant concentrations as shown in Figure 4-43. (a) 0.003 mM $C_{12\text{-}18}E_7$ with the load on the surface in Figure 4-43 (a), set point 0.28 V, the maximal adhesive force 0.501 nN. (b) 0.003 mM $C_{12\text{-}18}E_7$ with the load on the globular structure in Figure 4-43 (a), set point 0.28 V, the maximal adhesive force 0.209 nN. (c) 0.1 mM $C_{12\text{-}18}E_7$, set point 0.33 V. (d) 50 mM $C_{12\text{-}18}E_7$, set point 0.15 V, the tip jumps to contact with the graphite surface at a force of 0.081 nN and jumps off contact at a force of 0.894 nN (maximal adhesion). The thickness of adsorbed layer determined by the approach curve is 3.2 nm, indicating a monolayer of hemicylindrical surfactant aggregates.

The F-D curves in Figure 4-44 (a) relate to the surface for the mixture of PVPVI with 0.003 mM $C_{12\text{-}18}E_7$, where there is no globular structure (ref. Fig. 4-43 (a)). The F-D curves in Figure 4-44 (b) were obtained, when the force was loaded on the globular structure in Figure 4-43 (a). It can be seen here that the curves for the surface without adsorbed polymer in (a) have higher gradients of force with respect to the distance than those for the adsorbed polymer

globule in (b). The retraction curve of (a) shows a distinct adhesion of tip to the surface, where the pull-off force is 0.501 nN. The pull-off force is lower than that for graphite in water. This implies that the graphite surface is covered by surfactant molecules to some extent. The pull-off force of the globular structure is 0.209 nN, which is comparable with that measured force of 0.244 nN for the polymer globule adsorbed on graphite (see Fig. 4-39 (c)).

At 0.1 mM of $C_{12\text{-}18}E_7$ (Fig. 4-44 (c)), no adhesion was observed in the F-D measurement. At the very high $C_{12\text{-}18}E_7$ concentration of 50 mM (Fig. 4-44 (d)), the tip jumps to contact with the graphite surface at a force of 0.081 nN and a maximal adhesion occurs at a force of 0.894 nN. According to four F-D measurements at different loaded positions for the mixture of the polymer with 50 mM $C_{12\text{-}18}E_7$, the thickness of the adsorbed surfactant layer in the presence of 0.1 mM PVPVI is evaluated to be 3.2 nm, which is in good agreement with the thickness of the monolayer of hemicylindrical $C_{12\text{-}18}E_7$ micelles alone (3.1 nm), as stated in Section 4.5.1. Hence, the periodic structures presented in Figure 4-43 refer to the monolayer of hemicylindrical surfactant aggregates adsorbed.

Therefore, by the AFM study it is concluded that the adsorption of PVPVI onto graphite is markedly inhibited in mixture with $C_{12\text{-}18}E_7$ of even very low concentrations below the CMC. Thus, the hemicylindrical structure of surfactant aggregates is not changed in the presence of the polymer. This indicates that the adsorption of surfactant and that of polymer onto surface is also competitive in surfactant-polymer binary mixtures.

4.5.9 SDS-PVPVI at the graphite-solution interface

The structures of mixtures of 0.1 mM PVPVI and SDS at different surfactant concentrations are shown in Figure 4-45. At 0.1 mM of SDS the globular structure of PVPVI can still be seen on the graphite surface (Fig. 4-45 (a)). It was found that the size of globules is not changed compared with that in the absence of SDS. As shown in Figure 4-45 (b), up to 0.8 mM SDS no globular structure of polymer can be seen on the surface. At the high SDS concentration of 100 mM the periodic parallel structures of surfactants are shown (Fig. 4-45 (c)). The periodicity of the parallel structures is 5.3 ± 0.3 nm. This periodicity is in good agreement with that of SDS alone adsorbed on graphite. A height profile of the periodic structure is shown in Figure 4-45 (d), corresponding to the indicated line in (c). The height of structure is about 200 pm, which is in the range of that for SDS alone. Therefore, it is concluded that the adsorption of PVPVI onto graphite is inhibited by low SDS concentrations ($<$ CMC). Nevertheless, the hemicylindrical structure of surfactant aggregates is not changed in the presence of the polymer.

As shown in (c), the surfactant aggregate structure in the presence of the polymer is not completely seen in the image. This may be on the one hand due to the instability of surfactant aggregates adsorbed owing to the repulsion between ionic headgroups of SDS as mentioned in Section 4.5.2, and on the other hand, to the loosely overlying polymer chains on surfactants which may be scratched by the AFM tip during imaging, resulting in the partial destruction of surfactant aggregates.

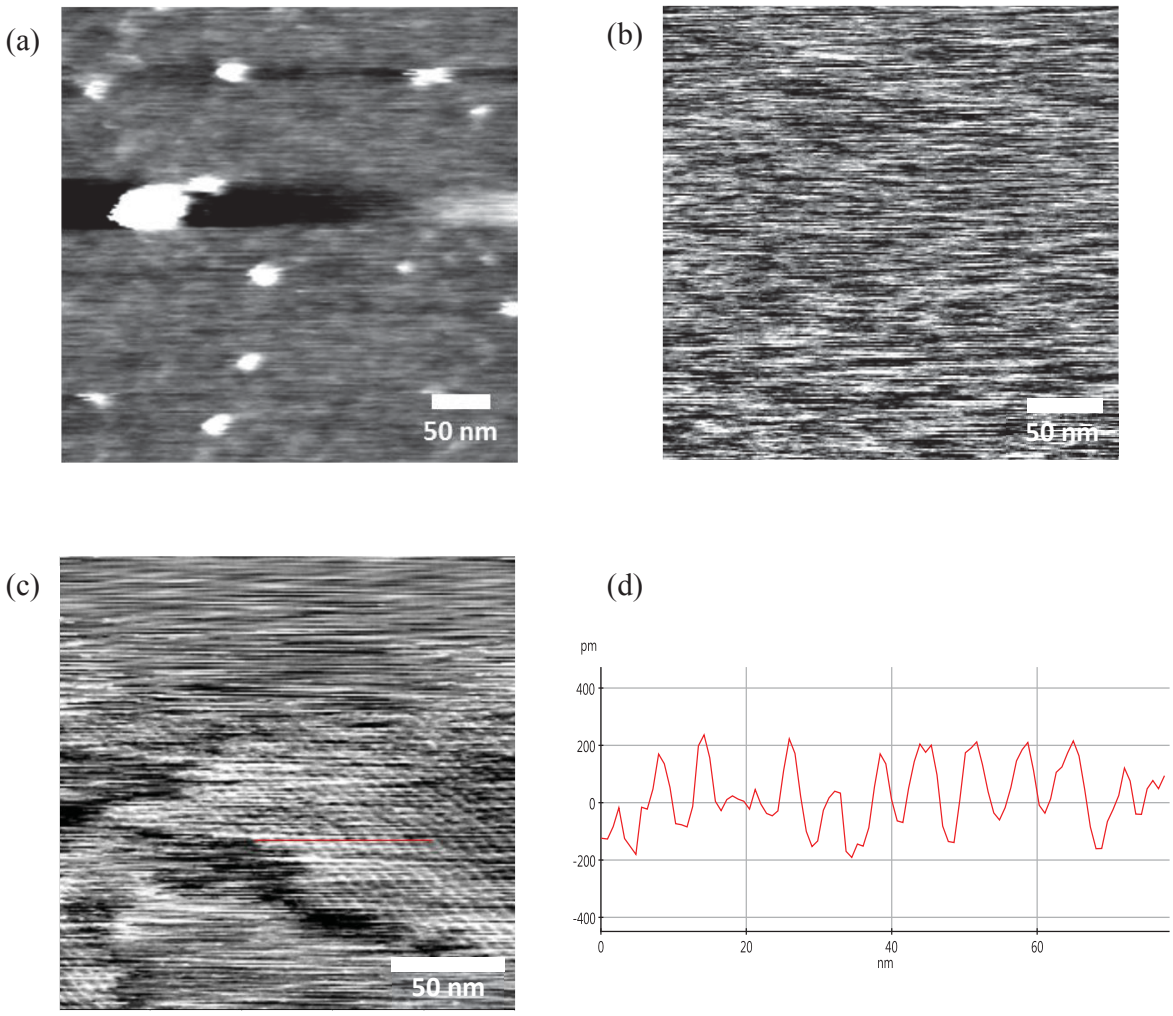

Figure 4-45 AFM images of mixtures of 0.1 mM PVPVI with (a) 0.1 mM, (b) 0.8 mM and (c) 100 mM SDS at the graphite-solution interface. (d) Height profile of the indicated line in (c). At a very low surfactant concentration of 0.1 mM (below the CMC), the globular structure of polymer can still be seen on the surface. At the surfactant concentration of 0.8 mM (~0.1×CMC), the adsorption of polymer is inhibited and the graphite surface shows an unstructured layer. At the high surfactant concentration of 100 mM (> CMC), it shows periodic parallel structures. The periodicity and height of the structure agree well with those of surfactants alone. This indicates that the hemicylindrical aggregate structure of SDS is not changed in the presence of PVPVI.

Fleming et al.[127] demonstrated the adsorption of the mixture of poly(vinylpyrrolidone) (PVP) with SDS at the graphite-solution interface by the study of interaction force using AFM. In addition, the adsorbed amounts of PVP in mixture with SDS on carbon black reported by Ma et al.[128] and in mixture with LiDS on graphite by Otsuka et al.[129] using electron spin resonance (ESR) are enhanced in the presence of surfactants, indicating the formation of surfactant-polymer complexes at solid-liquid interfaces. Thus, one may expect here a cooperative adsorption of SDS and PVPVI at low surfactant concentrations (below the CMC) as shown in Figure 4-45 (b), since the interaction of SDS with PVPVI was verified both at the air-water interface and in the bulk phase. However, at high surfactant concentrations ($>$ CMC), the graphite surface is dominated by surfactants, whereas the adsorption of polymer is inhibited due to the competitive adsorption of surfactant. Therefore, the adsorption of the DTI polymer can be inhibited also by the anionic surfactant SDS at higher surfactant concentrations than that by the nonionic surfactant $C_{12\text{-}18}E_7$.

Table 4-24 Structures of the mixtures of PVPVI (0.1 mM) with SDS at different surfactant concentrations adsorbed at the graphite-solution interface.

SDS in mM	**Surface**	**Periodicity in nm**
0.1	polymer globules	-
0.8	no polymer globule (unstructured)	-
100	hemicylindrical surfactant structure	5.3 ± 0.3

In this study, AFM proves to be an approachable and a very informative method to identify the adsorption structures of single components and of binary mixtures of dye, surfactant and DTI polymer on graphite. The AFM studies provide information about the structures of adsorbed layers of binary aqueous mixtures at solid-liquid interfaces and allow the allocation of individual components, which is difficult to access with other methods. The identification of adsorption structures on the model surface gives an understanding of the adsorption of the dye in mixture with surfactant and DTI polymer and a clarification of the influence of surfactant and DTI polymer on the dye adsorption for a hydrophobic surface. To give an overview of AFM studies at the graphite-solution interface regarding different systems, the AFM results are summarized in Table 4-25.

Table 4-25 Summary of results from the AFM study with respect to the adsorption structures for different systems.

System	Concentration in mM	Surface	Periodicity or Diameter in nm	Roughness in nm
$C_{12\text{-}18}E_7$	0.1−50	hemicylindrical structure	5.9 ± 0.3	
SDS	50−100	hemicylindrical structure	5.4 ± 0.2	
Acid blue 113	0.009−0.073	unstructured adlayer		S_q: 0.180−0.240 S_a: 0.142−0.180
PVPVI	0.01	no adsorbed polymer		
	0.05	polymer layer		S_q: 0.348 ± 0.056 S_a: 0.272 ± 0.040
	0.1	globular structure	13−18 (52%)	
$C_{12\text{-}18}E_7$/ Acid blue 113	0.003/0.009	no adsorbed dye		
	0.1/0.009	hemicylindrical structure	7.0 ± 0.5	
	50/0.009	hemicylindrical structure	7.3 ± 1.0	
SDS/ Acid blue 113	100/0.009	hemicylindrical structure	n.a.	
PVPVI/ Acid blue 113	10^{-6}−0.1/0.009	unstructured adlayer		S_q: 0.180−0.503 S_a: 0.137−0.360
	0.01/0.073	unstructured adlayer		S_q: 0.262 ± 0.020 S_a: 0.204 ± 0.016
$C_{12\text{-}18}E_7$/PVPVI	0.003/0.1	few polymer globules	12−18 (67%)	
	0.1/0.1	hemicylindrical structure	6.1 ± 0.7	
	50/0.1	hemicylindrical structure	6.2 ± 0.8	
SDS/PVPVI	0.1/0.1	polymer globules	13−18 (57%)	
	0.8/0.1	no polymer globule (unstructured layer)		
	100/0.1	hemicylindrical structure	5.3 ± 0.3	

n.a.: not available.

It was found that the dye Acid blue 113 adsorbs on graphite in an unstructured way, forming single dye molecules and small dye aggregates. The adsorbed amount of the dye on graphite is increased at high dye concentrations, which agrees well with the results on carbon black.

At the concentration of 0.05 mM, the DTI polymer PVPVI adsorbed on graphite favors an expanded conformation differing from the conformation of coiling chains in the bulk phase at the same concentration derived by DLS. At the concentration of 0.1 mM, PVPVI forms single globular structures mostly with a diameter of 15−17 nm, which is in agreement with the size of one polymer molecule in the bulk phase determined by DLS.

It is demonstrated that in binary systems the adsorption of individual components onto graphite is competitive. In general, surfactants have higher adsorption preference for the graphite than the dye and DTI polymer, which can be arranged in the order: $C_{12\text{-}18}E_7$, SDS > Acid blue 113 ≳ PVPVI. Both the adsorption of the dye and of the DTI polymer on graphite can be inhibited by surfactants. In the mixture of the dye with the nonionic surfactant (> CMC), the size of the hemicylindrical surfactant structure is increased, indicating the incorporation of the dye into surfactant aggregates adsorbed on graphite. The incorporation of the dye into surfactant micelles was also found in solution above the CMC according to studies by UV-Vis spectroscopy and DLS. Therefore, the adsorption of the dye on the surface is affected by two factors: the competitive adsorption and the incorporation of the dye into micellar surfactant aggregates adsorbed on surface. Additionally, it was observed that the dye forms a dye-polymer complex with the DTI polymer on graphite above the CAC of the polymer, which is in correspondence with the UV-Vis spectroscopic and DLS study for the dye-polymer interaction in solution.

4.6 Outlook: polyamide surfaces

The investigation on the model surface graphite by AFM, supplemented by the studies in solution and at air-solution as well as carbon black-solution interfaces, clarified the influence of surfactants and the DTI polymer on the adsorption of the dye on hydrophobic model surfaces. In order to get a further understanding of adsorption mechanism of dyes on textile or textile-like surfaces, the polyamide surface is chosen as such an applicable surface. As preparation for future studies, different polyamide (PA) surfaces are characterized by AFM to expand the knowledge and know-how acquired to study on textile-like surfaces and allow the comparison on different surfaces (substrates).

4.6.1 Preparation of polyamide films

The polyamide (PA) films are prepared from commercial PA fabrics (EMPA 406, Swissatest Testmaterialien) or PA 66 granules (Sigma-Aldrich). The preparation of these PA films is described in Table 4-26. The material was dissolved in formic acid or in a mixture of formic acid and acetic acid in a certain ratio by weight to produce the polyamide solution. After mixing, the polyamide solution was spread on a flat glass using an applicator (Thierry) with the thickness of 500 µm and then dried in air at room temperature. The dry film was fixed on the magnetic disk using double-sided tape for imaging in air. For the imaging in liquid the film was fixed at the bottom of a petri dish (PS) with a 2-part epoxy adhesive (UHU).

Table 4-26 Preparation of PA films for AFM studies.

Sample	Material	Solvent	Ratio of material and solvents in w %	Dissolution time in h	Dissolution temperature in °C
PA-A1	PA 66 granule	AS	1 : 9	3	40
PA-A2	PA 66 granule	AS : ES	1 : 6 : 3	4	40
PA-B1	PA fabric	AS	1 : 9	3	22
PA-B2	PA fabric	AS : ES	1 : 6 : 3	4	22

AS: formic acid.
ES: acetic acid.

4.6.2 Characterization of polyamide surfaces by AFM

As reference, the surface structures of PA fibers are compared with those of PA films measured in air. As can be seen in Figure 4-46 (a) and (b), the surface of PA fibers after washing was not essentially changed in comparison with that of untreated fibers. The PA fiber surface appears as nodular structures, the length of which varies from several tens to hundreds of nanometers. The roughness S_q of the surface in the micrometer size is about 2 ± 0.5 nm. Moreover, the elongated nodules show a preferred orientation in which the fiber may be drawn during the production. The reproduced PA-B1 film from PA fabrics (Fig. 4-46 (c)) by dissolving in formic acid exhibits a similar surface structure to that of original PA fibers (Fig. 4-46 (a) and (b)). In contrast, the PA-B2 film prepared with a mixed solvent of formic acid:acetic acid (2:1) shows a different feature, where the nodular structure is not elongated (Fig. 4-46 (d)).

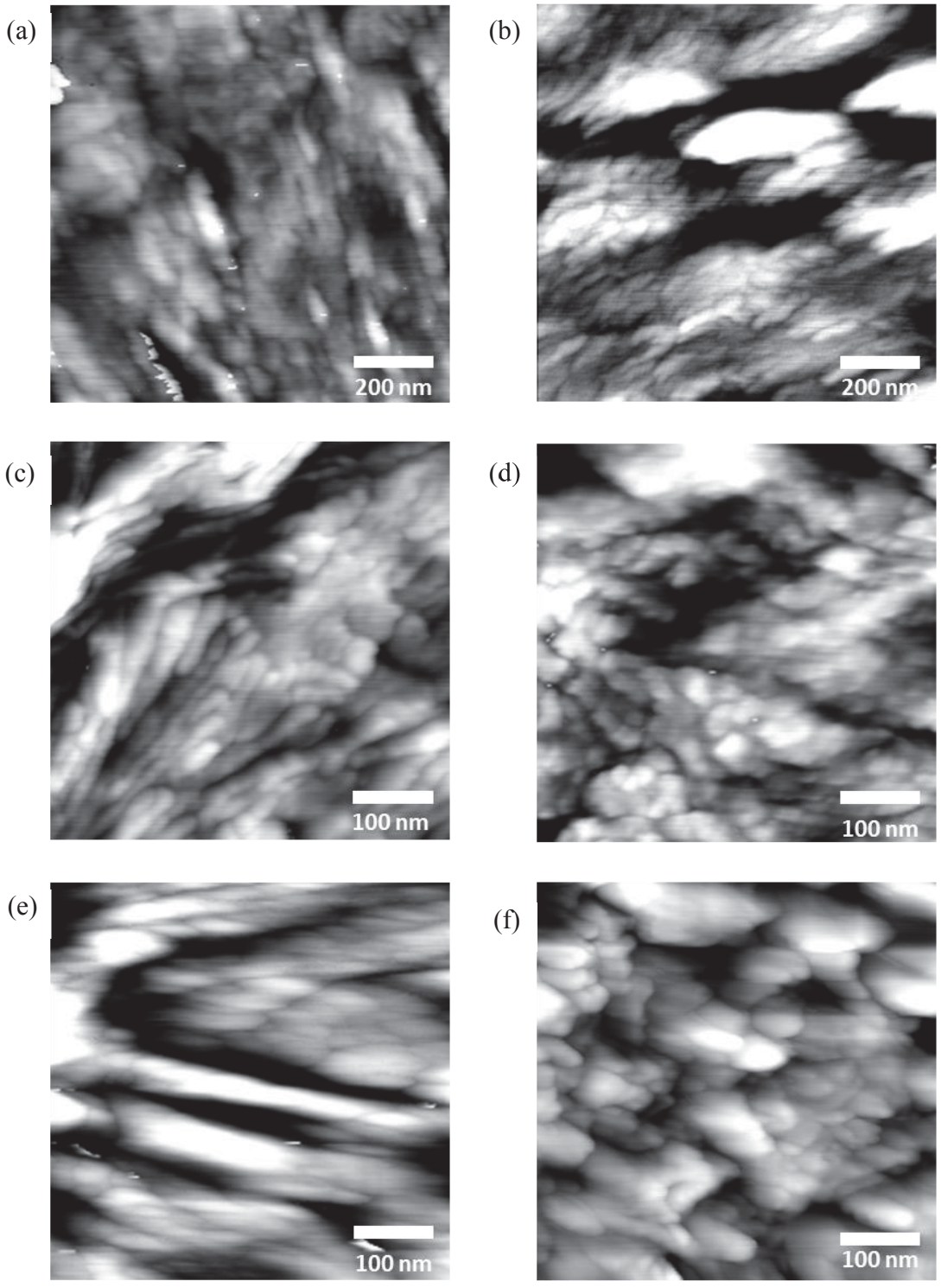

Figure 4-46 AFM images of (a) untreated PA fiber, (b) PA fiber dried after washing in water, (c) PA-B1 film, (d) PA-B2 film, (e) PA-A1 film and (f) PA-A2 film. The imaging of (a) and (b) was conducted in air by noncontact mode and the imaging of (c)-(f) in air by Tapping mode. The structure of PA surfaces appears generally as nodular structures.

Both PA films from PA granules have also nodular surface structures, as seen in Figure 4-46 (e) and (f), however, the nodules seem to be greater compared to those of PA-B1 and PA-B2 films. This may be attributed to the higher purity of the polymer in granules than that in fabrics. The fabrics may contain other additives, such as TiO_2 or antistatic agents besides the major polyamide,[130] which can cause nucleation of small assemblies resulting in more heterogeneous surfaces. Moreover, the reproduced PA films have generally a greater roughness and roughness variation (5 ± 2 nm) than PA fibers.

It was found that the PA films from PA fabrics (PA-B1 and PA-B2) were not resistant to the 2-part epoxy adhesive, hence, the surface structures of the PA-A1 and PA-A2 films from PA granules in water were studied by AFM. For the AFM study of polyamide surfaces in liquid, the measurements were carried out by different scan modes. Although the Tapping mode is traditionally considered to be more appropriate for the polymer surface due to the significantly reduced force acting on the sample,[131,132] it was found, however, in the study of polyamide surfaces in water that the contact mode brought the best resolution, despite the surface might be damaged to some extent during imaging.

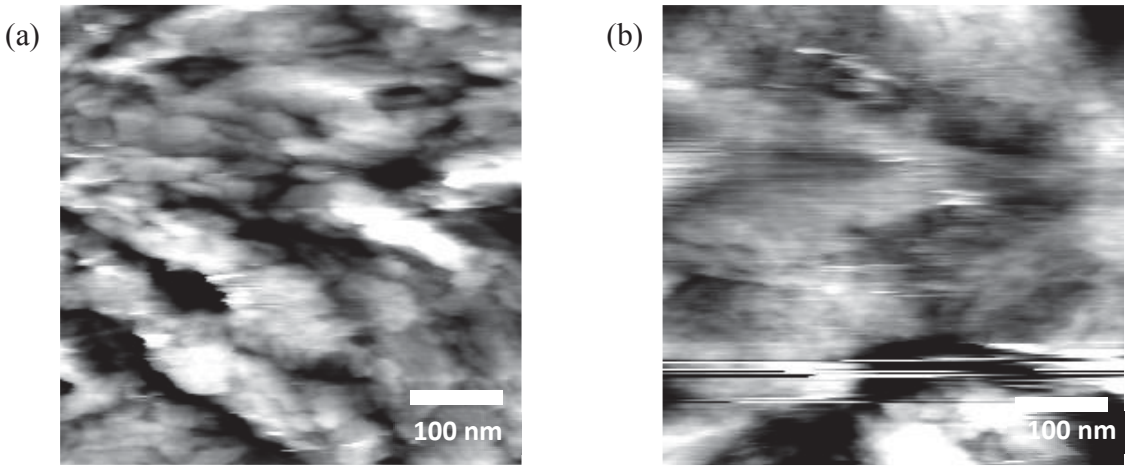

Figure 4-47 AFM images of (a) PA-A1 film and (b) PA-A2 film in water. All images were captured in liquid by contact mode.

Figure 4-47 (a) and (b) show the PA-A1 and PA-A2 films in water respectively. Comparing with the surfaces in air (Fig. 4-46), the nodular structure of the PA film in water looks fuzzy, but the roughness of surface is still in the same order of magnitude as the surfaces in air. This implies that the film has swelled after immersion in water. On the other hand, due to the wetting

the film can be very soft, where the tip-induced force may result in a compliable deformation of the local structure while scanning over the surface.

As seen in the study conducted in air, the surfaces of the commercial polyamide fibers and reproduced polyamide films can be well identified by AFM. The surface resemblance between the fiber and the reproduced film is very important for further studies. That means the PA films can serve as substrates for the further investigation, providing information that can also be applicable for textile surfaces.

However, because of the wetting of the PA fibers and films in liquid the identification of their surface structures or the adsorption structures on these surfaces can be difficult by AFM directly in solution. An AFM study showed that SAC micelles with a diameter of 25−60 nm are formed on nylon surfaces, which are immersed in sulfonated aromatic compounds (SACs) and then dried in air.[133] Hence, the further study of interactions of the dye with additives on textile surfaces by AFM is suggested to be carried out under dry conditions.

5 Summary and conclusions

In this work, the adsorption structures of single components and of binary mixtures of the dye Acid blue 113, the nonionic surfactant $C_{12\text{-}18}E_7$ as well as the anionic surfactant SDS and the DTI polymer PVPVI on graphite were identified for the first time by AFM in solutions. In addition, the adsorption of the dye and the dye in mixture with SDS on carbon black was quantified and compared with AFM studies. To develop structural models for the model systems, additionally, the interaction of these components in solution was studied by UV-Vis spectroscopy and DLS and the interaction at the air-solution interface was determined by surface tension measurements. In combination of results obtained, structural models for the interaction between surfactant, polymer and dye in solution and at solid-liquid interfaces are suggested to gain an understanding of the influence of surfactant and DTI polymer on dye transfer at a molecular level.

5.1 Interaction in solution

By UV-Vis spectroscopy it was found that the dye Acid blue 113 interacts with the nonionic surfactant $C_{12\text{-}18}E_7$, the anionic surfactant SDS and the DTI polymer PVPVI respectively, all resulting in a bathochromic shift of the dye absorption spectrum, which indicates the dye-surfactant and dye-polymer interaction in solution. Acid blue 113 interacts with surfactants above the CMC, indicating the incorporation of the dye into surfactant micelles. At saturation one $C_{12\text{-}18}E_7$ micelle can bind 2−3 dye molecules and on average 7−8 SDS micelles can bind only one dye molecule. Therefore, the dye shows a weak interaction with SDS, which can be attributed to the repulsion of anionic groups of the dye and SDS. Acid blue 113 interacts with the DTI polymer PVPVI above the CAC of the polymer ($\sim 1 \cdot 10^{-4}$ mM) forming the 1:1 dye-polymer complex at an initial saturation. The binding preference of additives for the dye determined by the UV-Vis spectroscopic study can be ordered: $C_{12\text{-}18}E_7$ > PVPVI > SDS (in terms of mass) and PVPVI > $C_{12\text{-}18}E_7$ > SDS (in terms of mole/molecule).

Figure 5-1 shows structural models suggested for the interaction of Acid blue 113 with $C_{12\text{-}18}E_7$, SDS and PVPVI in solution respectively in dependence of surfactant and polymer concentrations. According to the DLS study, Acid blue 113 forms aggregates in aqueous solution. In mixture with surfactants above the CMC, the dye is incorporated into surfactant micelles. Above the CAC of the polymer, the dye forms dye-polymer complexes with the

polymer. The dye-surfactant and dye-polymer interaction results in the dissolution of dye aggregates in surfactant and polymer solution.

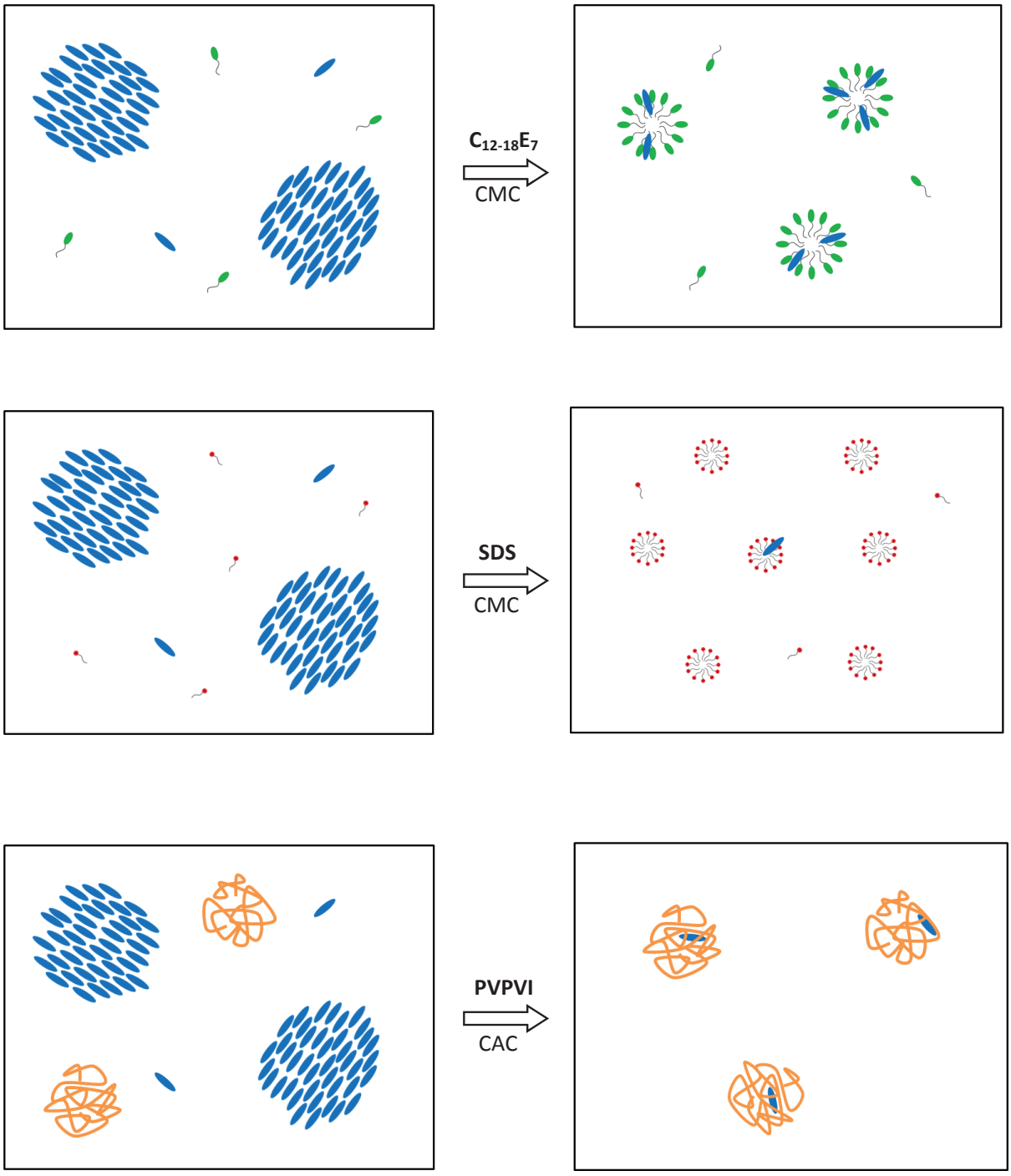

Figure 5-1 Schematic illustrations for the interaction of the dye Acid blue 113 (blue) with the nonionic surfactant $C_{12\text{-}18}E_7$ (green), the anionic surfactant SDS (red) and the DTI polymer PVPVI (orange) (not precisely scaled). Acid blue 113 interacts with $C_{12\text{-}18}E_7$ and SDS above the CMC by incorporation of the dye into surfactant micelles. One $C_{12\text{-}18}E_7$ micelle can bind 2−3 dye molecules at saturation and on average 7−8 SDS micelles can bind only one dye molecule, where the dye may be situated in the hydrophilic shell partially penetrating in the hydrophobic region. Acid blue 113 interacts with PVPVI above the CAC of the polymer, forming a (1:1) dye-polymer complex at an initial saturation.

In addition, in the study of three-component systems of dye + polymer + surfactant it was found that the binding of the dye to additives is competitive. At high polymer concentrations, the dye has a higher preference to the polymer than surfactants. Nevertheless, at low polymer concentrations the anionic surfactant SDS can influence the dye-polymer binding indicating the dye-polymer-surfactant complex due to the SDS-PVPVI interaction, which was also observed in the DLS study. The interaction between SDS and PVPVI in the bulk phase is interpreted in the next section as shown in Figure 5-2.

5.2 Interaction at the air-solution interface

According to the study at the air-solution interface by surface tension measurements, the anionic surfactant SDS interacts with the DTI polymer PVPVI at the air-solution interface. In contrast, no interaction between the nonionic surfactant $C_{12\text{-}18}E_7$ and PVPVI at the air-solution interface was observed. It is suggested that the association of SDS with PVPVI is due to the electrostatic attraction between the anionic surfactant and the polyelectrolyte,[109] as illustrated in Figure 5-2 (left). The surfactant-polymer interaction at the air-solution interface results in a surface tension reduction of the mixture at lower surfactant concentrations compared to the surfactant alone.

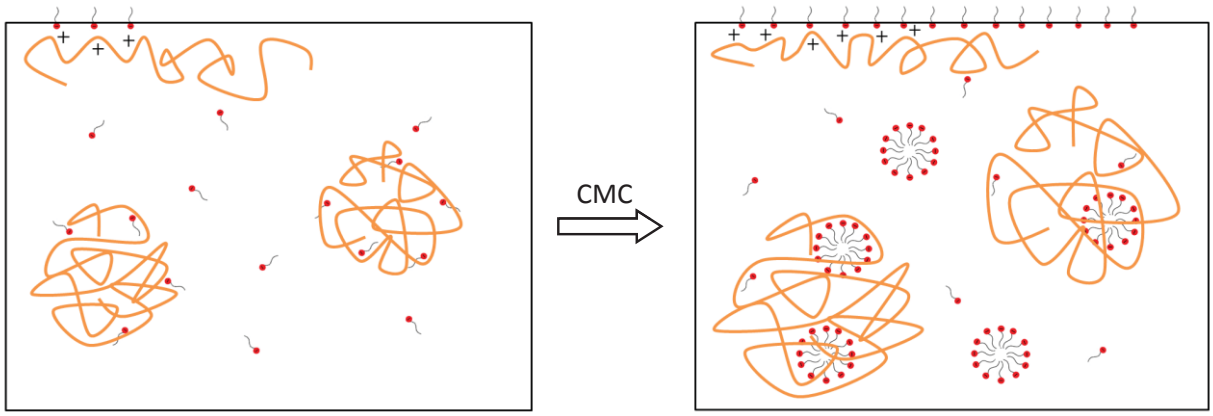

Figure 5-2 Illustration of the interaction between SDS (red) and PVPVI (orange) at the air-solution interface and in the bulk phase (not precisely scaled), suggested on the basis of the literature[108,109]. Left: the association of the surfactant and the polymer at the air-water interface results in the surface tension reduction at lower surfactant concentrations compared to the surfactant alone. Right: above the CMC surfactants continue to aggregate to form micelles bound with the polymer, resulting in a size increase of the polymer due to the surfactant-polymer complex in comparison with the polymer alone.

The DLS study showed that, at surfactant concentrations above the CMC the size of polymer is obviously increased, which can be explained by the formation of surfactant micelles bound with the polymer (Fig. 5-2, right). It is assumed that above the CMC surfactants aggregate at specific

sites of the polymer chain to form micelles, driven by the hydrophobic interaction between surfactants[108]. At the region above the CMC surfactant-polymer complexes and polymer-free surfactant micelles are coexistent.

5.3 Interaction at the carbon black-solution interface

In order to understand the adsorption mechanism of the dye on solid surface and supplement AFM studies on graphite, the adsorption of the dye and the dye in mixture with SDS at the carbon black-solution interface was quantified by analysis of adsorption isotherms. The adsorption of the dye Acid blue 113 alone on carbon black follows the Freundlich adsorption model, which indicates a heterogeneous adsorption. The adsorbed amount of the dye increases with increasing dye concentrations until to its solubility limit in water. Considering the molecular area of the dye, the maximal adsorbed amount of the dye corresponds to a coverage of about 40% for the total carbon black surface, indicating averagely a monomolecular adsorption.

In mixture with the anionic surfactant SDS, the adsorption of the dye on carbon black becomes more homogeneous obeying the Langmuir adsorption model. The change in the adsorption model from Freundlich to Langmuir can be explained by the finely divided dye adsorption due to the finer dispersion of the dye by addition of surfactants. In mixture with SDS, the adsorption of the dye at low dye concentrations is not influenced by surfactant concentrations, showing comparable Langmuir constants ($522-535$ m^3/mol) and at high dye concentrations the adsorbed amounts of the dye decrease in the presence of high surfactant concentrations ($>$ CMC), resulting in a plateau of lower level in the adsorption isotherm. This indicates that the adsorption of the dye on the surface can be inhibited by the surfactant of high concentrations ($>$ CMC) to some extent.

5.4 Interaction at the graphite-solution interface

The AFM studies at the graphite-solution interface gave an understanding of adsorption structures of individual components and the binary mixtures at the solid-liquid interface. The adsorption structures of single components are shown in Figure 5-3.

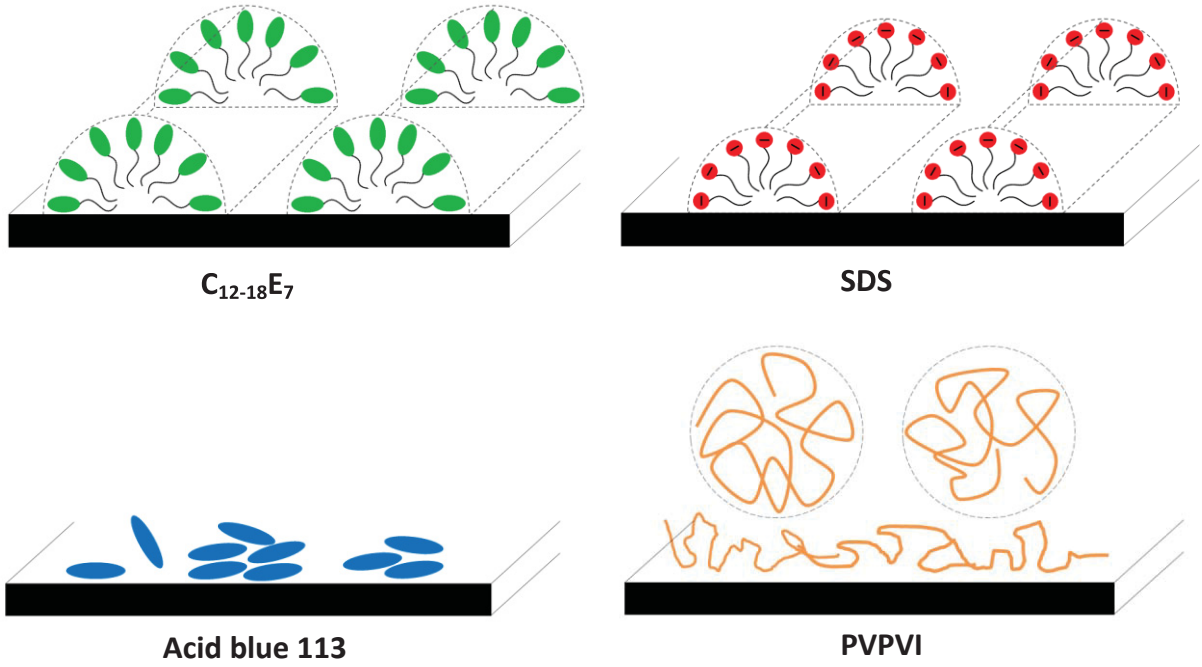

Figure 5-3 Schemas of the structures of surfactants $C_{12\text{-}18}E_7$ and SDS, the dye Acid blue 113 and the DTI polymer PVPVI at the graphite-solution interface (not precisely scaled). $C_{12\text{-}18}E_7$ and SDS form hemicylindrical aggregates[7,8] on graphite above the CMC. The periodicity of the hemicylindrical structure for $C_{12\text{-}18}E_7$ is 5.9 ± 0.3 nm and the thickness of a monolayer of hemicylindrical aggregates is 3.1 nm. The periodicity for SDS is 5.4 ± 0.2 nm. Acid blue 113 adsorbs on graphite in an unstructured way, forming structures relating to single dye molecules and small dye aggregates. At low polymer concentrations, PVPVI adsorbed favors an expanded conformation on graphite. With further increasing polymer concentrations, PVPVI prefers to form globular structures corresponding to polymer coils in the bulk phase.

On graphite, above the CMC both the nonionic surfactant $C_{12\text{-}18}E_7$ and the anionic surfactant SDS form hemicylindrical aggregates,[7,8] which appear as periodic parallel stripes in AFM images. The periodicity of the hemicylindrical structure for $C_{12\text{-}18}E_7$ is 5.9 ± 0.3 nm and for SDS 5.4 ± 0.2 nm. The thickness of a monolayer of hemicylindrical $C_{12\text{-}18}E_7$ aggregates determined by F-D curves is 3.1 nm.

The dye Acid blue 113 adsorbs on graphite in an unstructured way, forming structures with a lateral dimension in the range of 1−13 nm, which can be related to single dye molecules and small dye aggregates. The adsorbed amount of the dye on graphite is increased at high dye concentrations. This observation on graphite agrees with the results on carbon black (ref. Section 5.3).

At low concentrations of the DTI polymer PVPVI, the graphite surface is covered by a polymer layer. Up to the high polymer concentration of 0.1 mM single polymer globules can be seen on the surface, the size of which derived by AFM is mostly in the range of 15−17 nm, which

corresponds to the size of one polymer molecule in water determined by DLS. As proposed in Figure 5-3, at low polymer concentrations PVPVI adsorbed favors an unfolded conformation due to the adsorbate-substrate interaction. The polymer adsorbs on graphite in such a conformation with some attached segments to the surface (trains), some detached segments (loops) and the ends (tails) protruded from the surface stretching toward the bulk phase. With further increasing polymer concentrations, because of the intrinsic intramolecular interaction and the weakened polymer-graphite interaction by the preadsorbed polymer layer, PVPVI prefers to form globular structures corresponding to the polymer coils in the bulk phase.

Dye-Surfactant

In mixtures of the dye with the nonionic surfactant $C_{12\text{-}18}E_7$ of even a very low concentration (0.003 mM) below the CMC, the typical dye structure was not seen on graphite. At the surfactant concentration above the CMC only the hemicylindrical structure of surfactants was observed on the surface and the size of the hemicylindrical structure is increased in the presence of the dye, with respect to a periodicity of the structure from about 5.9 nm to 7.2 nm. This indicates the incorporation of the dye into surfactant aggregates adsorbed on graphite (Fig. 5-4), as it was also observed in solution (ref. Section 5.1, Fig. 5-1).

Therefore, two different adsorption mechanisms on graphite were identified for the mixture of the dye with $C_{12\text{-}18}E_7$. On the one hand, the adsorption of the dye on the surface is inhibited due to the strong adsorption of the surfactant. On the other hand, the dye may be incorporated into surfactant aggregates adsorbed in small amounts at surfactant concentrations above the CMC.

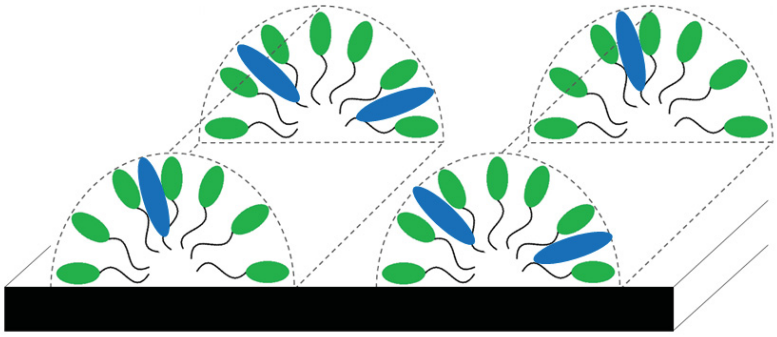

Figure 5-4 Schema of the structure for the mixture of the dye with $C_{12\text{-}18}E_7$ above the CMC at the graphite-solution interface (not precisely scaled). Surfactant aggregates adsorbed on graphite maintain the hemicylindrical structure, where the dye is incorporated into surfactant aggregates, resulting in a size increase of surfactant aggregates from about 5.9 nm to 7.2 nm regarding the periodicity of the structure.

The similar effect was also found for the mixture of the dye with the anionic surfactant SDS only at high surfactant concentrations. At high SDS concentrations (> CMC), only the hemicylindrical structure of surfactants was observed on graphite, while the typical dye structure was not seen. However, the surfactant structure could not be further quantified due to less clear hemicylindrical structures for the system with SDS in the AFM study, as also described in literature[13(p. 77-78)]. According to the study on carbon black (ref. Section 5.3), it can be concluded that SDS has a higher adsorption preference than the dye for the nonpolar model surfaces and can inhibit the adsorption of the dye on surface to some extent at high concentrations (> CMC).

Dye-Polymer

As known, the DTI polymer PVPVI forms single globular structures on graphite at high concentrations (≥ 0.1 mM) (ref. Fig. 5-3). In mixture of the dye with the polymer, the dye structure was seen at different polymer concentrations, but the polymer globules was not observed even at high polymer concentrations, which indicates that Acid blue 113 has a relatively higher affinity for graphite than the DTI polymer. Above the CAC of the polymer ($\sim 1 \cdot 10^{-4}$ mM), an adsorption of the dye-polymer complex was found on the surface, showing an unstructured layer. This interaction between Acid blue 113 and PVPVI was also observed in solution above the CAC forming the dye-polymer (1:1) complex. As proposed in Figure 5-5, the polymer shows the traditional conformation consisting of trains, loops and tails on graphite, where the dye adsorbed is bound with the polymer at specific sites.

Figure 5-5 Proposed structure for the mixture of the dye with PVPVI at the graphite-solution interface (not precisely scaled). The DTI polymer forms a dye-polymer complex with the dye on graphite above the CAC of the polymer, showing an unstructured layer. Moreover, it was found that the dye-polymer complexes adsorbed seem to prevent further adsorption either of the dye and the polymer onto the surface.

Moreover, it was found that the dye-polymer complexes adsorbed seem to prevent further adsorption either of the dye and the polymer onto the surface. The inhibition of the further adsorption of the dye may be attributed on the one hand to occupancy of the active adsorption sites of the surface for the dye and on the other hand to the change of surface property due to the adsorbed dye-polymer complex.

Surfactant-Polymer

In the presence of $C_{12\text{-}18}E_7$ of a very low concentration (0.003 mM) below the CMC, the globular structure of the DTI polymer was hardly observed on graphite, whereas the globular polymers could still be seen at the SDS concentration of 0.1 mM.

For both surfactants at concentrations above the CMC, the adsorption of the polymer on the surface is markedly inhibited, where almost only the hemicylindrical structure of surfactants was observed, which is not changed in the presence of polymer. This indicates that surfactants have a higher adsorption preference than the DTI polymer for graphite. The periodicity of the hemicylindrical structure for the mixture of $C_{12\text{-}18}E_7$ + PVPVI is 6.2 $\pm$ 0.1 nm and for SDS + PVPVI is 5.3 $\pm$ 0.3 nm.

As shown in Figure 5-6, above the CMC the graphite surface is covered by surfactant aggregates. According to the study in solution and at the air-solution interface, there is no interaction between $C_{12\text{-}18}E_7$ and PVPVI. However, SDS interacts with PVPVI both in solution and at the air-solution interface (ref. Fig. 5-2). It is therefore assumed that the polymer is loosely bound with SDS adsorbed, which could not be further verified by the AFM study yet due to the scratch of tip during imaging.

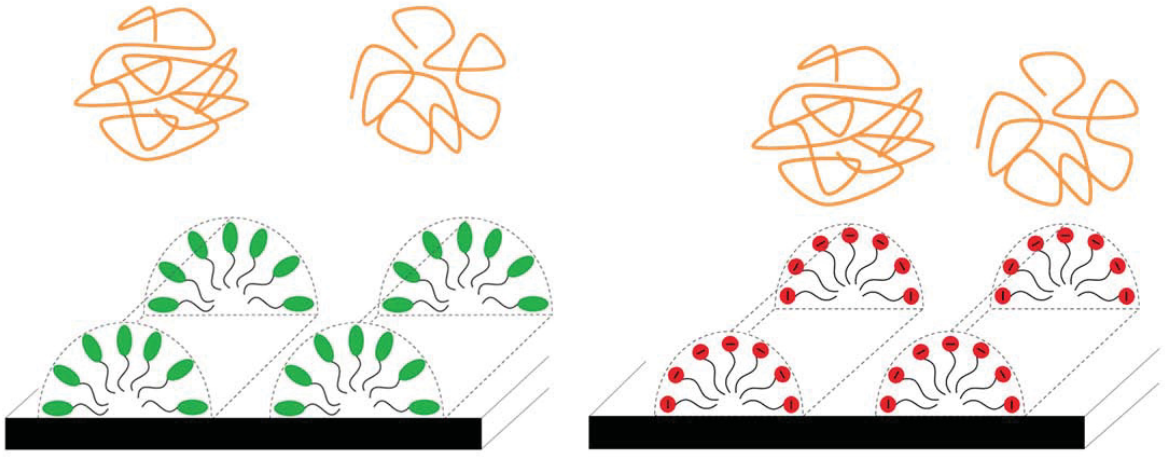

Figure 5-6 Schemas of the structures for the mixtures of surfactants above the CMC with the DTI polymer at the graphite-solution interface (not precisely scaled). The adsorption of polymer is inhibited owing to the adsorption of surfactants on the surface. The hemicylindrical aggregate structure of surfactants is not changed in the presence of polymer. This indicates that surfactants have a higher adsorption preference than the DTI polymer for graphite.

The studies at the graphite-solution interface by AFM demonstrate that the adsorption of individual components onto surfaces in the binary system is competitive, which has a very

important influence on the adsorption of dye on surfaces. The adsorption preference for the graphite surface can be generally arranged in the order: $C_{12\text{-}18}E_7$, SDS > Acid blue 113 ≳ PVPVI.

In summary, AFM proves to be a very powerful tool to characterize the adsorbed layers of binary aqueous mixtures of dye, surfactant and DTI polymer at solid-liquid interfaces. The studies on nonpolar model surfaces reveal that two mechanisms play a decisive role in the adsorption of dye onto surfaces in the presence of surfactants: the competitive adsorption of individual components and the incorporation of dyes into micellar surfactant aggregates on model surfaces. The nonionic surfactant $C_{12\text{-}18}E_7$ has a higher adsorption preference than the dye to model surfaces, and on the other hand, the dye can be incorporated into surfactant micelles in solution as well as into surfactant aggregates adsorbed on surface, which can result in additive or adverse effects on dye transfer inhibition. In comparison with the anionic surfactant SDS, the nonionic surfactant $C_{12\text{-}18}E_7$ shows a greater effect due to its higher affinity for model surfaces and stronger incorporation of the dye into surfactant micelles in solution. The DTI polymer PVPVI probably forms the dye-polymer complex with the dye on model surfaces above the CAC of the polymer, as it is proven in solution. In the presence of surfactants (> CMC), the adsorption of the polymer onto surfaces is inhibited due to the dominant adsorption of surfactants.

This work developed the model description for the molecular interaction between surfactant, DTI polymer and dye in solution and at interfaces in binary systems, which brings a further contribution to understanding of the molecular mechanism of surfactants and DTI polymers in influencing dye adsorption and consequently dye transfer in washing processes.

6 Outlook

It was shown that the DTI efficacy is related to the interaction of dyes with surfactants and DTI polymers both in solution and at solid-liquid interfaces. The DTI effect by the stabilization of dyes in solution is affected not only by the interaction of dyes with additives respectively but also by the interaction between additives. Because of the additive and adverse effect of the two different mechanisms on dye transfer inhibition at the solid-liquid interface in the presence of surfactants, the type and composition of surfactants is critical for the DTI efficacy. In addition, the relative affinity of dyes and DTI polymers for surfaces accounts for the selectivity of DTI polymers for dyes and textiles. The identification of adsorption mechanisms on model surfaces is of vital importance for the understanding of the influence of detergent components such as surfactants and DTI polymers on dye transfer as well as for the improvement of detergent formulations.

Based on these results on model surfaces, the study on textile or textile-like surfaces can be established. Therefore, in this work the surface of commercial polyamide fibers and polyamide films were characterized by AFM both in air and in water, as described in Section 4.6. The characterization of the polyamide surfaces verifies the feasibility of study on such textile-like surfaces by AFM. This provides the first basic information for the further investigation of the DTI mechanism on textile surfaces, which can lead to a deeper insight into the mode of action of DTI in real washing processes.

The present AFM studies of model systems identified the adsorption structures of individual components as well as binary mixtures of surfactant, DTI polymer and dye on the model surface graphite and clarified the adsorption mechanism of the dye in binary systems. This makes it possible to extend the AFM study to ternary systems of the dye and surfactant mixtures as well as of the dye, surfactant and DTI polymer, in order to understand more about the correlation of dyes with detergent components in a complex system during dye transfer.

Furthermore, with the knowledge and know-how acquired in this work the studies in terms of other dyes and surfaces (model or textile surfaces) can also be expanded to make comparisons between different dyes and substrate surfaces.

References

1. B. Simončič, J. Špan, "A Study of Dye-Surfactant Interactions. Part 1. Effect of Chemical Structure of Acid Dyes and Surfactants on the Complex Formation," Dyes and Pigments **36** (1), 1–14 (1998).

2. B. Simončič, J. Špan, "A study of dye-surfactant interactions. Part 3. Thermodynamics of the association of C.I. Acid Orange 7 and cetylpyridinium chloride in aqueous solutions," Dyes and Pigments **46**, 1–8 (2000).

3. P. F. Tavčer, J. Špan, "Dye-Surfactant Interactions Studied Using Job's Method," Textile Research Journal **69** (4), 278–284 (1999).

4. J. Oakes, P. Gratton, "Solubilisation of dyes by surfactant micelles. Part 1: Molecular interactions of azo dyes with nonionic and anionic surfactants," Coloration Technology **119**, 91-99 (2003).

5. J. Oakes, P. Gratton, S. Dixon, "Solubilisation of dyes by surfactant micelles. Part 3: A spectroscopic study of azo dyes in surfactant solutions," Coloration Technology **119** (5), 301–306 (2003).

6. H.-U. Jäger, W. Denzinger, "Wirkungsweise von Polymeren mit farbübertragungsinhibierenden Eigenschaften," Tenside Surfactants Detergents **28** (6), 428–433 (1991).

7. E. J. Wanless, W. A. Ducker, "Organization of Sodium Dodecyl Sulfate at the Graphite−Solution Interface," J. Phys. Chem. **100** (8), 3207–3214 (1996).

8. H. N. Patrick, G. G. Warr, S. Manne, I. A. Aksay, "Self-Assembly Structures of Nonionic Surfactants at Graphite/Solution Interfaces," Langmuir **13** (16), 4349–4356 (1997).

9. S. Manne, H. E. Gaub, "Molecular Organization of Surfactants at Solid-Liquid Interfaces," Science **270** (1995).

10. W. von Rybinski, M. Jabnoun, J. van Megen, F. Oesterhelt, C. Seidel, "Structures of adsorption layers of surfactant mixtures on nonpolar solid surfaces," Colloid and Polymer Science **293** (11), 3107–3117 (2015).

11. C. E. Hoeft, R. L. Zollars, "Adsorption of Single Anionic Surfactants on Hydrophobic Surfaces," Journal of Colloid and Interface Science **177**, 171–178 (1996).

12. B. Tamamushi, K. Tamaki, "Adsorption of long-chain electrolytes at the solid/liquid interface. Part 2.-The adsorption on polar and non-polar adsorbents," Trans. Faraday Soc. **55**, 1007-1012 (1959).

13. M. Jabnoun, *Adsorption layers of surfactant mixtures on non-polar solid particles and stability of dispersions* (PhD thesis, Heinrich-Heine-Universität Düsseldorf, 2012).

14. T. Uchiyama, A. Kawauchi, D. L. DuVal, "Quick identification of polymeric dye transfer inhibitors in laundry detergents by pyrolysis-gas chromatography/mass spectrometry," Journal of Analytical and Applied Pyrolysis **45**, 111–119 (1998).

15. M. J. Schwuger, "Zur Kenntnis der Zusammenhänge zwischen Adsorption und Waschwirkung von Tensiden," Chemie Ingenieur Technik **43** (12), 705–710 (1971).

16. A. Tehrani-Bagha, K. Holmberg, "Solubilization of Hydrophobic Dyes in Surfactant Solutions," Materials **6** (2), 580–608 (2013).

17. J. W. McBain, R. C. Merrill, J. R. Vinograd, "The Solubilization of Water-insoluble Dye in Dilute Solutions of Aqueous Detergents," J. Am. Chem. Soc. **63** (3), 670–676 (1941).

18. R. C. Merrill, J. W. McBain, "Studies on Solubilization," J. Phys. Chem. **46** (1), 10–19 (1942).

19. A. A. Green, J. W. McBain, "Solubilization of water-insoluble dye by pure soaps and detergents of different types," The Journal of Physical and Colloid Chemistry **51** (1), 286–298 (1947).

20. J. W. McBain, A. G. Wilder, R. C. Merrill, "Solubilization of water-insoluble dye by colloidal electrolytes and non-ionizing detergents," The Journal of Physical and Colloid Chemistry **52** (1), 12–27 (1948).

21. T.-S. Choi, Y. Shimizu, H. Shirai, K. Hamada, "Solubilization of disperse dyes in cationic gemini surfactant micelles," Dyes and Pigments **45** (2), 145–152 (2000).

22. M. N. Amin, R. S. Blackburn, "Sustainable Chemistry Method to Improve the Wash-off Process of Reactive Dyes on Cotton," ACS Sustainable Chem. Eng. **3** (4), 725–732 (2015).

23. J. Oakes, S. Dixon, "Physical interactions of dyes in solution-influence of dye structure on aggregation and binding to surfactants/polymers," Review of Progress in Coloration and Related Topics **34** (1), 110–128 (2004).

24. J. Oakes, P. L. Gratton, P. K. C. Paul, "A spectroscopic and modelling study of polymer/dye interactions," Coloration Technology **119** (3), 150–157 (2003).

25. J. Oakes, S. Dixon, "Adsorption of dyes to cotton and inhibition by polymers," Coloration Technology **119** (3), 140-149 (2003).

26. J. Oakes, S. Dixon, "Adsorption of dyes to cotton and inhibition by surfactants, polymers and surfactant–polymer mixtures," Coloration Technology **119** (6), 315–323 (2003).

27. I. Holme, “Recent developments in colorants for textile applications,” Surface Coatings International Part B: Coatings Transactions **85** (4), 243–264 (2002).

28. V. K. Gupta, B. Gupta, A. Rastogi, S. Agarwal, A. Nayak, “A comparative investigation on adsorption performances of mesoporous activated carbon prepared from waste rubber tire and activated carbon for a hazardous azo dye--Acid Blue 113,” Journal of Hazardous Materials **186** (1), 891–901 (2011).

29. G. Wagner, *Waschmittel: Chemie, Umwelt, Nachhaltigkeit*, 5th ed. (WILEY-VCH, Weinheim, Germany, 2017).

30. H. Schott, “Solubilization of a Water-Insoluble Dye as a Method for Determining Micellar Molecular Weights,” J. Phys. Chem. **70** (9), 2966–2973 (1966).

31. K. Holmberg, *Surfactants and polymers in aqueous solution*, 2nd ed. (John Wiley & Sons, Chichester West Sussex England, Hoboken NJ, 2003).

32. A. R. Tehrani-Bagha, R. G. Singh, K. Holmberg, “Solubilization of two organic dyes by anionic, cationic and nonionic surfactants,” Colloids and Surfaces A: Physicochemical and Engineering Aspects **417**, 133–139 (2013).

33. J. Oakes, P. Gratton, S. Dixon, “Solubilisation of dyes by surfactant micelles. Part 4: Influence of dye fixatives,” Coloration Technology **120** (6), 267–275 (2004).

34. B. Simončič, M. Kert, “A study of anionic dye–cationic surfactant interactions in mixtures of cationic and nonionic surfactants,” Dyes and Pigments **54**, 221–237 (2002).

35. K. W. Kolasinski, *Surface Science: Foundations of Catalysis and Nanoscience*, Second edition (John Wiley & Sons Ltd, West Chester, USA, 2008).

36. G. Attard, C. Barnes, *Surfaces* (Oxford University Press, USA, 1998).

37. H.-D. Dörfler, *Grenzflächen und kolloid-disperse Systeme: Physik und Chemie* (Springer-Verlag, 2002).

38. H. Y. Erbil, *Surface Chemistry of Solid and Liquid Interfaces* (Blackwell Publishing Ltd, 2006).

39. T. Cosgrove (Editor), *Colloid Science: Principles, Methods and Applications*, Second edition (WILEY, 2010).

40. K. Y. Foo, B. H. Hameed, “Insights into the modeling of adsorption isotherm systems,” Chemical Engineering Journal **156** (1), 2–10 (2010).

41. L. M. Grant, F. Tiberg, W. A. Ducker, “Nanometer-Scale Organization of Ethylene Oxide Surfactants on Graphite, Hydrophilic Silica and Hydrophobic Silica,” J. Phys. Chem. B **102**, 4288–4294 (1998).

42. L. M. Grant, W. A. Ducker, “Effect of Substrate Hydrophobicity on Surface−Aggregate Geometry. Zwitterionic and Nonionic Surfactants,” J. Phys. Chem. B **101** (27), 5337–5345 (1997).

43. E. J. Wanless, W. A. Ducker, “Weak Influence of Divalent Ions on Anionic Surfactant Surface-Aggregation,” Langmuir **13** (6), 1463–1474 (1997).

44. H. N. Patrick, G. G. Warr, “Self-assembly structures of nonionic surfactants at graphite–solution interfaces. 2. Effect of polydispersity and alkyl chain branching,” Colloids and Surfaces A: Physicochemical and Engineering Aspects **162** (1), 149–157 (2000).

45. J. Dong, G. Mao, R. M. Hill, “Nanoscale Aggregate Structures of Trisiloxane Surfactants at the Solid−Liquid Interface,” Langmuir **20** (7), 2695–2700 (2004).

46. A. J. Groszek, “Selective adsorption at graphite/hydrocarbon interfaces,” Proc. Roy. Soc. Lond. A. **314**, 473–498 (1970).

47. R. J. Anderson, D. J. Bendell, P. W. Groundwater, *Organic Spectroscopic Analysis* (The Royal Society of Chemistry, Cambridge, UK, 2004).

48. W. Schmidt, *Optische Spektroskopie*, 2. Auflage (WILEY-VCH, 2000).

49. M. Born, R. Oppenheimer, “Zur Quantentheorie der Molekeln,” Ann. Phys. **389** (20), 457–484 (1927).

50. E. Lippert, W. Lüder, F. Moll, W. Nägele, H. Boos, H. Prigge, I. Seibold-Blankenstein, “Umwandlung von Elektronenanregungsenergie,” Angew. Chem. **73** (21), 695–706 (1961).

51. E. Condon, “A Theory of Intensity Distribution in Band Systems,” Physical Review **28**, 1182–1201 (1926).

52. C. Reichardt, *Solvents and Solvent Effects in Organic Chemistry*, Third edition (WILEY, 2003).

53. E. Buncel, S. Rajagopal, “Solvatochromism and solvent polarity scales,” Acc. Chem. Res. **23** (7), 226–231 (1990).

54. M. J. Kamlet, R. W. Taft, “The solvatochromic comparison method. I. The β-scale of solvent hydrogen-bond acceptor (HBA) basicities,” Journal of the American Chemical Society **98** (2), 377–383 (1976).

55. H.-H. Perkampus, *UV-VIS Spectroscopy and Its Applications* (Springer-Verlag, 1992).

56. B. J. Ree, J. Lee, Y. Satoh, K. Kwon, T. Isono, T. Satoh, M. Ree, "A Comparative Study of Dynamic Light and X-ray Scatterings on Micelles of Topological Polymer Amphiphiles," Polymers **10** (12) (2018).

57. C. Czeslik, H. Seemann, R. Winter, *Basiswissen Physikalische Chemie*, 2. überarbeitete Auflage (B. G. Teubner, Wiesbaden, 2007).

58. B. Chu, *Laser Light Scattering: Basic Principles and Practice*, Second edition (Academic Press, 1991).

59. R. Pecora, "Doppler Shifts in Light Scattering from Pure Liquids and Polymer Solutions," The Journal of Chemical Physics **40** (6), 1604–1614 (1964).

60. C. Washington, *Particle Size Analysis in Pharmaceutics and Other Industries: Theory and Practice* (Ellis Horwood, 1992).

61. J. Stetefeld, S. A. McKenna, T. R. Patel, "Dynamic light scattering: A practical guide and applications in biomedical sciences," Biophysical Reviews **8** (4), 409–427 (2016).

62. D. E. Koppel, "Analysis of Macromolecular Polydispersity in Intensity Correlation Spectroscopy: The Method of Cumulants," The Journal of Chemical Physics **57** (11), 4814–4820 (1972).

63. Malvern Instruments Limited, *Dynamic light scattering - common terms defined*. *Whitepaper*, 2017.

64. L. Wilhelmy, "Ueber die Abhängigkeit der Capillaritäts-Constanten des Alkohols von Substanz und Gestalt des benetzten festen Körpers," Ann. Phys. **195** (6), 177–217 (1863).

65. DataPhysics Instruments GmbH, *https://www.dataphysics-instruments.com/products/dcat* (Germany, 2020).

66. G. Meyer, N. M. Amer, "Novel optical approach to atomic force microscopy," Appl. Phys. Lett. **53** (24), 2400–2402 (1988).

67. F. J. Giessible, "Advances in atomic force microscopy," Review of Modern Physics **75**, 949–983 (2003).

68. K. S. Birdi, *Scanning probe microscopes: Applications in science and technology* (CRC Press, Boca Raton Florida, 2003).

69. B. Cappella, *Mechanical Properties of Polymers Measured through AFM Force-Distance Curves* (Springer, 2016).

70. B. Cappella, G. Dietler, “Force-distance curves by atomic force microscopy,” Surface Science Reports **34**, 1–104 (1999).

71. J. S. Villarrubia, “Algorithms for scanned probe microscope image simulation, surface reconstruction, and tip estimation,” J. Res. Natl. Inst. Stand. Technol. **102** (4), 425 (1997).

72. F. Zenhausern, M. Adrian, B. Ten Heggeler-Bordier, L. M. Eng, P. Descouts, “DNA and RNA polymerase/DNA complex imaged by scanning force microscopy: Influence of molecular-scale friction,” Scanning **14** (4), 212–217 (1992).

73. A. Yacoot, L. Koenders, “Aspects of scanning force microscope probes and their effects on dimensional measurement,” J. Phys. D: Appl. Phys. **41** (10), 103001 (46pp) (2008).

74. “Geometrische Produktspezifikation (GPS)-Oberflächenbeschaffenheit: Flächenhaft - Teil 2: Begriffe und Oberflächen-Kenngrößen (ISO 25178-2:2012),”.

75. K. Holmberg (Editor), *Handbook of applied surface and colloid chemistry* (John Wiley & Sons, 2002).

76. J. Oakes, P. Gratton, S. Dixon, “Solubilisation of dyes by surfactant micelles. Part 3: A spectroscopic study of azo dyes in surfactant solutions,” Coloration Technology **119** (5), 301–306 (2003).

77. H. P. Frank, S. Barkin, F. R. Eirich, “The Interaction of Polyvinylpyrrolidone with Some Azo Dyes,” J. Phys. Chem. **61** (10), 1375–1380 (1957).

78. T. Takagishi, N. Kuroki, “Interaction of polyvinylpyrrolidone with methyl orange and its homologs in aqueous solution: Thermodynamics of the binding equilibria and their temperature dependences,” J. Polym. Sci. Polym. Chem. Ed. **11** (8), 1889–1901 (1973).

79. R. L. Reeves, S. A. Harkaway, A. R. Sochor, “Spectral and thermodynamic studies of the interaction of binding site probes with poly(vinylpyrrolidone),” Journal of Polymer Science (Polymer Chemistry Edition) **19**, 2427–2441 (1981).

80. W. Brown, Z. Pu, R. Rymdén, “Size and shape of nonionic amphiphile micelles: NMR self-diffusion and static and quasi-elastic light-scattering measurements on $C_{12}E_5$, $C_{12}E_7$, and $C_{12}E_8$ in aqueous solution,” J. Phys. Chem. **92**, 6086–6094 (1988).

81. C. D. Bruce, M. L. Berkowitz, L. Perera, M. D. E. Forbes, “Molecular Dynamics Simulation of Sodium Dodecyl Sulfate Micelle in Water. Micellar Structural Characteristics and Counterion Distribution,” J. Phys. Chem. B **106** (15), 3788–3793 (2002).

82. J.-B. Jeong, S.-R. Yang, J.-D. Kim, “Micellar Aggregation and Structure of Dodecyl Heptaethoxylates ($C_{12}E_7$) with Different Oxyethylene Distributions in Aqueous Media,” Langmuir **18** (23), 8749–8755 (2002).

83. C. D. Bruce, S. Senapati, M. L. Berkowitz, L. Perera, M. D. E. Forbes, "Molecular Dynamics Simulations of Sodium Dodecyl Sulfate Micelle in Water: The Behavior of Water," J. Phys. Chem. B **106** (42), 10902–10907 (2002).

84. N. Yoshii, K. Iwahashi, S. Okazaki, "A molecular dynamics study of free energy of micelle formation for sodium dodecyl sulfate in water and its size distribution," The Journal of Chemical Physics **124** (18), 184901 (1-6) (2006).

85. Y. Croonen, E. Gelade, M. Van der Zegel, M. Van der Auweraer, H. Vandendriessche, F. C. De Schryver, M. Almgren, "Influence of salt, detergent concentration, and temperature on the fluorescence quenching of 1-methylpyrene in sodium dodecyl sulfate with m-dicyanobenzene," J. Phys. Chem. **87** (1426-1431) (1983).

86. J.-Y. Park, Y. Hirata, K. Hamada, "Relationship between the dye/additive interaction and inkjet ink droplet formation," Dyes and Pigments **95** (3), 502–511 (2012).

87. B. M. Folmer, K. Holmberg, "The cross-sectional headgroup area of nonionic surfactants: the influence of polydispersity," Colloids and Surfaces A: Physicochemical and Engineering Aspects **180**, 187–191 (2001).

88. M. Miyake, A. Asano, Y. Einaga, "Size change of the wormlike micelles of pentaoxyethylene, hexaoxyethylene, and heptaoxyethylene dodecyl ethers with uptake of n-dodecane," The Journal of Physical Chemistry B **112** (15), 4648–4655 (2008).

89. S. Shirai, E. Yoshiyuki, "Wormlike Micelles of Polyoxyethylene Dodecyl $C_{12}E_j$ and Heptaoxyethylene Alkyl C_iE_7 Ethers. Hydrophobic and Hydrophilic Chain Length Dependence of the Micellar Characteristics," Polymer Journal **37** (12), 913–924 (2005).

90. O. Valdes-Aguilera, D. C. Neckers, "Aggregation phenomena in xanthene dyes," Acc. Chem. Res. **22**, 171–177 (1989).

91. K. Hamada, T. I. S. Take, "Effects of Electrostatic Repulsion on the Aggregation of Azo Dyes in Aqueous Solution," J. Chem. Soc. Faraday Trans. 1 **82**, 3141–3148 (1986).

92. K. L. Kendrick, W. R. Gilkerson, "The state of aggregation of methyl orange in water," Journal of Solution Chemistry **16** (4), 257–267 (1987).

93. P. J. Hillson, R. B. McKay, "Aggregation of Dye Molecules in Aqueous Solution A Polarographic Study," Transactions of the Faraday Society **61**, 374–382 (1965).

94. R. L. Reeves, M. S. Maggio, S. A. Harkaway, "A critical spectrophotometric analysis of the dimerization of some ionic azo dyes in aqueous solution," The Journal of Physical Chemistry **83** (18), 2359–2368 (1979).

95. I. A. Vasil'eva, R. O. Anarbaev, N. A. Moor, O. I. Lavrik, “Dynamic light scattering study of base excision DNA repair proteins and their complexes,” Biochimica et Biophysica Acta. Proteins and proteomics **1867** (3), 297–305 (2019).

96. M. Guettari, A. Belaidi, S. Abel, T. Tajouri, “Polyvinylpyrrolidone Behavior in Water/Ethanol Mixed Solvents: Comparison of Modeling Predictions with Experimental Results,” J. Solution Chem. **46** (7), 1404–1417 (2017).

97. T. G. Fox, P. J. Flory, “Intrinsic Viscosity-Molecular Weight Relationships for Polyisobutylene,” The Journal of Physical and Colloid Chemistry **53** (2), 197–212 (1949).

98. S. M. Bhattacharjee, A. Giacometti, A. Maritan, “Flory theory for polymers,” Journal of Physics: Condensed Matter: An Institute of Physics Journal **25** (50), 503101 (2013).

99. C. M. Kok, A. Rudin, “Relationship between the hydrodynamic radius and the radius of gyration of a polymer in solution,” Makromol. Chem. Rapid Commun. **2**, 655–659 (1981).

100. L. J. Fetters, N. Hadjichristidis, J. S. Lindner, J. W. Mays, “Molecular Weight Dependence of Hydrodynamic and Thermodynamic Properties for Well-Defined Linear Polymers in Solution,” J. Phys. Chem. Ref. Data **23** (4), 619–640 (1994).

101. P. Kékicheff, C. Grabielle-Madelmont, M. Ollivon, “Phase diagram of sodium dodecyl sulfate-water system. 1. A calorimetric study,” J. Colloid Interface Sci. **131** (1), 112–132 (1989).

102. Z. Liu, Y. Shang, J. Feng, C. Peng, H. Liu, Y. Hu, “Effect of hydrophilicity or hydrophobicity of polyelectrolyte on the interaction between polyelectrolyte and surfactants. Molecular dynamics simulations,” The Journal of Physical Chemistry. B **116** (18), 5516–5526 (2012).

103. N. J. Turro, B. H. Baretz, P. L. Kuo, “Photoluminescence probes for the investigation of interactions between sodium dodecyl sulfate and water-soluble polymers,” Macromolecules **17** (7), 1321–1324 (1984).

104. H. Arai, M. Murata, K. Shinoda, “The interaction between polymer and surfactant. The composition of the complex between polyvinylpyrrolidone and sodium alkyl sulfate as revealed by surface tension, dialysis and solubilization,” J. Colloid Interface Sci. **37** (1), 223–227 (1971).

105. Y. Fan, H. Tang, R. Strand, Y. Wang, “Modulation of partition and localization of perfume molecules in sodium dodecyl sulfate micelles,” Soft Matter **12** (1), 219–227 (2016).

106. R. L. Reeves, S. A. Harkaway, “Surface tensions of aqueous solutions of some azo dye sulfonates and analogs,” J. Colloid Interface Sci. **64** (2), 342–347 (1978).

107. A. D. Fenta, “Surface and thermodynamic studies of micellization of surfactants in binary mixtures of 1,2-ethanediol and 1,2,3-propanetriol with water,” International Journal of Physical Sciences **10** (8), 276–288 (2015).

108. P. Hansson, B. Lindman, “Surfactant-polymer interactions,” Current Opinion in Colloid & Interface Science **1** (5), 604–613 (1996).

109. E. D. Goddard, T. S. Phillips, R. B. Hannan, “Water Soluble Polymer-Surfactant Interaction-Part I.,” J. Soc. Cosmet. Chem. **26**, 461–475 (1975).

110. Y. Guo, X. Dong, W. Ruan, Y. Shang, H. Liu, “A thermo-sensitive OEGMA-based polymer: Synthesis, characterization and interactions with surfactants in aqueous solutions with and without salt,” Colloid and Polymer Science **295** (2), 327–340 (2017).

111. M. Lundin, L. Macakova, A. Dedinaite, P. Claesson, “Interactions between Chitosan and SDS at a Low-Charged Silica Substrate Compared to Interactions in the Bulk–The Effect of Ionic Strength,” Langmuir **24** (8), 3814–3827 (2008).

112. Y. Touhami, D. Rana, G. H. Neale, V. Hornof, “Study of polymer-surfactant interactions via surface tension measurements,” Colloid Polymer Science **279**, 297–300 (2001).

113. B. Cabane, “Structure of some polymer-detergent aggregates in water,” The Journal of Physical Chemistry **81** (17), 1639–1645 (1977).

114. D. Langevin, “Complexation of oppositely charged polyelectrolytes and surfactants in aqueous solutions. A review,” Adv. Colloid Interface Sci. **147-148**, 170–177 (2009).

115. R. Nagarajan, *Polymer-surfactant interactions*. In “New Horizons: Detergents for the New Millennium Conference Invited Papers” (American Oil Chemists Society and Consumer Specialty Products Association, 2001).

116. S. Nethaji, A. Sivasamy, A. B. Mandal, “Adsorption isotherms, kinetics and mechanism for the adsorption of cationic and anionic dyes onto carbonaceous particles prepared from Juglans regia shell biomass,” Int. J. Environ. Sci. Technol. **10** (2), 231–242 (2013).

117. M. T. Amin, A. A. Alazba, M. Shafiq, “Adsorptive Removal of Reactive Black 5 from Wastewater Using Bentonite Clay: Isotherms, Kinetics and Thermodynamics,” Sustainability **7** (11), 15302–15318 (2015).

118. S. S. Tahir, N. Rauf, “Removal of a cationic dye from aqueous solutions by adsorption onto bentonite clay,” Chemosphere **63** (11), 1842–1848 (2006).

119. B. H. Hameed, D. K. Mahmoud, A. L. Ahmad, “Equilibrium modeling and kinetic studies on the adsorption of basic dye by a low-cost adsorbent: Coconut (Cocos nucifera) bunch waste,” Journal of Hazardous Materials **158** (1), 65–72 (2008).

120. M. Ahmaruzzaman, S. L. Gayatri, “Activated Tea Waste as a Potential Low-Cost Adsorbent for the Removal of p-Nitrophenol from Wastewater,” J. Chem. Eng. Data **55** (11), 4614–4623 (2010).

121. J. J. Porter, “Dyeing equilibria: interaction of direct dyes with cellulose substrates,” Coloration Technology **118** (5), 238–243 (2002).

122. M. Shirzad-Siboni, S. J. Jafari, O. Giahi, I. Kim, S.-M. Lee, J.-K. Yang, “Removal of acid blue 113 and reactive black 5 dye from aqueous solutions by activated red mud,” Journal of Industrial and Engineering Chemistry **20** (4), 1432–1437 (2014).

123. J. S. Villarrubia, “Algorithms for Scanned Probe Microscope Image Simulation, Surface Reconstruction and Tip Estimation,” J. Res. of the Natl. Inst. Stand. Technol. **102**, 425–454 (1997).

124. H. Wennerstrom, A. Khan, B. Lindman, “Ionic surfactants with divalent counterions,” Adv. Colloid Interface Sci. **34**, 433–449 (1991).

125. L. M. Grant, F. Tiberg, W. A. Ducker, “Nanometer-Scale Organization of Ethylene Oxide Surfactants on Graphite, Hydrophilic Silica, and Hydrophobic Silica,” J. Phys. Chem. B **102** (22), 4288–4294 (1998).

126. S. L. S. Stipp, “In Situ , Real-Time Observations of the Adsorption and Self-Assembly of Macromolecules from Aqueous Solution onto an Untreated, Natural Surface,” Langmuir **12** (7), 1884–1891 (1996).

127. B. D. Fleming, E. J. Wanless, S. Biggs, “Nonequilibrium Mesoscale Surface Structures: The Adsorption of Polymer−Surfactant Mixtures at the Solid/Liquid Interface,” Langmuir **15** (25), 8719–8725 (1999).

128. C. Ma, C. Li, “Interaction between polyvinylpyrrolidone and sodium dodecyl sulfate at solid/liquid interface,” J. Colloid Interface Sci. **131** (2), 485–492 (1989).

129. H. Otsuk, K. Esumi, “Interaction between Poly(N-vinyl-2-pyrrolidone) and Anionic Hydrocarbon/Fluorocarbon Surfactant on Hydrophobic Graphite,” Journal of Colloid and Interface Science **170** (1), 113–119 (1995).

130. R. H. Barker, “Additives in Fibers and Fabrics,” Environmental Health Perspectives **11**, 41–45 (1975).

131. Q. Zhong, D. Inniss, K. Kjoller, V. B. Elings, “Fractured polymer/silica fiber surface studied by tapping mode atomic force microscopy,” Surface Science Letters **290** (1-2), L688-L692 (1993).

132. K.C. Khulbe, C. Feng, T. Matsuura, G.C. Kapantaidakis, M. Wessling, G.H. Koops, "Characterization of polyethersulfone-polyimide hollow fiber membranes by atomic force microscopy and contact angle goniometery," Journal of Membrane Science **226** (1–2), 63–73 (2003).

133. J. Zhang, B. A. Watson, R. W. Keown, C. P. Malone, M. A. Barteau, "Investigation of Sulfonated Aromatic Compound (SAC) Modification to Nylon Film. 2. Study of SAC Sorption Isotherm and Atomic Force Microscopic Characterization of Nylon Surfaces," Langmuir **11** (8), 3018–3023 (1995).

Appendix

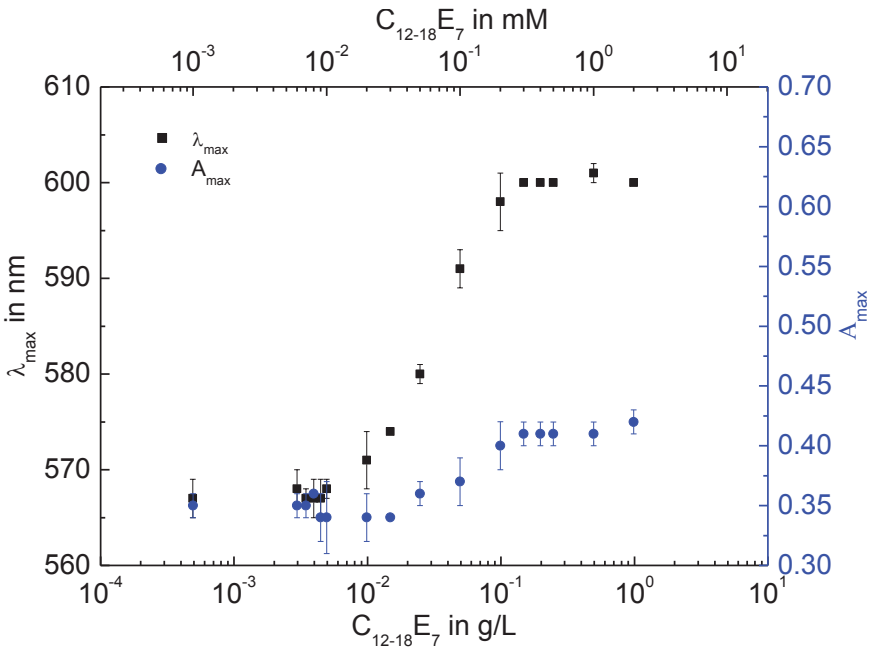

Figure 1 Plotting of the maximal absorbance values (A_{max}) and corresponding wavelengths (λ_{max}) of Acid blue 113 depending on $C_{12\text{-}18}E_7$ concentrations. The sample was the same as presented in Figure 4-2 but the equilibrium time was 20 h. The spectrum of Acid blue 113 begins to shift toward the larger wavelength at 0.02 mM of $C_{12\text{-}18}E_7$. The bathochromic shift reaches the maximum at 0.3 mM of $C_{12\text{-}18}E_7$. The absorption maximum (spectrum peak) shifts from 567 nm to 600 nm.

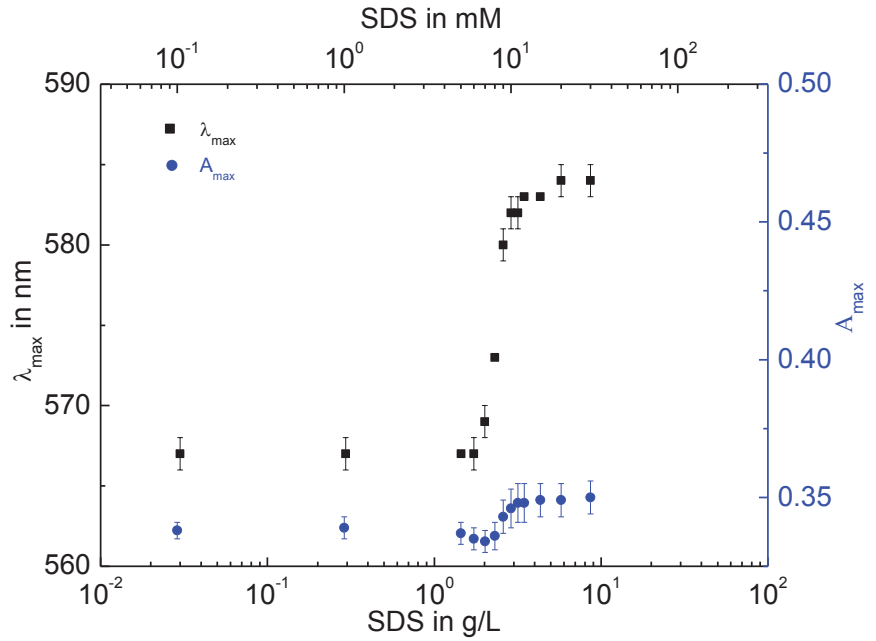

Figure 2 Plotting of the maximal absorbance values (A_{max}) and corresponding wavelengths (λ_{max}) of Acid blue 113 depending on SDS concentrations. The sample was the same as presented in Figure 4-4 but the equilibrium time was 21 h. The spectrum of Acid blue 113 begins to shift toward the larger wavelength at 7 mM of SDS. The bathochromic shift reaches the maximum at about 10 mM of SDS. The absorption maximum (spectrum peak) shifts from 567 nm to 584 nm.

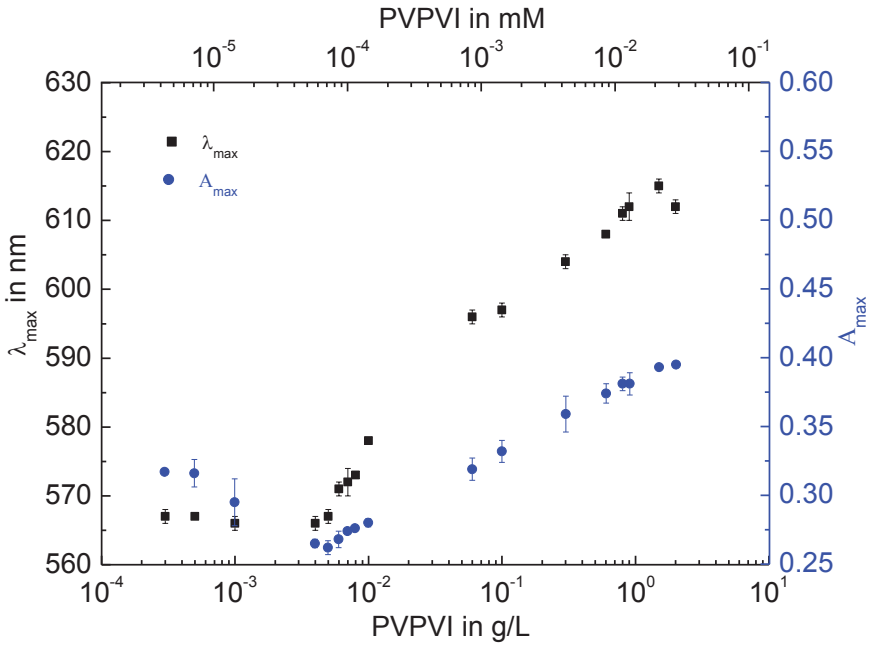

Figure 3 Plotting of the maximal absorbance values (A_{max}) and corresponding wavelengths (λ_{max}) of Acid blue 113 depending on PVPVI concentrations. The sample was the same as presented in Figure 4-6 but the equilibrium time was 27 h. The spectrum of Acid blue 113 begins to shift toward the larger wavelength at about 0.006 g/L ($\sim 1 \cdot 10^{-4}$ mM) of PVPVI. The bathochromic shift reaches the maximum at 0.6 g/L (~0.01 mM) of PVPVI. The absorption maximum (spectrum peak) shifts from 566 nm to 612 nm.

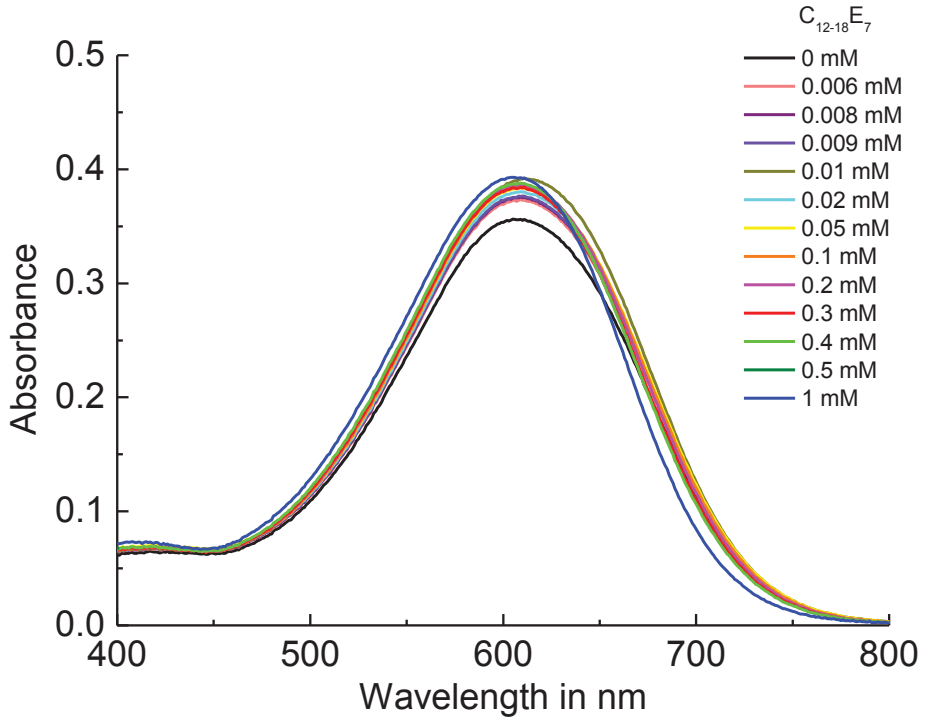

Figure 4 UV-Vis absorption spectra of mixtures of Acid blue 113 + PVPVI + $C_{12\text{-}18}E_7$, equilibrated for 24 h. The concentration of Acid blue 113 and PVPVI is 0.009 mM and $1 \cdot 10^{-2}$ mM respectively in all solutions. The concentration of $C_{12\text{-}18}E_7$ varies from 0 mM to 1 mM (0 g/L to 0.5 g/L).

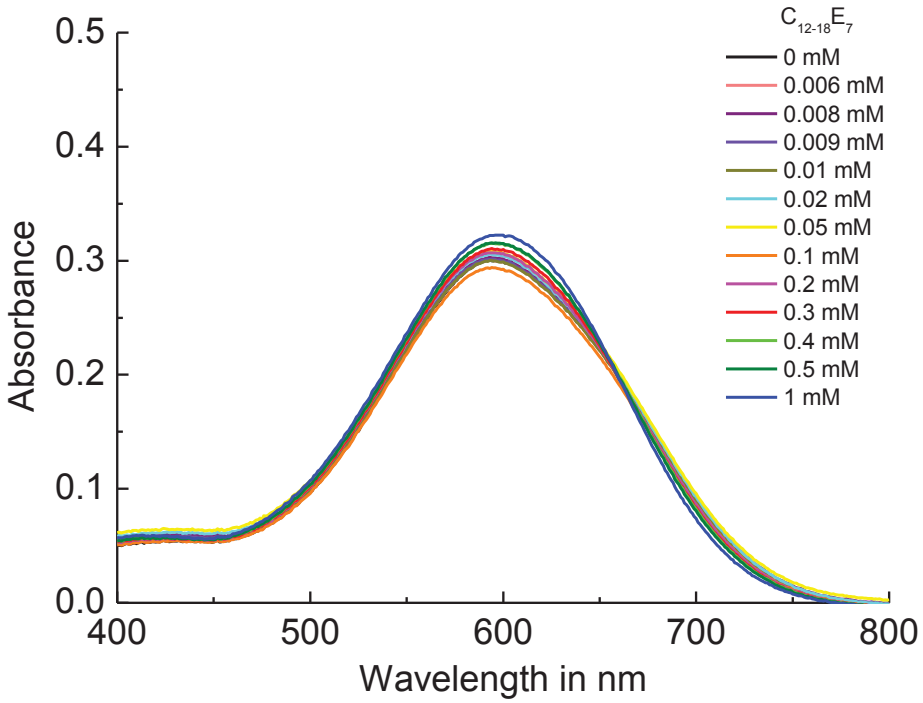

Figure 5 UV-Vis absorption spectra of mixtures of Acid blue 113 + PVPVI + $C_{12\text{-}18}E_7$, equilibrated for 24 h. The concentration of Acid blue 113 and PVPVI is 0.009 mM and $1 \cdot 10^{-3}$ mM respectively in all solutions. The concentration of $C_{12\text{-}18}E_7$ varies from 0 mM to 1 mM (0 g/L to 0.5 g/L).

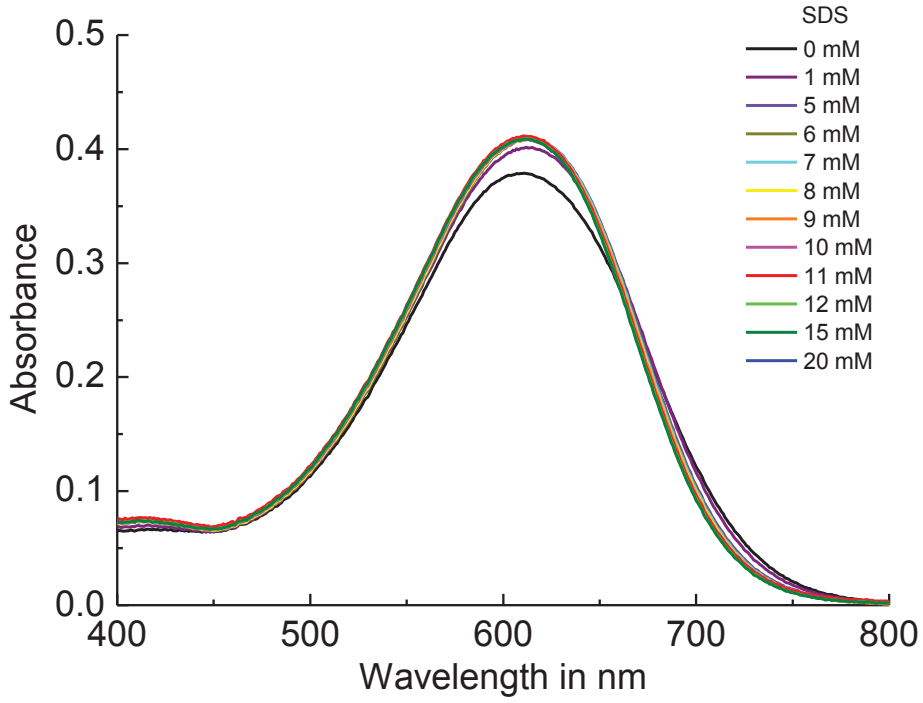

Figure 6 UV-Vis absorption spectra of mixtures of Acid blue 113 + PVPVI + SDS, equilibrated for 24 h. The concentration of Acid blue 113 and PVPVI is 0.009 mM and $1 \cdot 10^{-2}$ mM respectively in all solutions. The concentration of SDS varies from 0 mM to 20 mM (0 g/L to 5.8 g/L).

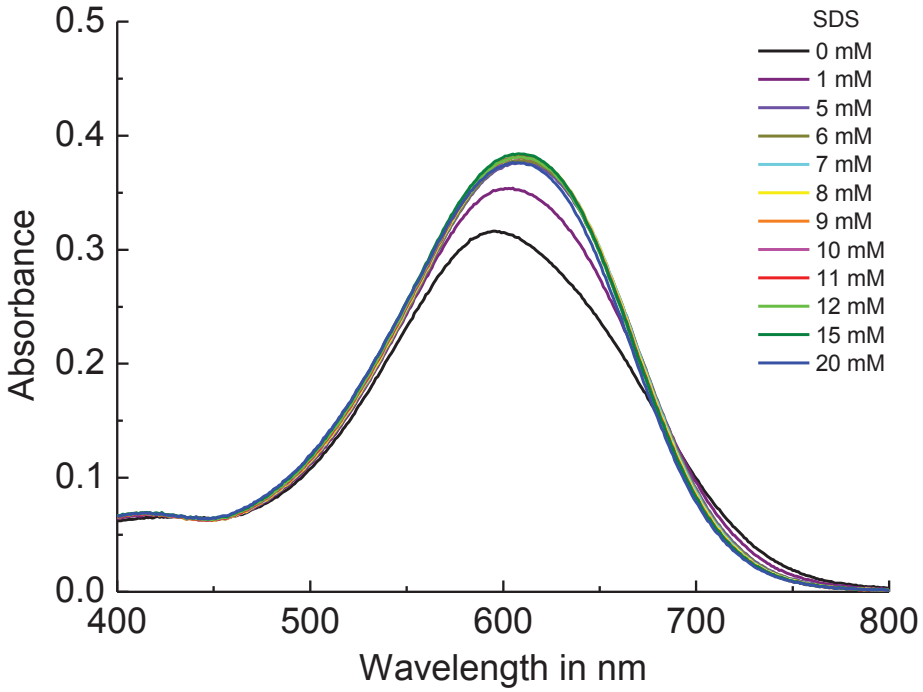

Figure 7 UV-Vis absorption spectra of mixtures of Acid blue 113 + PVPVI + SDS, equilibrated for 24 h. The concentration of Acid blue 113 and PVPVI is 0.009 mM and $1 \cdot 10^{-3}$ mM respectively in all solutions. The concentration of SDS varies from 0 mM to 20 mM (0 g/L to 5.8 g/L).

Table 1 The adsorbed amounts of Acid blue 113 on carbon black. The dye was dissolved in water. The carbon black was 0.4 g/L and the contact time was 2 h.

C_0 in g/L	C_0 in mol/L	C_{eq} in mol/m^3	C_{eq} deviation in mol/m^3	Γ in mol/m^2	Γ deviation in mol/m^2
0.002	$2.93 \cdot 10^{-6}$	$6.87 \cdot 10^{-4}$	0	$3.74 \cdot 10^{-8}$	0
0.003	$4.40 \cdot 10^{-6}$	$1.29 \cdot 10^{-3}$	$3.96 \cdot 10^{-4}$	$5.19 \cdot 10^{-8}$	$6.60 \cdot 10^{-9}$
0.004	$5.87 \cdot 10^{-6}$	$2.27 \cdot 10^{-3}$	0	$6.00 \cdot 10^{-8}$	0
0.006	$8.80 \cdot 10^{-6}$	$4.25 \cdot 10^{-3}$	$1.21 \cdot 10^{-4}$	$7.58 \cdot 10^{-8}$	$2.01 \cdot 10^{-9}$
0.008	$1.17 \cdot 10^{-5}$	$6.37 \cdot 10^{-3}$	$8.18 \cdot 10^{-5}$	$8.95 \cdot 10^{-8}$	$1.36 \cdot 10^{-9}$
0.01	$1.47 \cdot 10^{-5}$	$8.23 \cdot 10^{-3}$	$1.47 \cdot 10^{-4}$	$1.07 \cdot 10^{-7}$	$2.45 \cdot 10^{-9}$
0.02	$2.93 \cdot 10^{-5}$	$1.96 \cdot 10^{-2}$	$5.60 \cdot 10^{-4}$	$1.63 \cdot 10^{-7}$	$9.33 \cdot 10^{-9}$
0.03	$4.40 \cdot 10^{-5}$	$3.08 \cdot 10^{-2}$	$1.41 \cdot 10^{-3}$	$2.20 \cdot 10^{-7}$	$2.35 \cdot 10^{-8}$
0.04	$5.87 \cdot 10^{-5}$	$4.26 \cdot 10^{-2}$	$3.19 \cdot 10^{-4}$	$2.68 \cdot 10^{-7}$	$5.32 \cdot 10^{-9}$
0.05	$7.34 \cdot 10^{-5}$	$5.46 \cdot 10^{-2}$	$1.01 \cdot 10^{-3}$	$3.12 \cdot 10^{-7}$	$1.68 \cdot 10^{-8}$
0.06	$8.80 \cdot 10^{-5}$	$6.75 \cdot 10^{-2}$	$2.58 \cdot 10^{-3}$	$3.42 \cdot 10^{-7}$	$4.30 \cdot 10^{-8}$

C_0: the original dye concentration applied in adsorption measurements.
C_{eq}: the equilibrium concentration of the dye (the remaining dye concentration).
Γ: the adsorbed amount of the dye on carbon black.

Table 2 The adsorbed amounts of Acid blue 113 in mixture with 1.7 mM (< CMC) SDS on carbon black. The dye was dissolved in 1.7 mM SDS solution. The carbon black was 0.4 g/L and the contact time was 2 h. The remaining dye solution was filtrated prior to centrifugation.

C_0 in g/L	C_0 in mol/L	C_{eq} in mol/m^3	C_{eq} deviation in mol/m^3	Γ in mol/m^2	Γ deviation in mol/m^2
0.01	$1.47 \cdot 10^{-5}$	$1.55 \cdot 10^{-3}$	0	$2.19 \cdot 10^{-7}$	0
0.02	$2.93 \cdot 10^{-5}$	$5.21 \cdot 10^{-3}$	$9.83 \cdot 10^{-4}$	$3.91 \cdot 10^{-7}$	$1.63 \cdot 10^{-8}$
0.03	$4.40 \cdot 10^{-5}$	$1.57 \cdot 10^{-2}$	$1.41 \cdot 10^{-3}$	$4.55 \cdot 10^{-7}$	$2.40 \cdot 10^{-8}$
0.04	$5.87 \cdot 10^{-5}$	$3.02 \cdot 10^{-2}$	$2.83 \cdot 10^{-4}$	$4.72 \cdot 10^{-7}$	$3.54 \cdot 10^{-9}$
0.05	$7.34 \cdot 10^{-5}$	$4.35 \cdot 10^{-2}$	$9.19 \cdot 10^{-4}$	$4.87 \cdot 10^{-7}$	$1.63 \cdot 10^{-8}$

Table 3 The adsorbed amounts of Acid blue 113 in mixture with 10 mM (> CMC) SDS on carbon black. The dye was dissolved in 10 mM SDS solution. The carbon black was 0.4 g/L and the contact time was 2 h. The remaining dye solution was filtrated prior to centrifugation.

C_0 in g/L	C_0 in mol/L	C_{eq} in mol/m^3	C_{eq} deviation in mol/m^3	Γ in mol/m^2	Γ deviation in mol/m^2
0.006	$8.80 \cdot 10^{-6}$	$8.16 \cdot 10^{-4}$	$1.63 \cdot 10^{-5}$	$1.27 \cdot 10^{-7}$	$1.10 \cdot 10^{-8}$
0.008	$1.17 \cdot 10^{-5}$	$1.15 \cdot 10^{-3}$	$1.15 \cdot 10^{-4}$	$1.76 \cdot 10^{-7}$	$2.08 \cdot 10^{-9}$
0.01	$1.47 \cdot 10^{-5}$	$2.27 \cdot 10^{-3}$	$2.34 \cdot 10^{-4}$	$2.07 \cdot 10^{-7}$	$3.79 \cdot 10^{-9}$
0.015	$2.20 \cdot 10^{-5}$	$4.43 \cdot 10^{-3}$	$4.05 \cdot 10^{-4}$	$2.93 \cdot 10^{-7}$	$6.81 \cdot 10^{-9}$
0.02	$2.93 \cdot 10^{-5}$	$8.58 \cdot 10^{-3}$	$3.61 \cdot 10^{-4}$	$3.46 \cdot 10^{-7}$	$5.66 \cdot 10^{-9}$
0.03	$4.40 \cdot 10^{-5}$	$2.07 \cdot 10^{-2}$	$4.00 \cdot 10^{-4}$	$3.89 \cdot 10^{-7}$	$6.51 \cdot 10^{-9}$
0.04	$5.87 \cdot 10^{-5}$	$3.42 \cdot 10^{-2}$	$4.04 \cdot 10^{-4}$	$4.07 \cdot 10^{-7}$	$6.35 \cdot 10^{-9}$
0.05	$7.34 \cdot 10^{-5}$	$4.97 \cdot 10^{-2}$	$8.08 \cdot 10^{-4}$	$3.95 \cdot 10^{-7}$	$1.36 \cdot 10^{-8}$

Table 4 The adsorbed amounts of Acid blue 113 in mixture with 10 mM (> CMC) SDS on carbon black. The dye was dissolved in 10 mM SDS solution. The carbon black was 0.4 g/L and the contact time was 2 h.

C_0 in g/L	C_0 in mol/L	C_{eq} in mol/m^3	C_{eq} deviation in mol/m^3	Γ in mol/m^2	Γ deviation in mol/m^2
0.008	$1.17 \cdot 10^{-5}$	$2.06 \cdot 10^{-3}$	$1.35 \cdot 10^{-3}$	$1.61 \cdot 10^{-7}$	$2.25 \cdot 10^{-8}$
0.01	$1.47 \cdot 10^{-5}$	$2.49 \cdot 10^{-3}$	$8.87 \cdot 10^{-4}$	$2.03 \cdot 10^{-7}$	$1.48 \cdot 10^{-8}$
0.015	$2.20 \cdot 10^{-5}$	$4.88 \cdot 10^{-3}$	$6.12 \cdot 10^{-4}$	$2.85 \cdot 10^{-7}$	$1.02 \cdot 10^{-8}$
0.02	$2.93 \cdot 10^{-5}$	$9.41 \cdot 10^{-3}$	$7.67 \cdot 10^{-4}$	$3.32 \cdot 10^{-7}$	$1.28 \cdot 10^{-8}$
0.03	$4.40 \cdot 10^{-5}$	$2.17 \cdot 10^{-2}$	$3.91 \cdot 10^{-3}$	$3.72 \cdot 10^{-7}$	$6.52 \cdot 10^{-8}$
0.04	$5.87 \cdot 10^{-5}$	$3.46 \cdot 10^{-2}$	$1.79 \cdot 10^{-3}$	$4.01 \cdot 10^{-7}$	$2.98 \cdot 10^{-8}$
0.05	$7.34 \cdot 10^{-5}$	$4.86 \cdot 10^{-2}$	$1.01 \cdot 10^{-3}$	$4.13 \cdot 10^{-7}$	$1.69 \cdot 10^{-8}$

Table 5 The adsorbed amounts of Acid blue 113 on PTFE filter regarding three original dye concentrations. The dye was dissolved in water.

C_0 in g/L	C_0 in mol/L	C_{ad} in mol/L	C_{ad} deviation in mol/L	C_{ad} in %	C_{ad} deviation in %
0.005	$7.34 \cdot 10^{-6}$	$1.97 \cdot 10^{-6}$	$9.06 \cdot 10^{-7}$	27.66	12.69
0.01	$1.47 \cdot 10^{-5}$	$2.84 \cdot 10^{-6}$	$6.10 \cdot 10^{-7}$	19.00	4.09
0.05	$7.34 \cdot 10^{-5}$	$4.74 \cdot 10^{-6}$	$3.51 \cdot 10^{-7}$	6.24	0.46

C_0: the original dye concentration.
C_{ad}: the adsorbed dye concentration averaged from three experiments.

Table 6 The adsorbed amounts of Acid blue 113 on PTFE filter regarding three original dye concentrations. The dye was dissolved in 1.7 mM (0.5 g/L) SDS solution.

C_0 in g/L	C_0 in mol/L	C_{ad} in mol/L	C_{ad} deviation in mol/L	C_{ad} in %	C_{ad} deviation in %
0.005	$7.34 \cdot 10^{-6}$	$1.15 \cdot 10^{-7}$	$1.16 \cdot 10^{-8}$	1.58	0.16
0.01	$1.47 \cdot 10^{-5}$	$7.40 \cdot 10^{-7}$	$1.01 \cdot 10^{-7}$	4.76	0.65
0.05	$7.34 \cdot 10^{-5}$	$1.34 \cdot 10^{-6}$	$2.38 \cdot 10^{-7}$	1.80	0.32

Table 7 The adsorbed amounts of Acid blue 113 on PTFE filter regarding three original dye concentrations. The dye was dissolved in 10 mM (2.9 g/L) SDS solution.

C_0 in g/L	C_0 in mol/L	C_{ad} in mol/L	C_{ad} deviation in mol/L	C_{ad} in %	C_{ad} deviation in %
0.005	$7.34 \cdot 10^{-6}$	$1.59 \cdot 10^{-8}$	$2.04 \cdot 10^{-9}$	0.20	0.03
0.01	$1.47 \cdot 10^{-5}$	$3.39 \cdot 10^{-8}$	$6.91 \cdot 10^{-9}$	0.22	0.05
0.05	$7.34 \cdot 10^{-5}$	$2.40 \cdot 10^{-7}$	$2.57 \cdot 10^{-7}$	0.32	0.34

Table 8 The molar extinction coefficient ε of Acid blue 113 in different solvents determined by UV-Vis spectroscopy and the corresponding coefficient of determination R^2.

Solvent	ε in $L \cdot mol^{-1} \cdot cm^{-1}$	R^2
Water	38255	0.9999
1.7 mM SDS	36164	0.9998
10 mM SDS	37204	0.9999
1 g/L Na_2SO_4	29581	0.9985
Water + NaOH (pH = 10)	35949	0.9993
1 g/L NaCl + NaOH (pH = 10)	28756	0.9978
1 g/L Na_2SO_4 + NaOH (pH = 10)	29777	0.9973

The deviation in this thesis relates to the standard deviation based on a sample, given by using the STDEVA function in Microsoft Excel. The standard deviation describes how widely values are dispersed from the average value (the mean). The deviation is calculated using the following formula:

$$\text{Deviation} = \sqrt{\frac{\sum(x_i - \bar{x})^2}{N-1}} \quad (1)$$

where x_i is the value of data point i and $\bar{x}$ the mean value (average) of the sample. N is the sample size (the total number of data points).

Presentations at scientific conferences

Oral presentation:

Y. Zhan, C. A. M. Seidel, B. Glüsen and W. von Rybinski
Study on Interactions between Surfactant, Polymer and Dye in Solution and at Interfaces
14th Zsigmondy Colloquium of the German Colloid Society (April 2018 Mainz, Germany)

Poster:

Y. Zhan, C. A. M. Seidel, B. Glüsen and W. von Rybinski
Study of Interactions between Surfactant, Polymer and Dye in Solution and at Interfaces
Thermodynamics and Energetics in Soft Matter Systems summer school (July 2018 Grenoble, France)

Y. Zhan, C. A. M. Seidel, B. Glüsen and W. von Rybinski
Study of Interactions between Surfactant, Polymer and Dye in Solution and at Interfaces
STEPsCon 2018 (December 2018 Leverkusen, Germany)

Y. Zhan, C. A. M. Seidel, B. Glüsen and W. von Rybinski
Influence of Surfactant or Polymer on Dye Aggregation in Solution and at Interfaces
33rd ECIS Conference (September 2019 Leuven, Belgium)

Eidesstattliche Erklärung

Hiermit versichere ich an Eides statt, dass die vorliegende Dissertation von mir selbständig und ohne unzulässige fremde Hilfe unter Beachtung der „Grundsätze zur Sicherung guter wissenschaftlicher Praxis an der Heinrich-Heine-Universität Düsseldorf" erstellt worden ist sowie noch bei keiner anderen Institution in der vorgelegten oder in ähnlicher Form eingereicht wurde.

Es existieren keine vorherigen Promotionsversuche.

Düsseldorf, den 06.07.2020

Yifei Zhan